Long-term Measurement of Time-Dependent Pre-stressed Losses in the Westbound Gandy Bridge Project (Phase II)

PB2000-102811

Project Number: WPI-0510735

Final Report

Submitted to
Florida Department of Transportation
Project Manager : Dr. Moussa Issa, P.E.

By
Dr. Okey Onyemelukwe, P.E.
Civil & Environmental Engineering Department
University of Central Florida
Orlando, Fl. 32816

December 09,1999

Technical Report Documentation Page

1.Report No. WPI 0510735	2.Government Accession No.	3. Receipient's Catalog No.
4. Title and Subtitle Long-term Measurement of Time-Dependent Pre-Stressed Losses in the Westbound Gandy Bridge Project (Phase II)		5. Report Date 12/99
7. Author(s) Okey U.Onyemelukwe, Ph.D.,PE.		6. Performing Organization Code 8. Performing Organization Report
9.Performing Organization name and address University of Central Florida Civil & environmental Engineering Dept. 4000 Central Florida Blvd. Orlando,Fl. 32816		10. Work Unit No. 11. Contract or Grant No. B-A485
12. Sponsoring Agency name and address Florida Department of Transportation 605 Suwannee Street Tallahassee, FL 32399-0450		13. Type of Report and Period Covered Research 08/96 – 06/99 14. Sponsoring Agency Code
15.Supplementary Notes		

16. Abstract :

This report presents the analysis and results from the study of the time-dependent behavior of an actual pre-stressed concrete bridge as determined from field measurement of strains and temperature at various locations in the bridge structure. It further discusses the resulting pre-stress losses from creep and shrinkage of concrete, as well as, their effects on stress re-distribution in the bridge girders, and on camber and deflection of the girders. The bridge instrumentation techniques used and preliminary results from this bridge were subject of Phase I of this study which was presented in a previous FDOT report titled "Field Measurement and Evaluation of Time-Dependent Losses in Pre-stressed Concrete Bridges".

17. Key Words Prestressed Concrete Bridges Pretensioned Girders Prestressed Losses Time-Dependent Behavior Creep, Shrinkage, Steel Relaxation Camber and Deflection in Bridges	18. Distribution Statement

19. Security Classif.(of this report) Unclassified	20. Security classes (of this page) Unclassified	21. No. of pages 140	22. Price

Disclaimer Sheet

The opinions, findings and conclusions expressed in this publication are those of the authors and not necessarily those of the Florida Department of transportation or the US Department of Transportation.

This publication was prepared in cooperation with the state of Florida Department of Transportation & the US Department of Transportation.

SI* (MODERN METRIC) CONVERSION FACTORS

APPROXIMATE CONVERSIONS TO SI UNITS

Symbol	When You Know	Multiply By	To Find	Symbol
LENGTH				
in	inches	25.4	millimeters	mm
ft	feet	0.305	meters	m
yd	yards	0.914	meters	m
mi	miles	1.61	kilometers	km
AREA				
in^2	square inches	645.2	square millimeters	mm^2
ft^2	square feet	0.093	square meters	m^2
yd^2	square yards	0.836	square meters	m^2
ac	acres	0.405	hectares	ha
mi^2	square miles	2.59	square kilometers	km^2
VOLUME				
fl oz	fluid ounces	29.57	milliliters	ml
gal	gallons	3.785	liters	l
ft^3	cubic feet	0.028	cubic meters	m^3
yd^3	cubic yards	0.765	cubic meters	m^3

NOTE: Volumes greater than 1000 l shall be shown in m^3.

MASS				
oz	ounces	28.35	grams	g
lb	pounds	0.454	kilograms	kg
T	short tons (2000 lb)	0.907	megagrams	Mg
TEMPERATURE (exact)				
°F	Fahrenheit temperature	5(F-32)/9 or (F-32)/1.8	Celcius temperature	°C
ILLUMINATION				
fc	foot-candles	10.76	lux	l
fl	foot-Lamberts	3.426	candela/m^2	cd/m^2
FORCE and PRESSURE or STRESS				
lbf	poundforce	4.45	newtons	N
psi	poundforce per square inch	6.89	kilopascals	kPa

APPROXIMATE CONVERSIONS FROM SI UNITS

Symbol	When You Know	Multiply By	To Find	Symbol
LENGTH				
mm	millimeters	0.039	inches	in
m	meters	3.28	feet	ft
m	meters	1.09	yards	yd
km	kilometers	0.621	miles	mi
AREA				
mm^2	square millimeters	0.0016	square inches	in^2
m^2	square meters	10.764	square feet	ft^2
m^2	square meters	1.195	square yards	ac
ha	hectares	2.47	acres	mi^2
km^2	square kilometers	0.386	square miles	
VOLUME				
ml	milliliters	0.034	fluid ounces	fl oz
l	liters	0.264	gallons	gal
m^3	cubic meters	35.71	cubic feet	ft^3
m^3	cubic meters	1.307	cubic yards	yd^3
MASS				
g	grams	0.035	ounces	oz
kg	kilograms	2.202	pounds	lb
Mg	megagrams	1.103	short tons (2000 lb)	T
TEMPERATURE (exact)				
°C	Celcius temperature	1.8C + 32	Fahrenheit temperature	°F
ILLUMINATION				
lx	lux	0.0929	foot-candles	fc
cd/m^2	candela/m^2	0.2919	foot-Lamberts	fl
FORCE and PRESSURE or STRESS				
N	newtons	0.225	poundforce	lbf
kPa	kilopascals	0.145	poundforce per square inch	psi

* SI is the symbol for the International System of Units. Appropriate rounding should be made to comply with Section 4 of ASTM E380.

(Revised August 1992)

EXECUTIVE SUMMARY

Problem Statement

The Florida Department of Transportation (FDOT) is frequently confronted with contractor suggested redesigns of some of its pre-stressed concrete bridge projects. In which case most of them call for changing the bridge girder design from its original post-tensioned continuous members to longer simple supported spans. Often, these result in deeper simple span girders with larger cross-sectional areas, moment of inertia and consequently greater ultimate capacity. Thus, enabling the designer to eliminate the post-tensioning and change the statical scheme from continuous to simply supported.

However, although the girders are designed as simple spans, the attached deck slabs remain as continuous members. The final configuration of both the deck slab and the girder acting as a unit, is in essence a hybrid between a strictly statically indeterminate structure and a determinate structure. Further investigation of this sort of design is necessary, since the effect of the time-dependent behavior of these members with respect to creep, shrinkage and steel relaxation is drastically different for indeterminate structures as compared to simple ones.

Project Objectives

This study is a follow on to a previous one in which an actual pre-stressed concrete bridge, the West-Bound Gandy Bridge, was instrumented at the inception of construction with embedded strain gauges to measure both strain and temperature at select locations of the structure. The objective of this second phase of the research is to utilize the field measured strain and temperature readings in investigating the time-dependent behavior of this typical pre-tensioned concrete bridge with a hybrid structural configuration. The data collected is used to perform the following analysis and investigations:

- Determine the pre-stress losses at various locations and depth of the structure based on field measured data and compare them with those recommended for use by established codes such as ACI, AASHTO, PCI and the CEB-FIP.

- Utilize the field measured data and the pre-stress losses derived from them in investigating any stress redistribution that may result from the time-dependent behavior of the concrete, and from the hybrid structural configuration of the bridge.

- Establish any serviceability issues that may result from this hybrid structural configuration by using the field measured data, to investigate any effects the time-dependent behavior may have on the camber and deflection of the members.

Project Findings

This report concentrates on field measured and bridge monitoring data for up to 390 days from the date of initial instrumentation of the bridge girders in the pre-cast yard. By this time, most of the pre-stress losses in the members had occurred and the remaining data, which is available in a database for up to three years of measurement, has become essentially constant and shows negligible variations in time. It is important to note that the composite bridge slab was cast at the 240^{th} day, and contributions due to this additional load and other superimposed loads on the structure were adequately accounted for in the analysis.

Consequent to the determination in the Phase I study that pre-stress losses varied across the depth of the girders, the ACI and PCI methods which account for time-dependency and the AASHTO lump sum value which is time and depth invariant were employed for comparison with those from field measurement. This study determines that the pre-stress losses from the field measured data compares well with those from the PCI and ACI time-dependent methods, while that from the AASHTO approach seemed overly conservative.

It was also determined that the variation of pre-stress loss with depth has a more profound effect on the camber values than on the stress distributions in the members.

Project Conclusions

The following important conclusions are drawn from this research project:

- It is established that the PCI and ACI-209 time-dependent methods for estimating pre-stress losses yield similar results to those from field measurements. However, it is necessary to note that the inability to utilize these code methodologies in depicting the effect of pre-stress loss at different depths of the concrete member may hamper their usefulness in accurate computation of camber and deflection values.
- This study proposes the use of K_d and K_t depth and time-dependent coefficients respectively, in implementing the variability of the effective creep coefficient with time and depth in a design.
- On account of the stress variations in the members, it is concluded that the time-dependency of the design is more significant than its depth dependency. Comparison of a continuous slab and a simple slab configuration indicates the stress variations at the mid-span were very similar, but were very different at regions close to the support, prompting for closer attention to the support region in such designs as this.
- The study also determines that the camber in the pre-stressed concrete girders varied significantly across its depth, thus, amplifying the importance of including the depth dependency of the creep coefficients in properly computing the camber for design.
- It is also observed that though the conventional use of higher concrete strengths in the field (more than what the actual design specifies) is a good practice with respect to stresses, it is not such a good thing for the camber and deflection, and must be done with care.

TABLE OF CONTENTS

LIST OF TABLES

LIST OF FIGURES

Chapter 1

INTRODUCTION

1.1 Westbound Gandy Bridge Project

This research project studied the effect of time-dependent pre-stress losses by using measurements from an actual bridge, the Westbound Gandy Bridge that connects Pinellas and Hillsborough counties in Florida. This report (phase II) presents a continuation of the work started in phase I of the project, and discusses mainly the pre-stressing effects as deduced from the measured strain data, the concrete stress re-distribution due to the bridge configuration, and computation of the bridge camber.

The bridge itself consists of typical segments of three simply supported spans of 43.9 m (144 ft) modified AASHTO type IV concrete girders with a continuous slab placed on these girders. The bridge instrumentation, data collection and data reduction techniques employed in the project were previously presented in the phase I report [1]. Pre-stress concrete losses are determined from using embedded vibrating wire strain gages to measure strain at different depths and locations along the girders. Centroids of steel, non-composite girder, and composite section were some of the different depths used. Other depths were top most, bottom most and some chosen in between. The

different instrumented locations along the bridge were at 1.52 m (5 ft), quarter, and mid-span of the girders with total span length of 43.9 m (144 ft). Modified AASHTO type VI girders were used for this bridge. Even though the modified AASHTO type VI girders look similar in shape to the standard ones, they are somewhat different in dimension. The modified girder is 15.2 cm (6 in) larger in height, 129 cm^2 ($20in^2$) bigger in area, 3.7 KN/m (21 Kpf) larger in self-weight, and has a moment of inertia of 0.842 m^4 (202,224 in^4) larger than the standard AASHTO type IV girder.

All strain gages are connected to a data collection system. The collection of data began in December of 1995 at the Hardaway Pre-stress Plant where the girders were cast. In April of 1996, the girders were transferred to the bridge from where data is still being collected, and is scheduled to end in August 1999. This draft report includes data reduced up to 390 days from the casting of the girders, and the final report will be include, the remainder of the data up to August 1999. The strain readings are used as a tool for studying the time dependent behavior of the pre-stressed concrete members. The behaviors that is of most importance in this study are the time-dependent losses such as creep, shrinkage and steel relaxation, and their effect on the amount of stresses as well as camber of the bridge.

The main objective of the study is to precisely measure the time-dependent components of the pre-stress loss. Although, calculating the total pre-stress loss is a vital task in pre-stressed concrete design, more important, is the proper calculation of the various components that make up the total loss. These components are creep, shrinkage and steel relaxation. Not only is computing these components of loss important for

achieving the total stress loss, but are also required for better computations of the amount of camber in the section.

This report presents the behavior of the beams instrumented with the strain gages. Data from these beams were collected from the time the girders were cast until 390 days later. This study represents the response of a pre-stressed section in the first thirteen months. During this period the slab was cast over the girders, hence, the addition of the superimposed dead load plays a role in this study. The change in behavior of the girders when the additional weight took effect was observed. Throughout the project, various stages such as initial transfer, prior and after the addition of the superimposed dead load were studied.

The content of this report can be summed in this paragraph. In chapter 2, related topics are mentioned under literature review. In chapter 3, location of girders and Bridge instrumentation is discussed. Reasons for selecting specific girders and locations for instrumentation are mentioned. In chapter 4, more detailed explanation of the method used in determining the field pre-stress loss is presented, along with the various design codes' pre-stress loss computation methodologies. In chapter 5, results in terms of pre-stress losses are presented and discussed. In chapter 6, results in terms of the effect of the pre-stress loss on stress and camber or deflection are shown and elucidated. In chapter 7, conclusions and future recommendations are made.

CHAPTER 2

LITERATURE SURVEY

2.1 Introduction

More accurate determination of pre-stress losses is an important task in the area of pre-stress concrete design. Common pre-stress designs utilize a lump sum value that reflects the various components of pre-stress losses. This lump sum value accommodates losses due to both immediate and time dependent factors. As research provides a better understanding of pre-stress concrete behavior, precise calculation of the various contributions to pre-stress loss becomes essential. Depending on the method of pre-stressing, the primary components of pre-stress losses are elastic shortening and steel relaxation which constitute immediate losses; creep, shrinkage and steel relaxation which make up time-dependent losses. The summation of the different contributions to pre-stress loss results in the total pre-stress loss value.

Several researchers recognized the importance of computing the various elements of pre-stress losses. Many common equations used by structural engineers depend on some of the individual elements of the total pre-stress loss. Obtaining the individual components of pre-stress loss will allow engineers to better compute some design aspects such as camber or deflection. Especially, since a parameter like creep may affect camber

and deflection more than the other time-dependent components. By the use of a simple mathematical equation, the several components can be added together to obtain the lump sum value of pre-stress loss.

2.2 Previous Work Related to this Study

The ACI 318R-92 code suggests the use of the work represented in some publications that discuss the methods for computing the various pre-stress loss components[2]. Among some of the suggested articles is the use of the PCI approach based on work by Zia et al.[3]. This method is also used in the PCI Handbook 4th edition[4]. This method presents a general method to compute the components of pre-stress loss as a function of time in which there is a strong interrelation between the various components. Alteration to one element affects the other elements. For example, the amount of steel relaxation is changed when the creep value is altered and vice versa. Due to the interaction between the various components of pre-stress loss, exact pre-stress values are hard to achieve. However, this method of computation is still a better estimation of the losses than the lump sum method commonly used in some codes[5].

This PCI article discusses losses in both pre-tensioned and post-tensioned members. The generality of this method extends to include factors that are altered to compensate for different concrete sectional properties. Normal weight vs. lightweight, moist cure vs. accelerated cure are some of the many factors taken into account in this study. This PCI article contains various equations that can be implemented to fit most

pre-stress concrete designs. However, if a project does not meet the specified conditions, another approach should be implemented. Some of the other factors affecting pre-stress loss discussed in this study include the unit weight of the member, the type of steel used and environmental conditions. In lightweight concrete, a unit weight between 1,442 and 2,002 kg/m^3 (90 and 125 lb/ft^3) must be used. In normal weight concrete, a unit weight of 2,323 kg/m^3 (145 lb/ft^3) must be used. Along with concrete weight specification, low relaxation steel must be used and a relative humidity of about 70 percent should exist.

Utilizing the findings from the work done by Zia et al., the PCI Committee report[3] on pre-stress losses suggests two methods that can be used to determine the amount of pre-stress losses. Both methods are a function of time. These methods are known as the General Method and the Simplified Method. Determination of these empirical pre-stress loss parameters is done using research data obtained from various projects.

The General Method of the PCI committee report on pre-stress loss discuses the various elements of pre-stress losses separately[3]. Each loss component is computed individually. Once the values of the various elements are achieved, the lump sum value is determined by summing the various components. The computations in these equations are time dependent, allowing the designer to view the behavior of the structure at various time intervals during the lifetime of the structure. Understanding the components of losses with respect to time is stressed in this method. The losses are divided into immediate and time dependent losses. Although both of these losses exist in pre-tensioned and post-tensioned concrete members, the composition of immediate losses differs between the two methods for pre-stressing concrete members. In pre-tensioned

members, the immediate loss includes initial steel relaxation and elastic shortening. Where in post-tensioned members, the immediate losses may consist of anchorage loss, frictional loss, elastic shortening, and misalignment of the ducts. The composition of the time dependent losses is primarily the same for both pre-stress and post-tensioned members. It consists of creep, shrinkage and steel relaxation. Each loss element is computed using a special equation that takes into account the sectional properties of a specific structure. Some of the many factors that play a role in computing the loss elements are the type of concrete and steel, the volume to surface area ratio, the length of curing, and age of concrete at steel transfer.

The Simplified Method of the PCI committee report on pre-stress loss presents the total pre-stress loss as one value. This method of loss computation is much simpler than the General Method. Its lack of generality is expressed in the specification required for the use of this method. Sectional properties, concrete and steel strength of the member are some of the specified requirements of interest. In pre-tensioned sections, accelerated cured concrete should be used, where in post-tensioned, a moist cured section should be used. The stress in the tendon at the critical location immediately after transfer should not exceed $0.7 f_{PU}$. The constraints in these equations make the implementation of this method in determining the lump sum loss of many pre-stress concrete sections an impossible task.

Another research of great significance to this project is the work done by the ACI Committee 209[6]. This study was based on both instantaneous and time dependent pre-stress losses. Equations for estimating the various components of pre-stress loss were

used in this study. The various equations used by ACI-209 will be presented and utilized in greater detail in chapter four of this report.

CEB-FIP European Code[7] captures the time-dependency of pre-stress loss as well. This code divides time-dependent pre-stress loss into two stress reductions. One is due to the creep and shrinkage of the concrete member or the reduction in strain of the concrete member. Two is due to the stress reduction within the steel. This steel reduction is caused by the relaxation of this material under constant tension.

Based on the various research projects presented on pre-stress loss, the AASHTO code suggests the use of time-dependent method for pre-stress loss calculation also[5]. It divides pre-stress losses into both instantaneous and time dependent pre-stress losses. The instantaneous losses include anchorage set, friction and elastic shortening. The time dependent losses are creep shrinkage and steel relaxation. The AASHTO code comments on the importance of calculating time-dependent pre-stress losses in accordance with a method supported by research data.

It is important to compare the work from this project with other studies and findings, in order to better understand the behavior of the pre-stress concrete members. In this work, time-dependent pre-stress loss with respect to depth is measured. Various strain gages were placed at different depths. Time-dependent pre-stress and its effect on the structures were determined at the various strain gage locations. The various findings of this research study were compared with other studies. Most of these studies capture time-dependent pre-stress loss at the steel centroid only. Others depict the non-time varying nor depth varying lump sum pre-stress loss. The difference in consequences

from using this research's method for pre-stress loss evaluation vs. the pre-stress losses obtain using other studies on the behavior of the member are elucidated later on in this report.

In a previous research study conducted by Christopher Mills[8], time-dependent pre-stress loss was measured and compared with the lump sum method of various codes. This study covered up to 150 days since the beams were cast. It is important to note that the additional superimposed dead load was applied at 240 days after the beams were cast. In Christopher Mills[8], it was found that the strain readings differed at various depths. Due the variation of strain reading at the different depths, a term herein referred to as apparent pre-stress loss was determined at different depths of the girder. It was also recommended in this study to separate the components of time-dependent pre-stress loss in order to study the effect of the individual components on the behavior of the structure.

Antonio Montiel[9] provides a simulation of time-dependent loss effects on a typical span of the Westbound Gandy Bridge. This study uses a computer program to predict what will occur over time. Comparison between results from the computer program and experimental estimation of the behavior of the member was investigated in this study. This study provides an analytical approach for estimating the affect of time-dependent pre-stress losses on the behavior of the structure.

The present project is aimed at continuing some of the work started by the above mentioned authors. In particular, determining the amount of time-dependent pre-stress loss since the beams were cast up to 390 days, which includes the effect of the additional superimposed dead load on pre-stress loss. Also this research project attempts to depict

pre-stress loss with respect to both time and depth, as well as separating the different components of pre-stress losses. The depth varying losses is what is called apparent pre-stress loss in this research, since they merely depict the equivalent losses at locations where actual strands do not exist. However, the value of the apparent pre-stress loss at the strand level will equal the true pre-stress loss at that level. One of the components of time-dependent pre-stress loss, creep, was incorporated into the camber and deflection's computation method used in this study. The implementation of time and depth dependent creep into the camber equations allows engineers to capture the magnitude of camber with respect to both time and depth as will be shown in chapter six.

CHAPTER 3

GIRDER AND BRIDGE INSTRUMENTATION

3.1 Introduction

Three typical simple spans of the Gandy Bridge were selected for this study. Each span consists of four 43.9 m (144 ft) long modified AASHTO type VI girders. Two of the spans were used for gage instrumentation. A couple of girders were selected from each span. All four girders were instrumented with strain gages across their depth. The thorough investigation of pre-stress loss and its affect on the section was based on these four girders. The significance of the selected girders is presented in Figure 3-1. Two of the four beams are exterior while the other two are interior. While both interior and exterior section behave differently, both end span beams and mid span beams are different as well. Atop the girders lie a continuous slab. The continuity of this slab spans along the three girder sections causing the slab and other superimposed dead loads to affect each selected span differently. From basic engineering, the moment caused by a continuos-superimposed dead load is different from one that is based on a simply supported dead load. Figure 3-1 and 3-2 show sketches of the Gandy Bridge configurations.

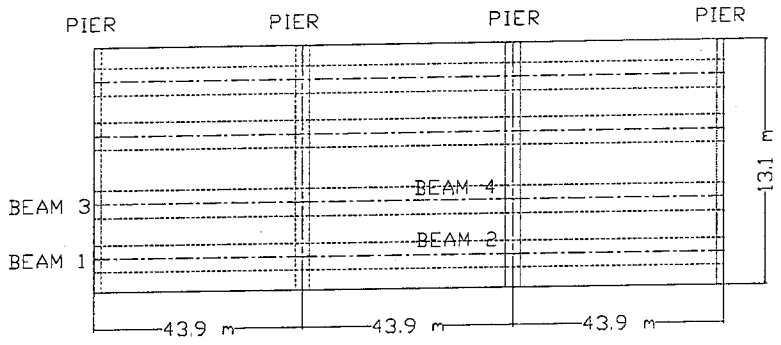

Figure 3-1 Bridge Configuration of the Westbound Gandy Bridge in Tampa, Florida.

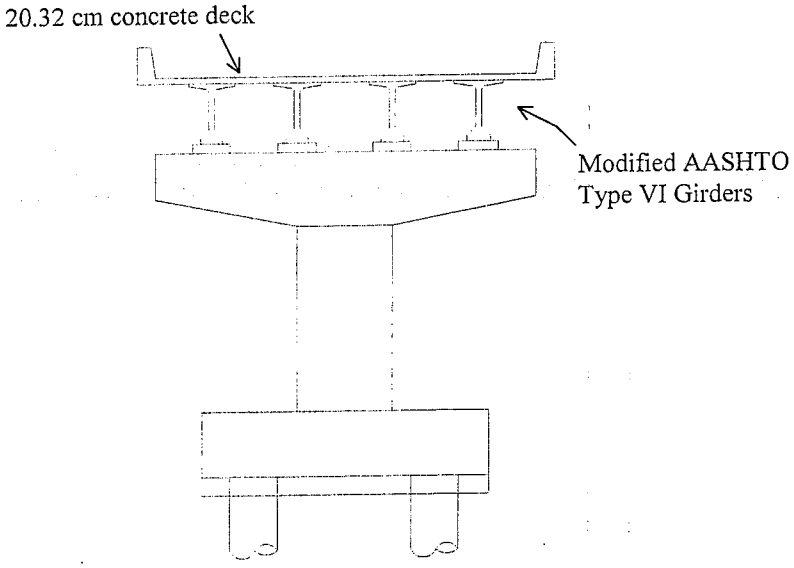

Figure 3-2 Cross-section of the Westbound Gandy Bridge.

3.2 The Gandy Bridge Design

A typical span of the Gandy Bridge consists of piers supporting four simply supported AASSTO type VI girders at both ends. These girders and the standard AASHTO type VI girder have the same general shape; however, they are different in dimensions. The modified AASHTO type VI girders are bigger in dimensions than the standard ones. They are 15.2 cm (6 in) deeper, 129 cm^2 (20 in^2) larger in area, and 3.7 KN/m (21 Kpf) heavier than the standard type VI. In the modified AASHTO type VI girders, the top flange width is 152.4 cm (60 in), the web height and thickness are 127.0 cm (50 in) and 17.8 cm (7 in) respectively. These values along with other dimensions are different from the standard AASHYO type VI girders. The increase in the dimensions of the modified sections has led to a 27.6 % increase in the moment of inertia of the section with only 1.84 % increase in the area over the standard type (See Table 3-1).

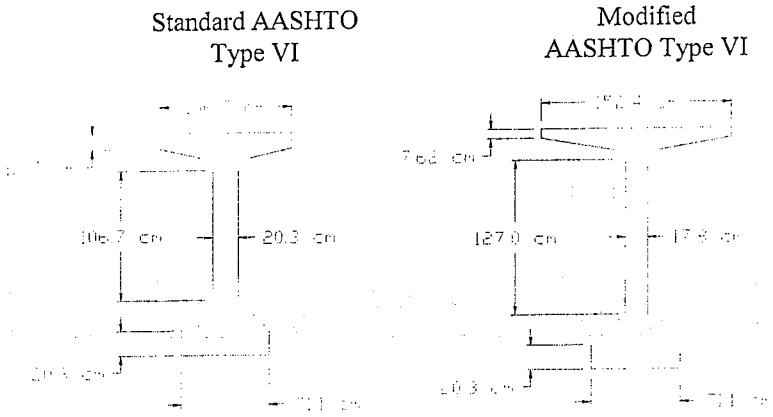

Figure 3-3 Standard and Modified AASHTO Type VI Girder Cross-sections.

Table 3-1 Properties for the Standard and Modified Type VI Girders

AASHTO Type VI	Height		Area		I_c		Girder Weight (w_0 = 0.145kpf)	
	cm	in	Cm^2	in^2	m^4	in^4	KN/m	kpf
Standard	182.9	72	7,000	1,085	0.3052	733,320	191.2	1.092
Modified	198.1	78	7,129	1,105	0.3894	935,544	194.9	1.113

These modified AASHTO type VI girders are pre-stressed using 64 number-1.27 cm (0.5 in) strands. Fifty of the 64 strands are tensioned straight along the bottom of these girders at 174.52 cm (68.7 in) from the top of the girders. The 14 remaining strands are doubly depressed. The tendon profile of the 14 double depressed strands is shown in Figure 3-4 and 3-5. The hold down points or points of depression can be clearly seen in Figure 3-4. Combinations of seven wire low relaxation 1862 MPa (270 ksi) strands are jacked with a tensile force of 150.3 kN (33.8 kips) on each strand. This tensile force results in a 1395.55 Mpa (202.4 ksi) tensile force on each of these strands.

Tendon Profile

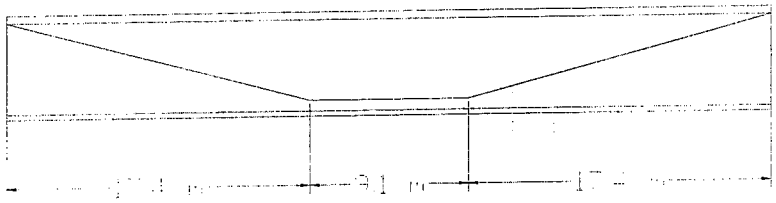

Figure 3-4 Tendon profile for Modified Type VI girder for Westbound Gandy Bridge.

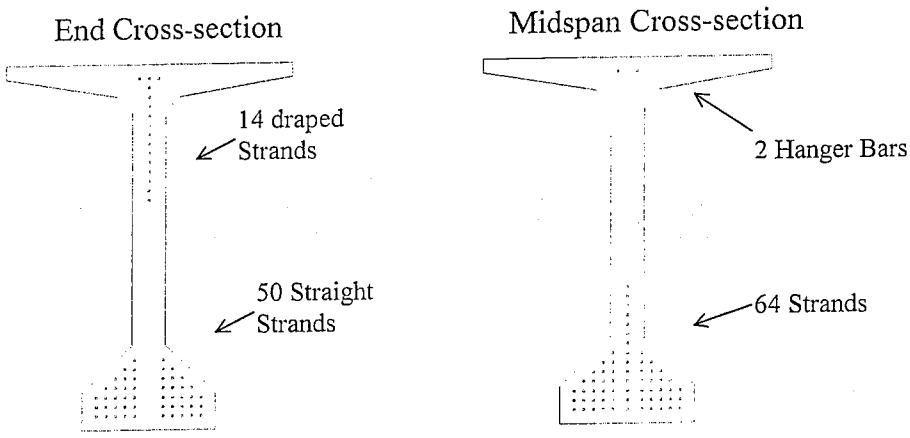

Figure 3-5 Ends and Mid-span cross-sections with tendons.

3.3 Instrumentation Used in the Gandy Bridge Project

Embedded vibrating wire strain gages were used to obtain the change in strain in the concrete. The entire data collection system is composed of three different equipment that can be used together to obtain meaningful strain measurements. They are strain gages, multiplexers and a data acquisition system. A description of each component is presented in the following paragraph.

Strain gages were embedded into the concrete. These gages are capable of measuring strain and temperature in the concrete section at the same location. These gages are composed of thermistor, vibrating wire protected in a tube and a wire that runs to a multiplexer. Once these gages are placed in the concrete, the concrete temperature is recorded. Any concrete movement results in a change in the tensioning of the vibrating wire. The concrete's strain and temperature data are then transmitted to the data

acquisition system, which stores them for a period of time. After a certain time, new data will over write the former obtained data; hence, data need to be collected periodically.

The data acquisition system uses the Micro-10 software program. This program allows both temperatures and strains values to be attained and presented in an understandable fashion. Along with this data acquisition system which contains the Micro-10 program, there is a cellular phone modem also. Downloading the data attained from the gages can be done by two methods. One of these methods is by connecting a computer system that contains the Micro-10 software to the data acquisition system directly, and downloading the data. This method is done at the site. The second method is done by activating the modem of this system via a phone line and downloading the contained data. In this method, the dialing computer must have the Micro-10 program and a modem and can be done from anywhere.

Proper placements of the equipment on the bridge were needed when the girders were moved to the site. The various multiplexers were attached to the four selected girders' inner side of the beams. This location placement is done for maximum protection of the equipment against all weather conditions. The data acquisition system was placed on pier 62, which is located between the four girders. The placement of the data acquisition atop the pier makes it possible to excess the system in case of any unfortunate problems that might occur. The power source of the data acquisition system is a 12-volt battery rechargeable by a solar panel. The solar panel is placed on the outer side of the pier where it can have the maximum amount of exposure to sunlight possible. A schematic approach of the equipment is shown in Figure 3-6.

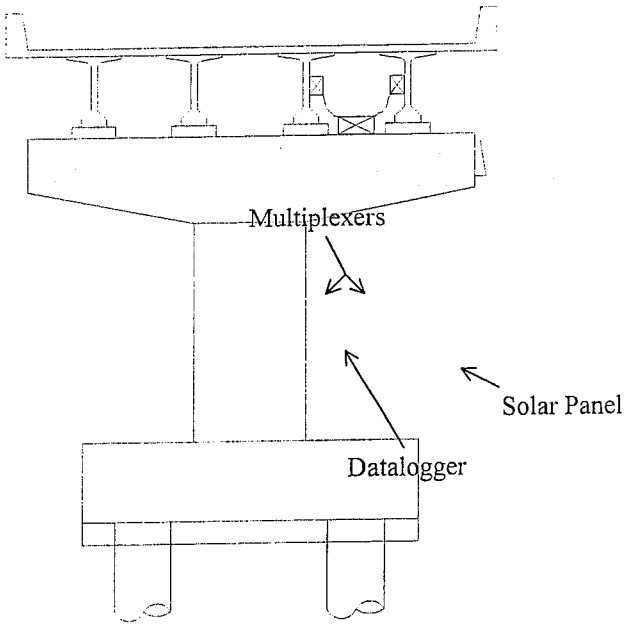

Figure 3-6 Bridge cross-section with equipment.

3.4 Placement of Gage Instrumentation

Gage instrumentation was done on both girders and slab. Different locations and depths were selected for gage instrumentation. The placement of the various gages was done to better our understanding of the pre-stress losses, and the behavior of the section at different locations and depths. The uniformity of sectional behavior is often assumed for design simplicity. Linear strains across the depth, one pre-stress loss value at steel centroid level and one camber value to represent the sectional behavior are among the many assumption used for simplifying the complex structural behavior. A better

understanding of the variation of concrete behavior across the depth was a major goal of this study. Pre-stress losses and its effect on stresses and camber values were done with respect to depth and time. In the following sequential sections, detailed explanations for choosing the location for gage placement in both girders and slab are shown.

3.4.1 Girder Instrumentation

Four girders that are of good representation of all other bridge girders were used for in this study as depicted earlier in the Figure 3-1. Various locations along these girders were selected for gage instrumentation. Among these selected sections are the mid-span of all studied girders which is one where the maximum moment and deflection occur. Another was at 1.52 m (5 ft) away from the support of Beam 1 and 4. The significance of this location is to represent the region that has a small moment and is close to the support. An intermediate location between the previous two was selected as well, this location is at quarter span of Beam 2 and 3. Figure 3-7 represents the four girders selected and the location of gage implementation.

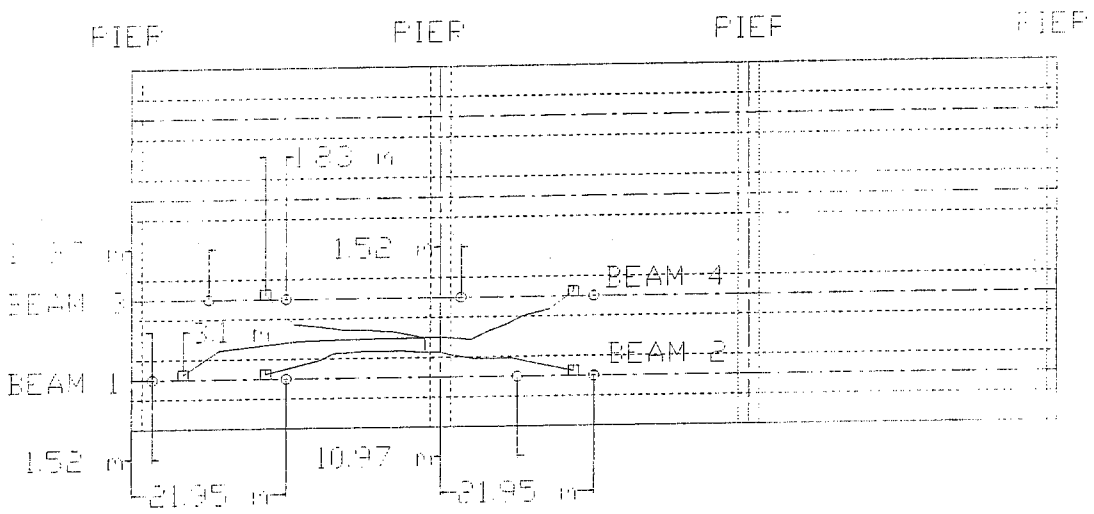

Figure 3-7 Instrumented locations along the studied girders.

At the locations specified, various depths were selected for gage placement. In the cross section of the mid-span, depths of some significance such as near the top most at 190.5 cm (75 in) and near the bottom most of the girders at 7.6 cm (3 in) from the bottom were selected. Other gages were instrumented at points within the centroid of the concrete girder at 99.06 cm (39 in), at the steel centroid of 23.57 cm (9.28 in), and the centroid of the composite section after the slab is placed of 154.9 cm (61 in). Some other points were selected to show the behavior of the section at points between the above mentioned ones. These are at, 53.34 cm (21 in), 65.58 cm (27 in), and 175.3 cm (69 in) within the girder depths. The reason for the selection of these points is to predict the sectional behavior at these depths as well. The selected depths for instrumentation at the mid-span are shown in Figure 3-8.

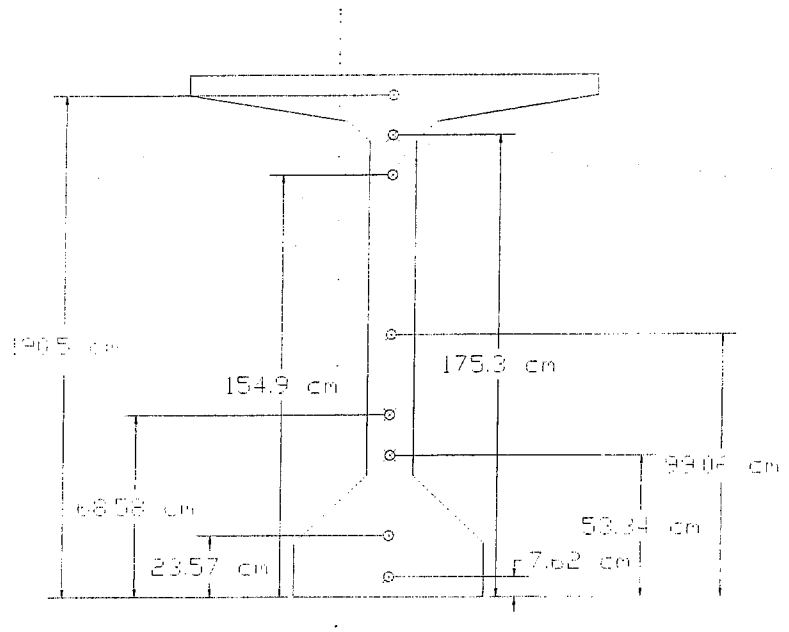

Figure 3-8 Mid-span gauge distribution for all Beams studied.

Both Beams 2 and 3 have six gages at quarter span away from the support. Some of these gages are placed at the same depth shown for mid-span. In both Beams 2 and 3, depths such as 190.5 cm (75 in), 175.3 cm (69 in) and 7.62 cm (3 in) are used for gage instrumentation. Note all these three gage locations are used in the mid-span also. Three new depth locations were also instrumented with strain gages at the quarter-span, depths such as 84.07 cm (33.1 in), 31.04 cm (12.22 in), and 18.80 cm (7.4 in). It is important to note that the depth of 84.07 cm (33.1 in) represents the steel centroid of the doubly depressed strands at quarter-span. Depth of 18.80 cm (7.4 in) represents the steel centroid of the 50 straight strands. Figure 3-9 shows the various depths used for gage instrumentation at quarter-span of Beams 2 and 3.

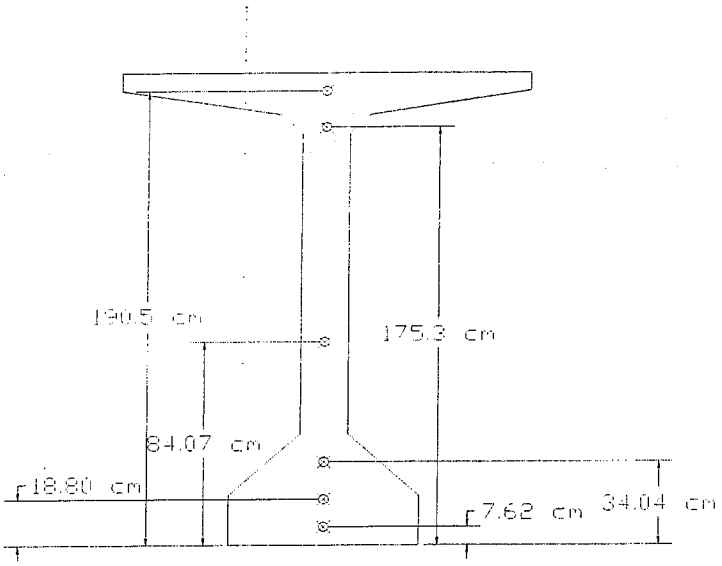

Figure 3-9 Quarter-span gauge distribution for Beams 2 and 3.

At 1.52 m (5 ft) away from the support of Beams 1 and 4, the strain instrumentation was implemented at the same depths shown in quarter-span. Five out of the six strain gages had the same depth location at 1.52m (5 ft) and quarter-span. The only difference in gage placement between the two locations was that of depth 147.0 cm (57.9 in) which was at the center of gravity of the 14 pre-stressed strands. These depth locations can be seen in Figure 3-10.

1.52 m from the End Support Gauge Distribution
6 Total Gauges

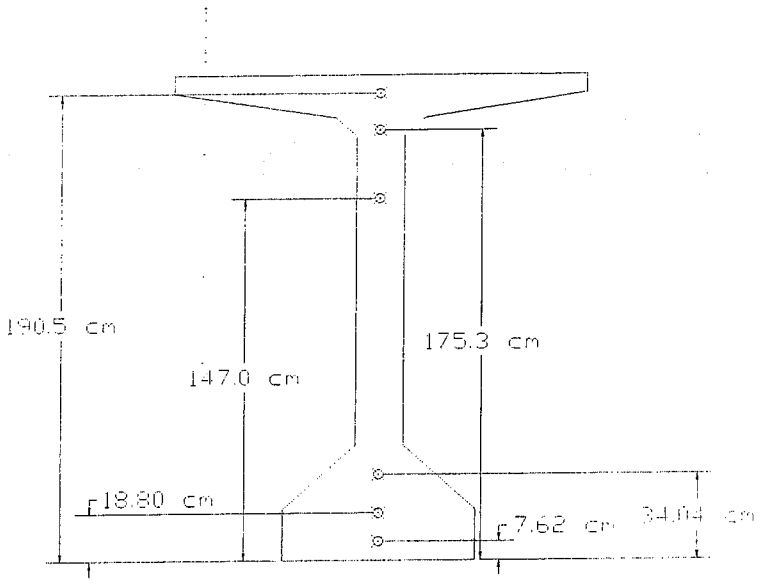

Figure 3-10 Gauge distribution for Beams 1 and 4 at 1.52 m away from the support

3.4.2 Slab Instrumentation

A continuos slab of 20.32 cm (8 in) was placed over the girders of the bridge. The continuity of the slab spans between three-span units. Due to slab continuity, significant location placement of strain gages must be made. Points near the maximum positive and at the maximum negative moments are of importance. Gage instrumentation at the mid-span and the support region were used. Strain gages at the mid-span are used to allow complete stress distribution to be obtained across the entire depth of the composite section. Strain placement at the support was equally as important. A thorough study of

the slab behavior at the maximum negative moment is essential. Depths at various locations were used for gage instrumentation also.

In the slab gage placement, both longitudinal and perpendicular stresses were of importance. Applied moment on the slab cause stresses in both longitudinal and perpendicular directions. Gages were placed at different depths. Studying the behavior of the section at the bottom of slab and centroid of the slab were considered to be a meaningful task. Hence a strain gage was placed at 0 cm from the bottom of the slab. This point represents the interface of the slab and the girder. It is going to be interesting to determine the true behavior at the interface of a simply supported girder and a continuous slab. The other strain gages were placed at a depth of 10.16 cm (4 in) which is at the centroid of the slab. This point provides a good representation of the slab behavior. These slab gage locations and depth can be clearly seen in Figure 3-11. Table 3-2 shows the detailed information about the slab gage placement.

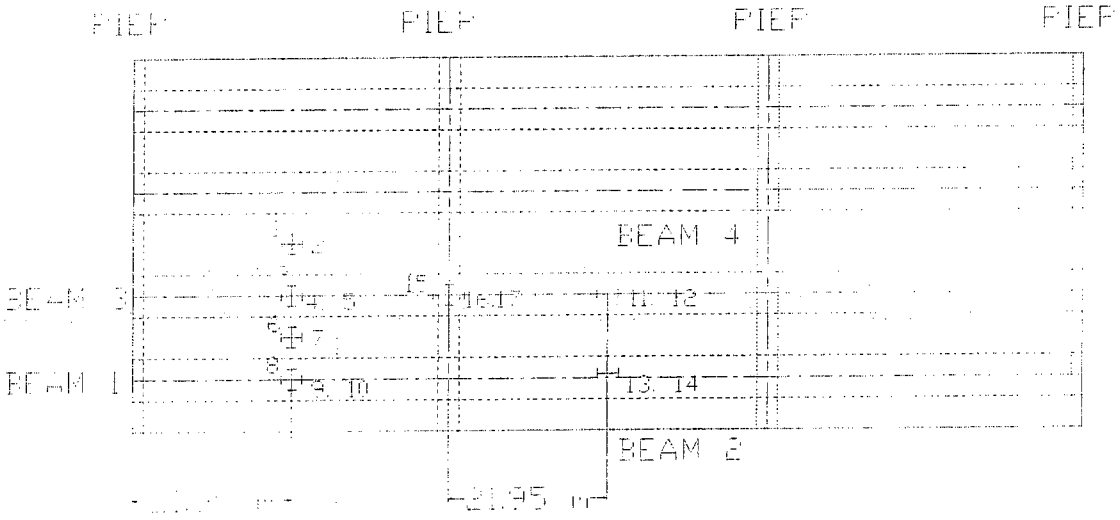

Figure 3-11 Slab gauge distribution for Westbound Gandy Bridge.

Table 3-2 Detailed information about composite slab gauges.

Slab Gauge #	Depth (measured from top of beam)		Location	Orientation (with respect to beam direction)
1	7.62 cm	3.0 in	Midspan of Slab between Beam 3 and North Beam	Perpendicular
2	10.16 cm	4.0 in	Midspan of Slab between Beam 3 and North Beam	Parallel
3	11.43 cm	4.5 in	Midspan of Beam 3	Perpendicular
4	10.16 cm	4.0 in	Midspan of Beam 3	Parallel
5	1.27 cm	0.5 in	Midspan of Beam 3	Parallel
6	13.97 cm	5.5 in	Midspan of Slab between Beam 1 and 3	Perpendicular
7	11.43 cm	4.5 in	Midspan of Slab between Beam 1 and 3	Parallel
8	10.80 cm	4.25 in	Midspan of Beam 1	Perpendicular
9	10.16 cm	4.0 in	Midspan of Beam 1	Parallel
10	2.54 cm	1.0 in	Midspan of Beam 1	Parallel
11	10.16 cm	4.0 in	Midspan of Beam 4	Parallel
12	0.76 cm	0.3 in	Midspan of Beam 4	Parallel
13	12.7 cm	5.0 in	Midspan of Beam 2	Parallel
14	1.27 cm	0.5 in	Midspan of Beam 2	Parallel
15	13.97 cm	5.5 in	At support between Beam 3 and 4	Perpendicular
16	12.7 cm	5.0 in	At support between Beam 3 and 4	Parallel
17	1.27 cm	0.5 in	At support between Beam 3 and 4	Parallel

CHAPTER 4

PRE-STRESS LOSSES AND TIME-DEPENDENT CONCRETE BEHAVIOR

4.1 Introduction

As described in chapter one, the initial tensile force applied to the strands and transferred to the concrete as a compressive force undergoes some losses. There are two methods of estimating these losses. One is the lump sum method; this method is widely used in civil engineering. Its main objective is defining the total loss. The lump sum method represents the losses as one value since the application of jacking stress. The other method is the detailed calculation of the various components of the total pre-stress loss. A full understanding and detailed calculation of all the components of the loss is performed and summed in order to compute the total pre-stress loss. The objective of this chapter is to elucidate the various equations incorporated into this study in order to capture the pre-stress concrete behavior. Since one of the main purposes of this study is the computation of time dependent pre-stress loss, it is very important to also show the effect of the pre-stress loss on the pre-stressed member behavior. A more detailed discussion on the pre-stressed concrete losses is discussed in the following section.

4.2 Total Pre-Stress Loss

AASHTO lump sum losses for the different types of pre-stressing steel is presented in Table 4-1. They depict the total pre-stressing loss in terms of one value. These values do not show any of the contribution of the various elements that make up the total pre-stressing loss. In order to apply Table 4-1 on any project, the design must meet some criteria. These lump sum values are applicable only under standard conditions of loading, types of concrete, construction procedures, and environmental conditions. The use of these lump-sum values in design does not allow for the inclusion of the time-dependency of the concrete behavior directly.

Table 4-1 AASHTO LUMP SUM LOSSES

Types of Pre-stressing Steel	Total loss fc' = 4000 psi (27600 KN/m^2)	fc' = 5000 psi (34500 KN/m^2)
Pre-tensioning strand		45000 psi (310000 KN/m^2)
Post-tensioning Wire of strand	32000 psi (220000 KN/m^2)	33000 psi (228000 KN/m^2)
Bars	22000 psi (152000 KN/m^2)	23000 psi (159000 KN/m^2)

Another method of computing pre-stress losses presented is the detailed method. Unlike the simple lump sum estimate of the pre-stress losses, this method involves the

computation of each element of the total loss. The summation of the various elements of the total pre-stress loss can be expressed in one simple equation.

$$\Delta fp_T = \Delta fp_{ES} + \Delta fp_R + \Delta fp_{CR} + \Delta fp_{SH} \quad (4.1)$$

Where Δfp_{ES} = the change in stress due to elastic shortening

Δfp_{PR} = the change in stress due to steel relaxation

Δfp_{CR} = the change in stress due to creep

Δfp_{SH} = the change in stress due to shrinkage

$\Delta f_{PR} = \Delta f_{PR}(t_o,t_{tr}) + \Delta f_{PR}(t_{tr},t_s)$

t_o = Time at jacking

t_{tr} = time at transfer

t_s = time at stabilized loss

This method which is time related starts with the first time interval between (t_o) and (t_{tr}) and so forth. One important aspect of equation (4.1) is the separation of instantaneous and time dependent losses. The instantaneous losses are elastic shortening and a part of the steel relaxation. Subtracting the instantaneous losses from the initial jacking stress results in the initial pre-stress as shown in the following equation.

$$fpi = fpj - \Delta fp_R(t_o,t_{tr}) - \Delta fp_{ES} \quad (4.2)$$

Where fpj = Pre-stress at jacking. In order to compute the actual amount of pre-stressed concrete loss, both instantaneous and time dependent losses should be calculated. In the subsequent sections of this chapter, instantaneous elastic shortening and time dependent pre-stress losses are discussed in more details.

4.3 Instantaneous Losses

Instantaneous losses are losses that occur immediately after transfer. The components of the instantaneous losses are dependent on the method of pre-stressing. In pre-tensioned sections, they consist of elastic shortening and initial steel relaxation. In post-tension, the instantaneous losses include elastic shortening, anchorage and frictional loss. Elastic shortening is a main component of pre-stress loss. In the following section, elastic shortening will be explained in further details.

4.3.1 Elastic Shortening

The transformation of stresses from the steel tendons to the concrete in the members results in some longitudinal deformation. This deformation is known as the elastic shortening of the member. It is defined through the following equations:

$$\varepsilon_{ES} = \frac{f_c}{E_c} = \frac{P_i}{A_C * E_c} \tag{4.3}$$

In the case of pre-tensioned concrete, it is commonly assumed that the application of the strands' stress to the concrete section takes place at one time. At that instantaneous time, some initial loss in stress occurs. This loss in pre-stress at that initial time is termed the elastic shortening loss. The following equation expresses the relationship between the change in stress and elastic shortening.

$$\Delta fp_{ES} = \varepsilon_{ES} * E_S = n * f_{CS} \tag{4.4}$$

$$n = \frac{E_S}{E_C} \tag{4.5}$$

$$f_{CS} = \frac{P_i}{A_C} \tag{4.6}$$

The instantaneous pre-stress loss value is an essential component in pre-stress concrete design. The total pre-stress loss consists of both instantaneous and time dependent pre-stress loss. The time dependent losses consist of various components. The separation of these components is of major importance in this study. The time dependent pre-stress loss and its separate components will be discussed next.

4.4 Time Dependent Pre-stress Loss

Time dependent pre-stress loss embodies inter-related components. These components consist of creep, shrinkage and steel relaxation. Interest for accurate calculation of the various components has grown lately in the area of pre-stress concrete design. Various institutes have realized the importance of separating the various components of pre-stress loss. In the subsequent sections the methods of the PCI and ACI for determining the time-dependent pre-stress loss will be presented.

4.5 Zia-PCI Committee Approach

The PCI committee[3] has studied and researched time dependent losses. Stress loss was put to the test in some pre-tensioned and post-tensioned specimens. The

different components of losses were expressed and will be shown later in this chapter. These losses were done with respect to time. Each component of the total pre-stress loss was expressed in a way to capture its time progression within the members. This method of computing losses with respect to time allows engineers to better depict the various critical stages of the structure's life. Some of the different stages of significance in the concrete structure's existence are as follows: The first stage is at the time of pre-stressing; the second stage is when additional weight (Superimposed dead loads and live loads) is imposed on the concrete member; the third stage is the behavior of the member between the preceding stages expressing the time-dependent behavior and; the last stage is up to the end of the service life.

4.5.1 Loss Due to Creep of Concrete

Loss due to creep is explained in chapter one and mathematically defined in this simple equation:

$$CR = (UCR)(SCF)(MCF)*(PCR)(f_c') \tag{4.7}$$

Where f_c is the compressive stress of concrete at a specific time period.

- Ultimate loss due to creep of concrete (UCR):
- UCR for moist cure not exceeding 7 days is shown in the following equation:

$$UCR = 95 - 20 * Ec / 10^6 \geq 11 \tag{4.8}$$

- Size and shape factor (SCF) is computed experimentally resulting in different factors depending on various volume to surface area ratios. Table 4-2 shows some of these findings.

Table 4-2 SCF for the various Volume to surface areas ratios.

Volume to surface area ratio	SCF
1	1.05
2	0.96
3	0.87
4	0.77
5	0.68
>5	0.68

- Effect of age at pre-stress and length of cure (MCF)

The creep factor (MCF) is affected by both the age of the concrete when the pre-stressing force is transferred and by the curing time of concrete in days. Table 4-3 shows some of these values.

Table 4-3 Creep factors for various ages of pre-stress and periods of cure.

Age at pre-stress Transfer, days	Period of cure days	Creep factor MCF
3	3	1.14
5	5	1.07
7	7	1.00
10	7	0.96
20	7	0.84
30	7	0.72
40	7	0.60

- Variation of creep with time (AUC):

Table 4-4 shows some of these variations. These creep variations depend on the time after pre-stress transfer. For any specific day in between the listed days on this Table, Linear interpolation may be used.

Table 4-4 Variation of creep with time (AUC)

Time after pre-stress Transfer, days	Portion of ultimate Creep, AUC
1	0.08
2	0.15
5	0.18
7	0.23
10	0.24
20	0.30
30	0.35
60	0.45
90	0.51
180	0.61
365	0.74
End of Service life	1.00

- Amount of Creep over each time interval (PCR):

In order to account for the time interval change of ultimate creep PCR, equation (4.9) should be used. AUC can be achieved from Table 4-4.

$$PCR = (AUC)_t - (AUC)_{t-1} \tag{4.9}$$

4.5.2 Loss Due to Shrinkage

Shrinkage as defined in chapter one is the loss of excess water in concrete members. This loss of water occurs as time progresses. Its effect is higher at the early age of the concrete and diminishes as the concrete ages. This relation is due to the fact that as concrete ages there is less excess water since most of it would have already evaporated.

$$SH = (USH) * (SSF) * (PSH) \tag{4.10}$$

- Ultimate loss due to shrinkage of concrete (USH):

For normal weight concrete USH is defined to be the following equation:

$$USH = 27{,}000 - 3{,}000 * \frac{E_C}{10^6} \geq 12{,}000 psi \tag{4.11}$$

For normal lightweight concrete USH is defined to be the following equation:

$$USH = 41{,}000 - 10{,}000 * \frac{E_C}{10^6} \geq 12{,}000 psi \tag{4.12}$$

- Effect of size and shape of the concrete member (SSF):

Size and shape factor is a major component of the shrinkage value. Bigger concrete members posses more water which lead to more water evaporation. On the other hand, smaller surface areas enable the concrete member to contain more water for a longer time period before it evaporates. Therefore, as the member's volume to surface ratio increases, the SSF will decrease leading to a decrease in the amount of shrinkage loss. This relationship can be observed in Table 4-5.

Table 4-5 Volume to Surface Area Ratio vs. SSF

Volume to Surface Shrinkage factor Ratio, in.	SSF
1	1.04
2	0.96
3	0.86
4	0.77
5	0.69
6	0.60

- Amount of shrinkage over each time step (PSH):

As time progresses excess water evaporates. Water evaporation is dependent on many factors as explained in chapter one. One of which is time. Every day some amount of water leaves the concrete. The rate at which water escapes the concrete's composition decreases with time making excess water diminish. PSH is the difference in the variation of shrinkage between sequential time periods. The following equation shows the relationship between the variation of shrinkage with time and amount of shrinkage over each step.

$$PSH = (AUS)_t - (AUS)_{t-1} \tag{4.13}$$

Values for the variation of shrinkage with time are shown in Table 4-6. Linear interpolations may be used for the unlisted values.

Table 4-6 Time after end of curing vs. portion of ultimate shrinkage

Time after end of curing, days	Portion of ultimate shrinkage, AUS
1	0.08
3	0.15
5	0.20
7	0.22
10	0.27
20	0.36
30	0.42
60	0.55
90	0.62
180	0.68
365	0.86
End of Service life	1.00

4.5.3 Loss Due to Steel Relaxation (RET)

Along with some of the factors that affect steel relaxation such as the initial pre-stressing force and elongation time is the type of strand used. The type of steel used affects the magnitude of steel relaxation. For any type of steel, tensioned steel tends to relax with time. As time progresses, this relaxation reduces the initial pre-stressing force. In looking at the following steel relaxation equations, it becomes apparent that the steel relaxation is a function of various factors. Among these factors are time, initial stress of steel, and the stress at a specific time.

For stress relived steel, RET is computed using the following equation:

$$RET = \frac{f_{St}[\log 24t - \log 24t_1]}{10} * (\frac{f_{St}}{f_{py}} - 0.55) \qquad (4.14)$$

Where

$$\frac{f_{St}}{f_{py}} - 0.55 \geq 0.05$$

$$f_{py} = 0.85 * f_{pu}$$

For low-relaxation Steel, time dependent loss due to steel relaxation is computed using the following equation:

$$RET = \frac{f_{St}[\log 24t - \log 24t_1]}{45} * (\frac{f_{St}}{f_{py}} - 0.55) \quad (4.15)$$

Where

$$\frac{f_{St}}{f_{py}} - 0.55 \geq 0.05$$

$$f_{py} = 0.90 * f_{pu}$$

4.6 Implementation of the PCI Approach in the Gandy Bridge Project

In previous research done at the University of Central Florida[8], codes' implementation in the Gandy Bridge Project did not account for the time dependency of pre-stress losses. It is vital in this study that field obtained pre-stress loss is compared to code findings that account for time-dependency. The PCI committee's research on time-dependent pre-stress loss captures the very same idea of this study. Its main purpose was to investigate the magnitude of the contributions of the various components of time dependent loss. In order to use the tables presented earlier on creep, shrinkage, and steel relaxation for any structure, many aspects about the design of the structure should be

known. Some of the most important aspects for calculating the various components of time dependent pre-stress losses are the type of concrete, curing time, weight, volume to surface ratio, and age of concrete at pre-stress transfer. In this study, These are available in the design report of the Gandy Bridge Project[11]. These values were computed for Beams 1 and 4 in this study, and are listed below.

- V/S = 3.7275 which results in SCF of 0.79725 and SSF = 0.794525
- Age at pre-stress transfer = 5 days & period of cure = 5 days. These value give an MCF value of 1.07
- Values of the ultimate creep and shrinkage vary with time. These values were computed from Table 4-4. Ages such as 4, 14, 28 days and so forth were not mentioned in the tables. Linear interpolation was used for their calculation.

In the previous work at the University of central Florida on pre-stress losses[8], it was determined that values of losses are not only dependent on time but also on the location within the depth of the concrete girder. As explained in chapter one, there were different strain gages placed at different depths of the concrete girders. The strain gage readings that have been collected throughout this project was carefully studied, and pre-stress losses for different gages were deduced. Plots of the pre-stress losses for the various depths will be shown and discussed in the next chapter.

4.7 ACI Committee 209 Approach

ACI Committee 209 considers time-dependent pre-stress losses in its approach also[6]. It divides losses into several categories. The ones of most concern for this study are the time dependent losses for a pre-tensioned element. These losses are creep, shrinkage and steel relaxation. Computation of each time dependent pre-stress loss component was done using the ACI suggested formulas. The ACI formulas that were used in this study were done to depict the stress losses in the members with respect to both time and location. In comparison between the use of both ACI and PCI equations, both methods were done to capture the pre-stress loss with respect to time, location and depth.

4.7.1 Losses Due to Creep

Creep is the deformation of the concrete member or flow of materials in the lateral direction due to longitudinal stress. Creep coefficient can be easily obtained from equation (4.15). In this equation the amount of ultimate creep is taken as the ratio of creep strain to the elastic strain.

$$Cu = \frac{\varepsilon_{CR}}{\varepsilon_{EL}} \tag{4.16}$$

Time is an important determinant of creep. In order to find the amount of creep at different times, the magnitude of ultimate creep is multiplied by a time factor. Equation (4.17) illustrates the relation between creep at a specific time period and ultimate creep.

$$C(t) = \frac{t^{0.6}}{(10 + t^{0.6})} * C_u \tag{4.17}$$

An average value of ultimate creep suggested by the ACI code is 2.35. Once the creep coefficient at any date is known, the loss in pre-stress due to creep can be computed. The change in the magnitude of pre-stress in a bonded member due to creep is the multiplication of the creep coefficient at a specific day by both the ratio of the modulus of elasticity of steel to concrete and by the stress of the concrete at the steel level. The following equation illustrates the method of computing the change in stress due to creep.

$$\Delta fp_{CR} = \frac{C_t * E_{PS}}{E_C} * f_{CS} \tag{4.18}$$

Where f_{CS} is the stress in the concrete at the level of the tendons' centroid.

4.7.2 Losses Due to Shrinkage

ACI 209 R- 92 findings on shrinkage play an important role in pre-stress concrete design. One of its findings was that 80 % of this loss occurs in the first year. Another was that the average ultimate shrinkage strain in both moist and steam-cured concrete was given as 780 * 10^{-6} in/in. This value is affected by many important components. Some of the components are the length of initial moist curing, ambient relative humidity, volume to surface ratio, temperature, and properties of concrete mixture. In order to

account for all these components, a correction factor is used to multiply the ultimate shrinkage value as shown in the following equation.

$$\varepsilon_{SH} = 780 * 10^{-6} \gamma_{SH} \quad (4.19)$$

Adjustment to the ultimate shrinkage equation to reflect the losses as a function of time can be obtained from two different equations:

One is for moist curing in seven days, as shown in the following equation:

$$\varepsilon_{SH} = \frac{t}{35+t} * (\varepsilon_{SH})_U \quad (4.20)$$

The other is for steam curing after one to three days, as shown below:

$$\varepsilon_{SH} = \frac{t}{55+t} * (\varepsilon_{SH})_U \quad (4.21)$$

4.7.3 Loss Due to Steel Relaxation

In pre-tensioned concrete, the steel tendons are under constant elongation. As time progresses the magnitude of the stress in the steel decreases. This stress reduction is dependent on the elongation time, the initial pre-stressing force and the type of tendons used as discussed in chapter one. The ACI code limits the tensile stress in the tendons as shown below.

- At jacking, the jacking force $f_{pj} = 0.94\ f_{py}$, but not greater than the lesser of $0.80\ f_{pu}$ and the maximum value suggested by the manufacturer.
- At pre-stress transfer, $f_{pi} = 0.94\ f_{py}$, but not greater than $0.74\ f_{pu}$.

ACI uses the following equation to find the steel relaxation loss.

$$\Delta f_{PR} = [K_{re} - J\,(f_{pES} + f_{pCR} + f_{pSH})] * C \qquad (4.22)$$

Where Kre, J, and C values are given in Tables 4-7 and 4-8.

Table 4-7 Values of C

Fpi /fpu	Stress-relieved Strand or wire	Stress-relieved bar or Low-relaxation Strand or wire
0.80		1.28
0.79		1.22
0.78		1.16
0.77		1.11
0.76		1.05
0.75	1.45	1.00
0.74	1.36	0.95
0.90	0.73	1.27
0.72	1.18	0.85
0.71	1.09	0.80
0.70	1.00	0.75
0.69	0.94	0.70
0.68	0.89	0.66
0.67	0.83	0.61
0.66	0.78	0.57
0.65	0.73	0.53
0.64	0.68	0.49
0.63	0.63	0.45
0.62	0.58	0.41
0.61	0.53	0.37
0.60	0.49	0.33

Table 4-8 Values of Kre and J

Type of tendons	K_{RE}	J
270 Grade stress-relieved strand or wire	20,000	0.15
270 Grade stress-relieved strand or wire	18,500	0.14
240 or 235 grade stress-relieved wire	17,600	0.13
270 Grade low-relaxation strand	5,000	0.040
250 Grade low-relaxation wire	4,630	0.037
240 or 235 Grade low-relaxation wire	4,400	0.035
145 or 160 Grade stress-relieved bar	6,000	
0.05		

4.8 Implementation of the ACI-209 Approach in the Gandy Bridge Project

The implementation of the ACI equations to the Gandy Bridge project was done for this study. The various components of pre-stress losses were computed. In the process of calculating those components of pre-stress losses, various design specifications were needed. Some of the design specification that played a role in the computation of losses were the type of tendons, the curing time and the ratio of the initial to the ultimate pre-stressing force.

4.9 Concrete Stress Computation in Pre-stressed Members

The concrete stress in any pre-stressed member can be divided into three components. The sum of all three, $f_{PRE\text{-}STRESS} + f_{WEIGHT} + f_{COMPOSITE}$, equals the total concrete stress in the member. $f_{PRE\text{-}STRESS}$ is the stress caused by the pre-stressing element. The transfer of the strand applied force to the concrete causes the concrete member to have stress variation within the depth of the concrete member. Due to eccentricity of the strands, the stress caused by the strands on the concrete member counteracts the other stresses on the same element. $f_{WEIGHT} + f_{COMPOSITE}$ are the stresses due to the weight and composite loads respectively. The dead load stress of the member causes the member to be in compression at top and tension at the bottom. The following equation shows the summation of the various components of stress in the girders.

$$f_c = f_{PRE\text{-}STRESS} + f_{WEIGHT} + f_{COMPOSITE} \tag{4.23}$$

$$f_{PRE-STRESS} = \frac{P_e}{A_c} * (1 - \frac{e_{STEEL}(e_{STEEL} - C_2)}{r^2}) \qquad \text{Depth} \geq c2 \tag{4.24}$$

$$f_{PRE-STRESS} = \frac{P_e}{A_c} * (1 + \frac{e_{STEEL}(C_2 - e_{STEEL})}{r^2}) \qquad \text{Depth} < c2$$

$$f_{WEIGHT} = -12 * (D - C_2) * \frac{M_{BEAM}}{I_{BEAM}} \qquad \text{Depth} \geq c2 \tag{4.25}$$

$$f_{WEIGHT} = 12 * (C_2 - D) * \frac{M_{BEAM}}{I_{BEAM}} \qquad \text{Depth} < c2$$

$$f_{COMPOSITE} = -12 * (D - C_2) * \frac{M_{COMP}}{I_{COMP}} \qquad \text{Depth} \geq c2 \tag{4.26}$$

$$f_{COMPOSITE} = 12 * (C_2 - D) * \frac{M_{COMP}}{I_{COMP}} \qquad \text{Depth} < c2$$

4.10 Camber and Deflection of Concrete Members

Due to the eccentricity of pre-stressing strands in the pre-stress concrete members, the initial pre-stressing force applied causes a negative deflection, i.e., camber, which produces a convex upward surface. In bridge design inadequate adjustment for camber values may cause uneven ridding surfaces and construction problems. The initial pre-stressing force decreases with time due to time dependent pre-stress losses causing its contribution to the initial magnitude of camber to decrease as well. On the other end of the spectrum, there is deflection. The weight of the concrete members, the superimposed dead load and life load cause the structure to deflect. A large magnitude of deflection is as undesirable as a large amount of camber. Computation of camber and deflection at different stages of construction and the structure's life is essential. In this study, the Approximate Time-Steps Method is used for calculating both positive and negative deflections as a function of time.

4.11 Approximate Time-Steps Method

The Approximate Time-Steps Method[10] is simplified to deal with the various time-dependent factors that make up the total deflection. These time-dependent factors

were mentioned earlier in this chapter and will be discussed in more details in this section in the context of camber and deflection. The summation of all these factors result in the total deflection which is achieved through the following equation for non-composite sections:

$$\delta_T = \delta_p [1-\Delta p/p_o + (1-\Delta p/2p_o)(k_r C_t)] + \delta_D [1+ k_r C_t] + \delta_{SD} [1 + K_a k_r C_t] + \delta_L \qquad (4.27)$$

Equation (4-27) consists of four different portions. The first portion is δ_p, which is the camber caused by pre-stressing alone. The second is, δ_D, the deflection caused by the dead load. The third is, δ_{SD}, the deflection caused by the super-imposed dead load. And the last is, δ_L, the deflection due to live load. The upward errors in equation (4.27) represent camber, while the downward errors represent deflection. In Chapter 6 of this report, more detailed information will be presented, regarding the implementation of this Time-Steps Method by accounting for composite action. The following two sections deal with both camber and deflection separately.

4.11.1 Camber

The method used to compute the amount of camber caused by pre-stressing involves the stresses and strains of the top and bottom of the girder. The eccentric compressive force applied to the concrete section causes different stresses at the upper

and lower part of the section. These stresses are used to calculate the camber of the girders at various depths.

The required sets of concrete stress equations can be calculated using the effective top and bottom stresses at various times. Since loss is a time dependent factor, the effective pre-stressing force must have that characteristic as well. As time progresses, the amount of loss increases leading to a decrease in the effective pre-stressing force. This decrease affects the behavior of the concrete section. Any effective pre-stress force miscalculations will result in different values for the top and bottom stresses of the section. In order to compute these stresses, the section properties must be known. Equations used to compute the stresses at both top and bottom at the mid-span are as follows:

$$f_{TOP} = \frac{-P_e}{A_c} * (1 - \frac{e_{STEEL} * C^t}{r^2}) \tag{4.28}$$

$$f_{BOT} = \frac{-P_e}{A_c} * (1 + \frac{e_{STEEL} * C_b}{r^2}) \tag{4.29}$$

Equation (4.28) and (4.29) depict the stresses due to the compressive stress from the steel alone and not the stresses due to the weight of the concrete section.

The top and bottom stresses are also calculated at the support section yielding almost identical equations. The following equations capture the top and bottom stresses at the end section.

$$f_{TOP} = \frac{-P_e}{A_c} * (1 - \frac{e_e * C_t}{r^2}) \tag{4.30}$$

$$f_{BOT} = \frac{-P_e}{A_c} * (1 + \frac{e_e * C_b}{r^2}) \quad (4.31)$$

The main difference between the mid-span and support pre-stress equations is the depth of the steel centroid, e_{steel}. Since a combination of straight and double depressed steel strands were used in this project, the distance to the steel centroid differs at both the mid-span and ends of the section.

The stresses at the top and bottom are then divided by the time dependent modulus of elasticity resulting in the extreme fiber strains ε_c^t, ε_{cb} and ε_e^t, ε_{eb}. The following equations show the computation of the concrete strains at both the mid-span and support respectively.

At mid-span:

$$\varepsilon_c{}^t = \frac{f_c{}^t}{E_c} \quad (4.32)$$

$$\varepsilon_{Cb} = \frac{f_{Cb}}{E_c} \quad (4.33)$$

At support:

$$\varepsilon_e{}^t = \frac{f_e{}^t}{E_c} \quad (4.34)$$

$$\varepsilon_{eb} = \frac{f_{eb}}{E_c} \quad (4.35)$$

Assuming the distribution of the strain across the depth of the section is linear, the curvature can be computed from the following equations:

$$\phi_c = \frac{\varepsilon_{cb} - \varepsilon_c^{t}}{h} \tag{4.36}$$

$$\phi_e = \frac{\varepsilon_{eb} - \varepsilon_e^{t}}{h} \tag{4.37}$$

Computing the magnitude of camber is done using equation (4.38) or (4.39). These equations depict the calculation of camber based on the curvature in the concrete. The amount of curvature of the section at both mid-span and support is a major factor in this equation. Another factor that affects camber is the profile of the steel in the concrete member. Different equations are used to account for the profile of steel in the concrete member. Equation (4.38) represent the magnitude of camber based on a double-depressed pre-stress beam. While equation (4.39) shows the camber magnitudes for a straight pre-stress concrete section.

$$\delta_i \uparrow = \phi_c \frac{L^2}{8} + (\phi_e - \phi_C) * \frac{a^2}{6} \tag{4.38}$$

$$\delta_i \uparrow = \phi_c \frac{L^2}{8} \tag{4.39}$$

Where L is the length of the section and a is the distance from the support to the first depressed point. The implementation of this equation for the Gandy Bridge with doubly depressed and straight strands is discussed in chapter 6.

4.11.2 Deflection

Computation of the amount of deflection is divided into three parts. All three parts cause the girders to deflect downwards. The first downward deflection is based on weight of the girder itself, the second is the deflection due to the superimposed dead and additional weight and the third is based on the live load. All three components of the downward deflections should be computed separately.

In a simple span bridge, the dead load contributions of deflection are computed using the same formula. This formula is affected by the time-dependent modulus of elasticity and moment of inertia along with the weight of the girder and the length of the span. The following equation was used to compute the magnitude of the various attributes to dead load deflection:

$$\delta = \frac{5 * W * L^4}{384 * E_c * I_g} \tag{4.40}$$

If the magnitude of camber from pre-stressing is higher than the magnitude of deflection, the member cambers up. On the other hand, if the last statement was the opposite the member will deflect down.

Chapter 5

MEASURED VS. CODE'S PRE-STRESS LOSS

5.1 Introduction

A great deal of strain measurements was obtained from the strain gages embedded into the girders of the Gandy Bridge. During this Project, strain measurements were studied at various times. Some of which included, the initial days of the project, the application of the superimposed dead load, one-year from casting, along with some other intermediate days. For each day, strain and temperature readings were collected for different hours. The hours that reflected the most reasonable and consistent samples of measurements were chosen for this study. The entire display of the specific days and hours selected for this study can be seen in Table 5-1. From the strain readings achieved for the various days of interest, time dependent pre-stress losses were calculated after correcting for temperature effects both locally and globally. Local temperature corrections involved gage corrections specified by the manufacturer, while the global one included correction from expansion and contraction of the concrete for each time interval in the girders. The various components of time-dependent pre-stress loss were then determined from these measurements, and compared with pre-stress loss from various codes. Numerous plots were made to determine the difference between various findings.

The Time-Dependent nature of the measured loss values were compared with those obtained from time dependent approaches of Zia-PCI[3] and ACI Committee 209[6].

5.2 Factors Effecting Pre-stress Loss

There are various factors that effect pre-stress loss. Among these factors are weather conditions, member shape and properties of the material composition. Relative humidity has a major effect on the amount of pre-stress loss. Under very humid conditions, the amount of water evaporation from the concrete member may be very small. Volume to surface ratio is a factor affecting the amount from water loss of the section also. Time is a major factor as well, and plays a significant role in pre-stress loss determination. The various times in days selected were introduced in the preceding section. Due to changes in the concrete as time progresses, the material property of the section undergoes some alterations. Adjustment to the modulus of elasticity of the section must be applied to reflect this change with respect to time. In time step calculation of pre-stress losses, a specific value of the modulus of elasticity can not be used. In order to account for the change with time, the value of the modulus of elasticity should be calculated with respect to age of concrete. The following equation depicts the modulus of elasticity as a function of time[12].

$$E_c(t) = \left[e^{[s(1-(\frac{28}{t})^{0.5})]} \right]^{\frac{1}{2}} * E_c(28) \qquad (5.1)$$

S = coefficient factor depending on the type of cement = 0.2 for this project

The modulus of elasticity of concrete at 28 days for normal-weight concrete can be estimated by:

$$E_c(28) = 21{,}500 * (\frac{f_{cm}}{f_{cmo}})^{\frac{1}{3}} \tag{5.2}$$

f_{cmo} =10 Mpa

Table 5-1 Sample of the gauge and temperature measurements.

Age (Days)					Gage	Temp.
After Prestress	Concrete	Ec(t)	Date	Time	G7	T7
0			12/26/95	700	2512.7	48.078
0.125	5.125	3900.662	12/26/95	1000	2253.9	50.437
1	6	3970.377	12/27/95	1700	2120	60.052
2	7	4034.514	12/28/95	100	2118	53.048
3	8	4086.966	12/29/95	1600	2106.3	61.497
7	12	4229.709	1/2/96	1000	2030.2	67.576
14	19	4364.442	1/9/96	600	2023.4	35.565
28	33	4494.132	1/23/96	1000	1896.3	57.657
50	55	4588.417	2/13/96	1000	1819.6	48.04
60	65	4614.727	2/24/96	800	1781.3	66.682
90	95	4667.371	3/20/96	800	1734.6	55.934
120	125	4699.975	4/30/96	700	1629.6	69.985
150	155	4722.713	5/24/96	800	1603	78.557
180	185	4739.738	6/12/96	1200	1599.2	80.797
240	245	4763.961	8/21/96	0	1248.2	81.208
240	245	4763.961	8/21/96	600	1244.9	80.175
270	275	4773.008	9/6/96	1200	1237.7	85.928
300	305	4780.699	10/21/96	1200	1246.8	78.172
330	335	4787.341	11/20/96	0	1287.4	72.111
360	365	4793.154	12/13/96	0	1247	65.961
390	395	4798.298	01/14/97	600	1250.2	55.264

5.3 Total Pre-stress Loss deduced from Measured Data

The attained readings from the strain gages embedded in the girders contain several components. Temperature and weight effects are some of the components that

are included in the strain values achieved. In order to compute the change in the strain values due to pre-stress loss solely, strains due temperature and weight effect need to be separated from the achieved readings. Once these changes in strain values are computed, calculating the total pre-stress loss of the pre-stress element becomes an easy task. Through the following equations the computation of the change in both instantaneous and time dependent strains become more understandable.

$$\Delta\varepsilon_{\text{Instantaneous}} = \Delta\varepsilon_{\text{Total}} - \Delta\varepsilon_{\text{Temperature}} \tag{5.3}$$

$$\Delta\varepsilon_{\text{Time-Dependent}} = \Delta\varepsilon_{\text{Total}} - \Delta\varepsilon_{\text{Temperature}} - \Delta\varepsilon_{\text{Weight effect}} \tag{5.4}$$

The total change in strain, $\Delta\varepsilon_{\text{Total}}$, is determined from summing the product of the difference in the temperature readings and the manufacturer provided correction factor, to the difference in strain readings as shown in the following equation:

$$\Delta\varepsilon_{TOTAL} = (\varepsilon_t - \varepsilon_o) + (T_t - T_{t-1}) * 6.78 \tag{5.5}$$

As obtained from the strain gages shown in Table 5.1, (ε) is the strain reading in micro-strain and (T) is the temperature in degrees Fahrenheit. Subscripts such as (t) and (o) and (t-1) represent time. The subscript (t) is any time, (t-1) is the preceding time from (t) and (o) is the initial time or a reference time. The factor used in equation (5.5) is the coefficient of thermal expansion of the steel used for the vibrating wires in the strain gages.

From equation (5.3) the effect of the temperature change on the strain measurement was subtracted from the total change in the strain of the member. The temperature change at this stage of the data processing serves as the global temperature correction. In equation (5.4), the effect of both temperature and weight effect change on

the strain measurement were subtracted. The following equations show the method of computing both strain defiling components.

$$\Delta\varepsilon_{Temperature} = (T_t - T_{t-1}) * 5.5 \tag{5.6}$$

$$\Delta\varepsilon_{WIEGH-EFFECT} = \frac{f_{wieght-effect}}{E_{C(t)}} * 10^6 - \frac{f_{wieght-effect}}{E_{C(t-1)}} * 10^6 \tag{5.7}$$

In contrast with the instantaneous strain change, the time dependent strain is affected by the change in strain due to the weight effect. The change in strain due to weight effect is partially shaped by the time dependency of the modulus of elasticity and by the change in strain due to the weight. The main equation that is used to determine $\Delta\varepsilon_{Weight\ effect}$ is shown in equation (5.7). This equation captures the difference between the strain at a specific time and the strain at the proceeding time. $f_{WEIGHT-EEFECT}$ is the stress due to the self weight of the member. $Ec_{(t)}$ and $Ec_{(t-1)}$ are the modulus of elasticity of the concrete at a specific time and its preceding time respectively.

Once the change in strain due to global temperature effect is subtracted from the total strain, the instantaneous strain is known at the time of transfer of stress from the strands to the concrete member. The instantaneous pre-stress loss is then easily computed by the simple equation of multiplying the modulus of elasticity of the steel by the change in strain in the concrete member to achieve the change in stress in the steel. This is enabled by the assumption that the bond between the steel and the concrete is strong enough. For the time dependent losses, the strain due to weight effect should also be computed and subtracted from the total strain as well as the strain due to temperature. Therefore, in comparison to the method of computing the instantaneous loss, the method

of computing the time dependent pre-stress loss is the same, except for the addition of subtracting the change due to weight effect from the total strain. The equation used for expressing the pre-stress loss of the steel at any day is equal to the product of the change in the concrete strain and the modulus of elasticity of the steel as shown in equation (5.9).

$$\text{Pre-stress loss of steel} = \Delta\varepsilon * E_s \tag{5.9}$$

For the losses from field measurement, the instantaneous loss due to the initial steel relaxation is included along with the loss due to elastic shortening in what is referred to as the Immediate Loss. For the time dependent losses, one must note that instantaneous loss such as elastic shortening becomes the initial loss or reference benchmark used for reducing this portion of the data. In the following figures, the pre-stress loss is plotted at both mid span and at 1.52 m away from the support for both Beams 1 and 4.

Figure 5-1 shows the relationship between the pre-stress loss and depth of Beam 1 at the mid-span for various days (i.e. the apparent pre-stress loss). The loss is increasing from the top to the bottom of the girder. Pre-stress loss comparison of the AASHTO and ACI-PCI codes for various days considered in this project, such as 150, 240, and 390 days is depicted in this figure. The apparent slope of the pre-stress loss at 390 days is much steeper than at 150 days. This behavior of the section is expected. When additional weight is imposed on a pre-stressed section, some tensioning or less compression occurs at the lower part of the section allowing the steel to regain some of its stress. The codes' findings seem to be very conservative when studying the mid-

section of the beam, especially since close to 80 % of the loss is expected to have occurred in the 1st year.

Figure 5-2 shows the relationship between the apparent pre-stress loss and depth for Beam 4 at 1.52 m away from the support at specific days. Similar to the mid-section of Beam 1, the loss is increasing from the top to the bottom of the girders. However, at 1.52 m, the apparent slope of the apparent pre-stress loss distribution after the formation of the composite section is not necessarily steeper than for the girder itself. This is attributed to the beam acting as a simple beam at the supports with little or no moment effect from any additional superimposed load. The apparent pre-stress loss seems to be much closer to the codes' findings at the bottom of the girder in this case. It can be observed that the codes suggest a one value pre-stress loss across the section. The codes' losses are based on the maximum pre-stress loss of the section.

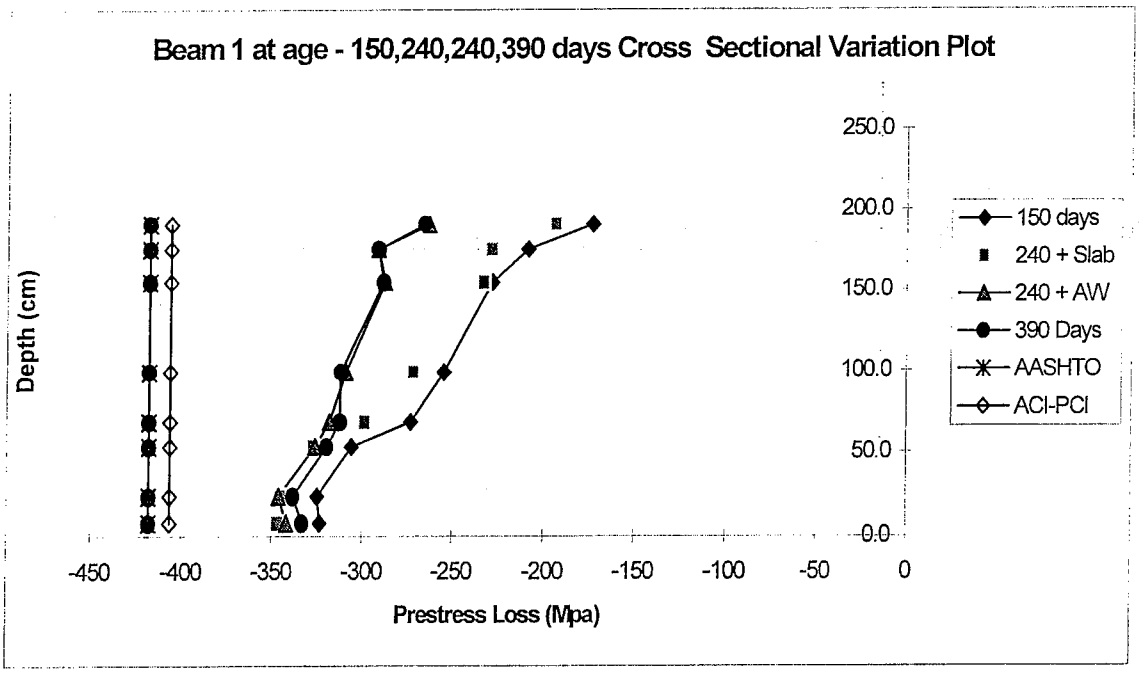

Figure 5-1: Apparent Pre-stress Loss Based on Strain Reading for Beam 1 at Mid-Span.

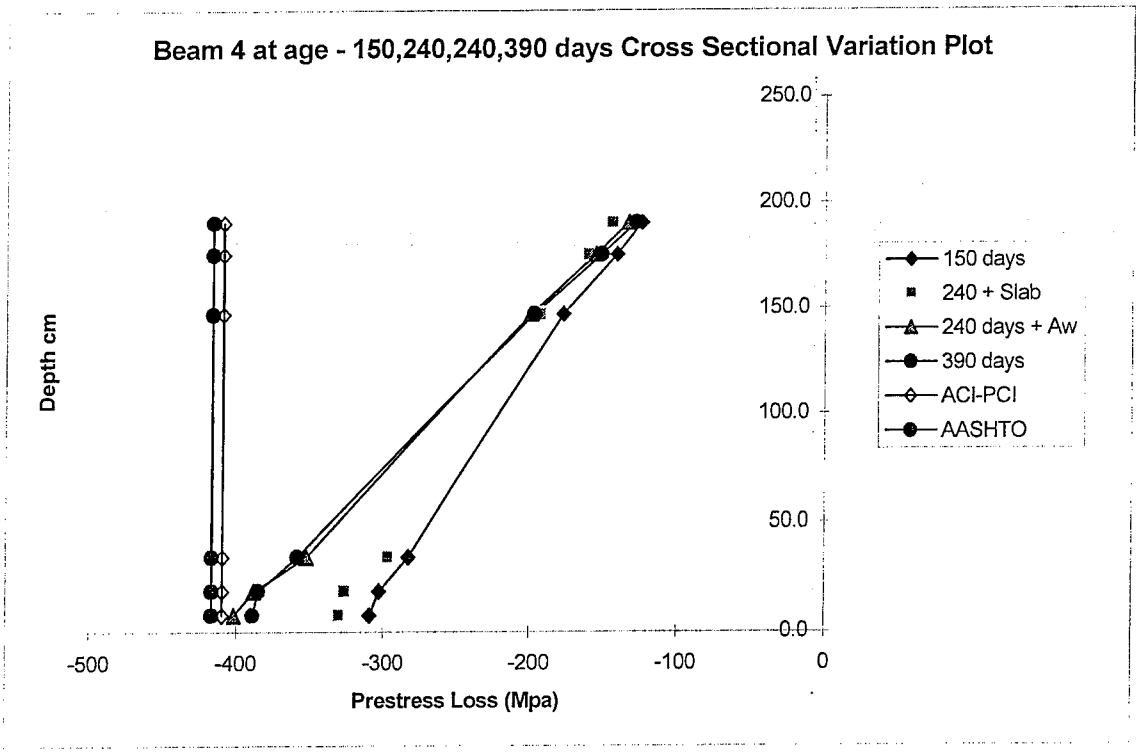

Figure 5-2: Apparent Pre-Stress Loss Based on Strain Reading for Beam 4 at 1.52m.

5.3.1 Ratio of Time-dependent Loss to Initial Pre-Stressing

The ratio of the effective pre-stress to the initial pre-stress is symbolized with letter R as shown in the following equation:

$$R = \frac{f_{pe}}{f_{pi}} \tag{5.10}$$

Where $f_{pe} = f_{pi} - loss$

Subtracting equation (5.10) from 1 will yield the ratio of the time-dependent pre-stress loss to the initial pre-stress. One must keep in mind that the initial pre-stress is equal to the jacking stress minus the immediate or instantaneous loss. Viewing this ratio in terms of a percentage allows structural engineers to better understand the amount of loss with respect to the initial pre-stressing force attributable to time-dependent effects. The following equation shows the transformation of equation (5.10) to depict the percentage of the time-dependent loss in any structural pre-stress member since the strands were cut:

$$1 - R = \frac{f_{pi} - f_{pe}}{f_{pi}} = \frac{loss}{f_{pi}} * 100\% \tag{5.11}$$

The implementation of the ratio of equation (5.11) into the sections of the Gandy Bridge is plotted in the subsequent figures. These ratios are computed across the various depths of the beam. Two specific days were selected for the study. The 150 and 390-day marks represent two significant stages in the project. At the 150-day mark, the slab and superimposed dead load were not yet a part of the bridge. At the 390-day mark, the

bridge included all superimposed dead loads. Along with the comparison between the two specific days of the project, comparison with the AASHTO and ACI-PCI code limitations is done for both figures.

Figure 5-3 represents the ratio of the apparent time-dependent loss to the initial pre-stressing at the mid-span of Beam 1. The marginal difference between the ratios at both days decreases from the top to the bottom of the member. At 150-days, the loss is increasing with depth. At 390-days, composite action had been applied causing the bottom portion to regain some of the losses hence, the loss decreases with depth.

Figure 5-4 represents the ratio of the apparent time-dependent loss to the initial pre-stressing of Beam 4 at 1.52m away from the support for various depths. The marginal difference between both days increases from the top to the bottom of the beam. At 390 days, the loss ratios at the lower part of the section are much higher than at the top. The value of the maximum ratio is 19.4 % and occurs at the lower part of this beam. In comparison with the mid-span of beam one, it is apparent that the ratios of losses to the initial pre-stressing are greater in the support region after the composite section is formed.

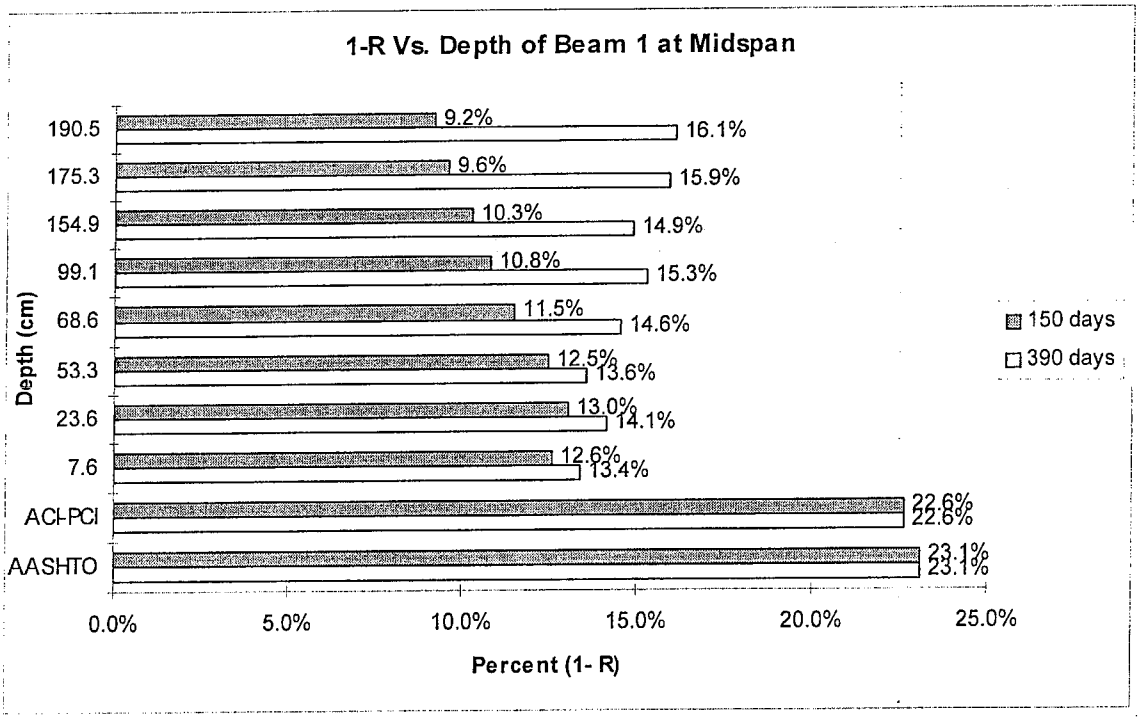

Figure 5-3: Apparent Pre-Stress Loss to initial Pre-Stressing ratio for Beam 1 at Midspan.

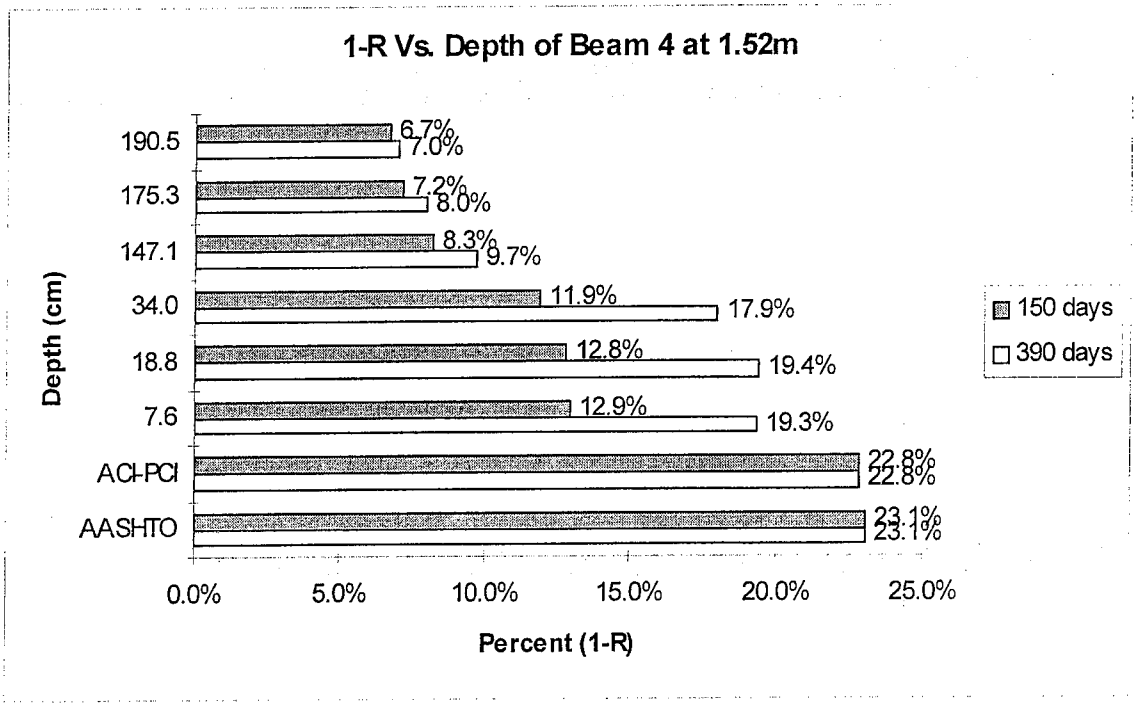

Figure 5-4: Apparent Pre-Stress Loss to initial Pre-Stressing ratio for Beam 4 at 1.52m.

5.3.2 Comparison of Actual Loss and TDL Ratios to the Various Code Estimates

Instantaneous loss plays a major role in the total pre-stress loss. The magnitude of the total loss is affected by both the instantaneous and the time-dependent contributions. Elastic shortening is one of the instantaneous components affecting the total pre-stress loss. The subtraction of the instantaneous loss enables us to capture the Time-Dependent Loss in these structural members. The major findings of both total and time-dependent losses are important; however, comparison of these values with various codes is necessary. Both these losses are divided by the code suggested values for total and time dependent losses respectively.

Figures 5-5 and 5-6 depict the percentage of total and time dependent loss at 390 days based on the codes' estimates for various depth of Beam 1 at the mid-span. The percentage is an indication of the amount of loss that occurred with respect to the code estimated values. For example, 90% of actual loss of the code estimate means that the actual loss is 90% of what the code suggested the loss to be for this specific member. From both figures, it is obvious that the code estimates for pre-stress losses are conservative. The closest actual loss to code estimate is 83.19 % where the closest TDL to code estimate is 74.75 %. On the other hand, comparison of percentage inconsistency when subtracting the elastic shortening leads to the conclusion that both the ACI and AASHTO codes underestimated the instantaneous losses and overestimated time dependent losses.

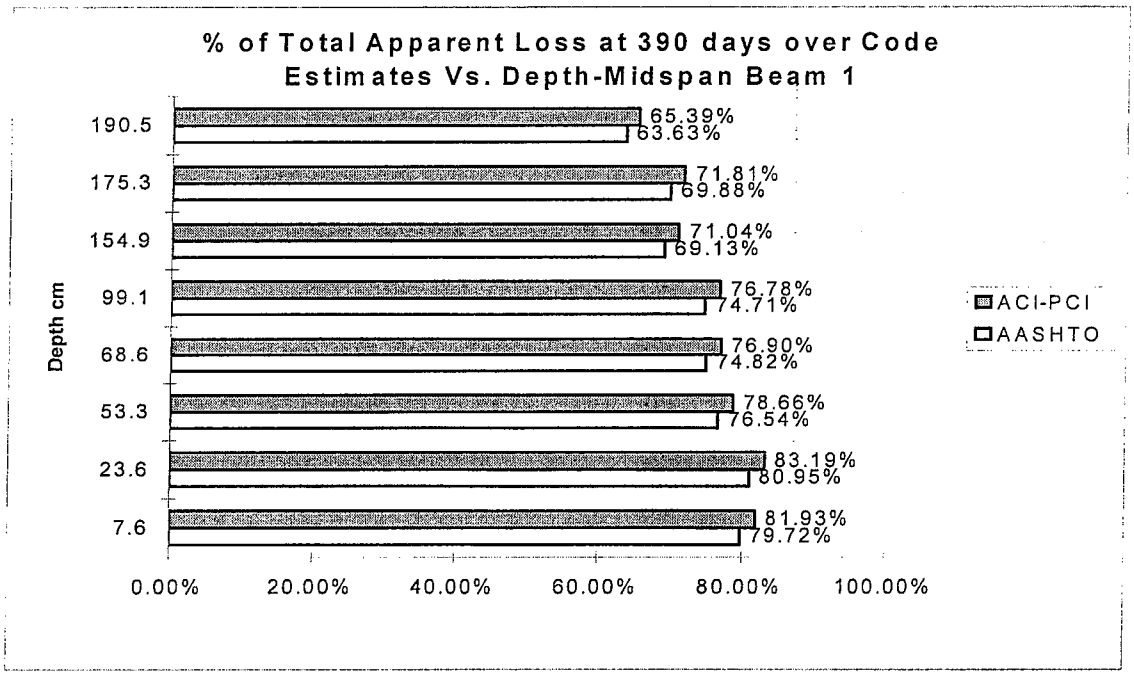

Figure 5-5: Ratios of Total Apparent loss to ACI-PCI and AASHTO of Beam One at Mid-Span.

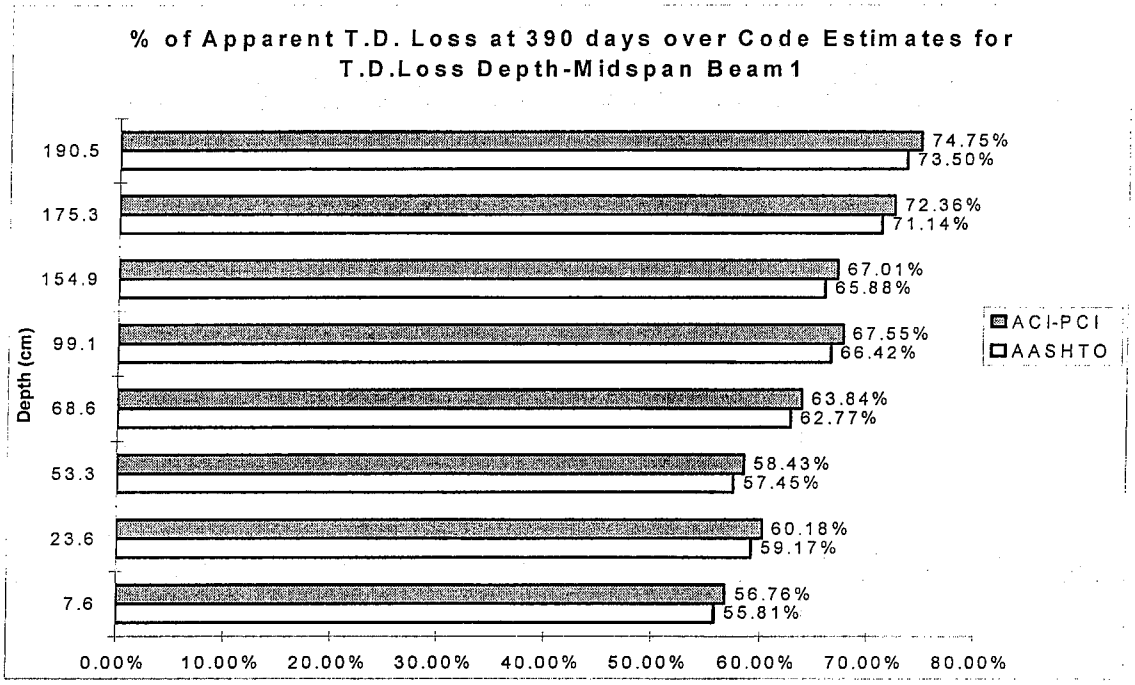

Figure 5-6: Ratios of Apparent TDL to ACI-PCI and AASHTO of Beam 1 at the Mid-span.

Figures 5-7 and 5-8 depict the percentage of total and time dependent loss at 390 days based on the codes' estimates for various depth of Beam 4 at 1.52m away from the support. In Figure 5-7, it can be observed that the losses computed are very close the codes estimates. 94.91 % of the codes estimate of losses had occurred. On the other hand, Figure 5-8 shows less conservative values. Only 83.24 % of the codes estimate of the TDL had occurred. Comparison of percentage inconsistency when subtracting the elastic shortening leads to the conclusion that the code seems to underestimate elastic shortening.

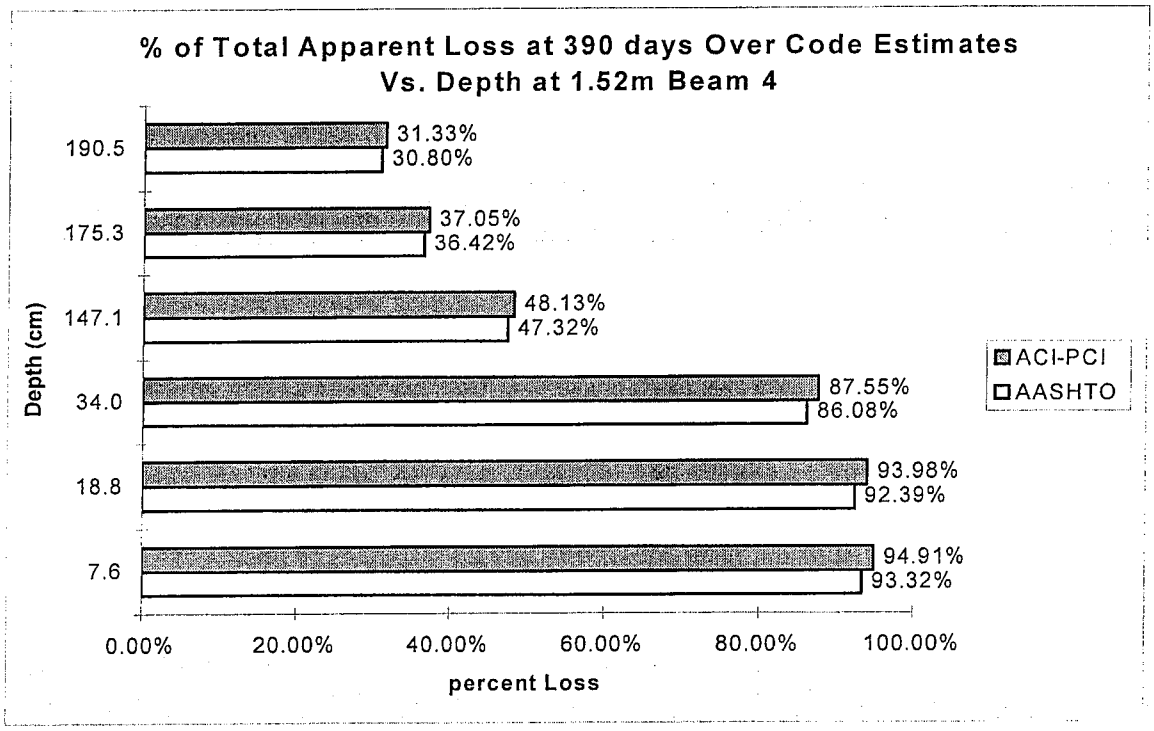

Figure 5-7: Ratios of Total Apparent Loss to ACI-PCI and AASHTO of Beam 4 at 1.52m.

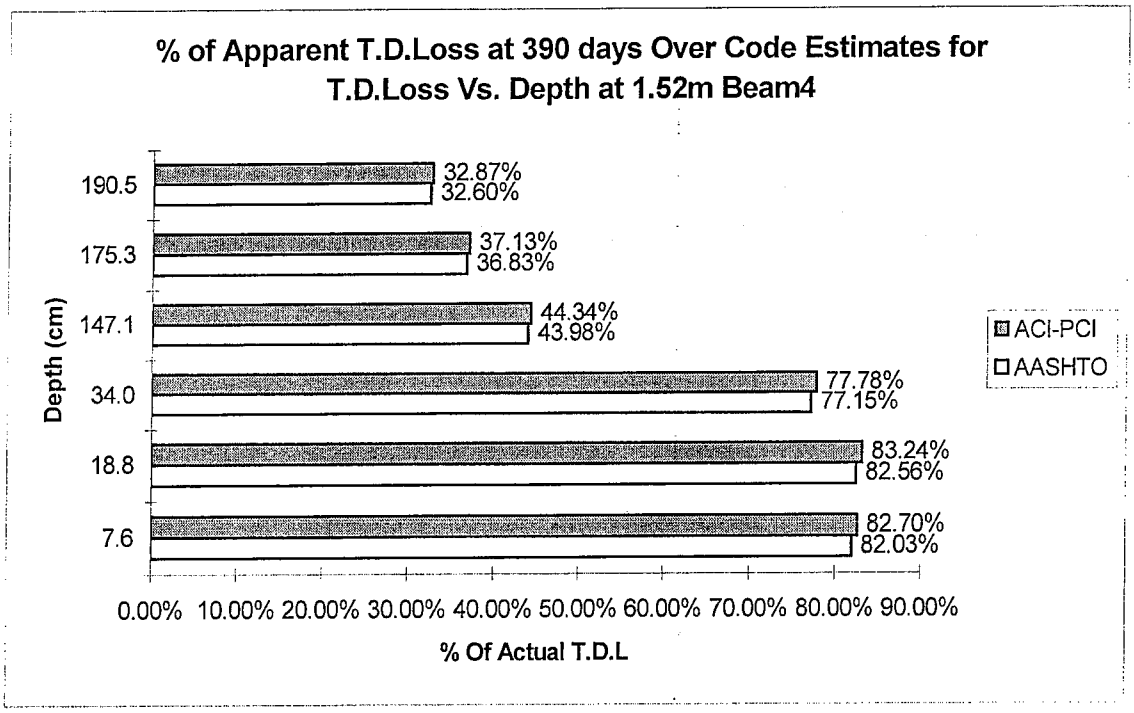

Figure 5-8: Ratios of Apparent TDL to ACI-PCI and AASHTO of Beam 4 at 1.52m.

5.4 Time-Dependent Factors Affecting Total Pre-Stress Loss

As discussed earlier in chapter four, there are two types of losses. One is the instantaneous loss and the other is the time dependent loss. Creep, shrinkage and steel relaxation are the components that make up the time dependent pre-stress loss. In this study two methods were used for computing these components. The first uses the readings obtained from the strain gages. This method is used to compute the net amount of creep. The second uses the PCI Committee and ACI-209 methods of computing the various time dependent factors of pre-stress losses. In the subsequent sections the two methods will be discussed sequentially.

5.4.1 Creep Using Data Obtained from Strain Gages

Creep has been defined as the deformation in the longitudinal direction under a sustained load. Another way to illustrate the effect of creep is in terms of the creep coefficient. Creep coefficient is the ratio of the strain due to creep at a specific time to an initial strain due to elastic shortening. It is important to note that the creep measured in this study may better be referred to as the effective creep. This is because the measured values already include the effect of all the factors that possibly alter the creep value. Both creep and shrinkage influence the strain readings of our data. In order to capture the creep coefficient exclusively, the amount of strain due to shrinkage must be subtracted as shown in the following equation:

$$\text{Creep Coefficient} = \frac{\varepsilon_{Time-dependent} - \varepsilon_{Time-dependent(due\cdot to\cdot shrinkage)}}{\varepsilon_{ins\,tan\,tan\,eous}} \tag{5.12}$$

Note that, in order to achieve $\varepsilon_{Time-dependent}$, Temperature and weight effects were subtracted from the measured strain as discussed earlier in section 5.3.

Figures 5-9 and 5-10 show what we refer to as the effective creep coefficient (Ce). This effective creep coefficient varies as a function of both time and depth. At 190.5 cm (75 in) from the bottom of the beam, the effective creep coefficient at 390 days is approximately 2, where it is much smaller in value at the lower region of concrete member. This variation may also be due to the fact that the steel concentration is at the lower part of the concrete section. The steel centroid at the mid-section of the beam is at 23.6 cm (9.29 in) from the bottom. Hence, the presence of the steel hinders the creeping

action of the concrete. This effective creep coefficient obtained from equation (5.12) is compared to the codes' findings of both ACI-209 and PCI Committee, which are computed at steel centroid only. It can be observed that the effective creep coefficient, at the strand level, measured from equation (5.12) lie in between the findings of both codes (ACI and PCI). In the mid-span of Beam 1 the creep coefficient measured compares well with PCI Committee at the early stages and better with ACI-209 at much later times. At 1.52 m from the support of Beam 4, Figure 5-10, the creep coefficient at steel centroid compares well with both ACI-209 and PCI committee. It is important to note that although the sustained loading of the dead load changes after 240 days, the elastic effect due to the addition of the superimposed dead load was removed at this juncture.

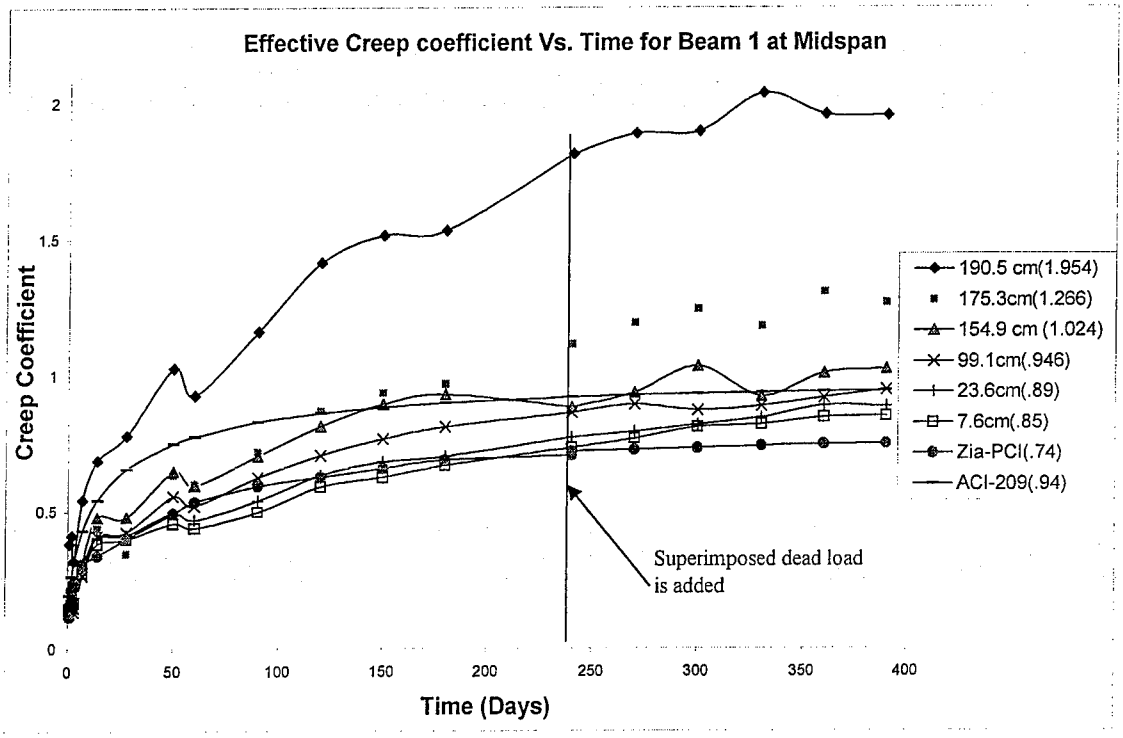

Figure 5-9: Creep Coefficient Based on Strain Reading for Beam 1 at Mid-Span.

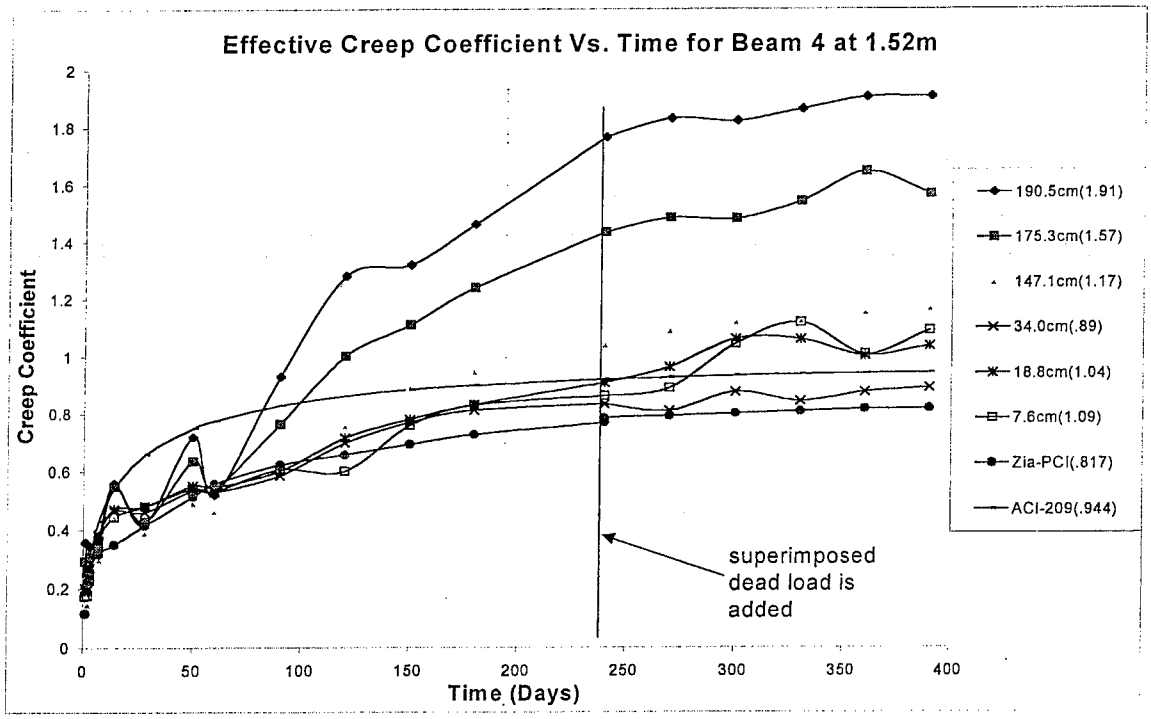

Figure 5-10: Creep Coefficient Based on Strain Reading for Beam 4 at 1.52m.

5.4.2 Effective Concrete Creep Modification Factors

To begin a process for implementation of effective creep coefficient in design, creep correction factor with respect to both time and depth are derived in this section. However, in comparison between the effective creep coefficient factor measured, and Zia-PCI[3] and ACI-209[6] time dependent creep coefficients, the effective creep coefficient similarly captures the time-dependency of creep. However, in contrast with both Zia-PCI and ACI-209, the effective creep coefficient captures the depth variation of the creep in addition. The ultimate concrete creep coefficient defined by various codes is often referred to as C_u. In design the time-dependency of creep is obtained by multiplying Cu

by a time function or factor. This factor is dependent on the method used to achieve the time-dependent creep coefficient. In order to achieve a time-dependent creep coefficient, C_u must be multiplied by $g_{(t)}$. $C_t = g_{(t)} * C_u$. It is important to note that the effective creep coefficient measured at 190.5 cm (75 in), where no pre-stressing strands exist compare, compare well with suggested values of $C_u = 2.0$ for concrete with strength of 55.16 Mpa (8000 psi)[13].

In this study, the effective creep coefficient can be determined by using two correction factors. One correction factor is with respect to time, called the Effective Time Correction factor, K_t. The other is with respect to depth, called the effective depth correction factor, K_d. K_t is obtained by dividing each effective creep coefficient value by the ultimate value (390-days in this case) for each depth considered. On the other hand, K_d is obtained by dividing the effective creep coefficients at each depth by the corresponding values at the steel centroid level. Both these factors are presented in the various plots shown later on in this section. In order to determine the effective creep coefficient values, equation (5.13) is used.

$$Ce = K_t * K_d \tag{5.13}$$

Figures 5-11 and 5-12 show the time and depth correction Factor for Beam 1 at the mid-span. Since the time correction factors are similar in values for the various depths, an average time correction factor was used. Similarly, an average depth correction factor was used as well. The average time and depth correction factors are shown in this section.

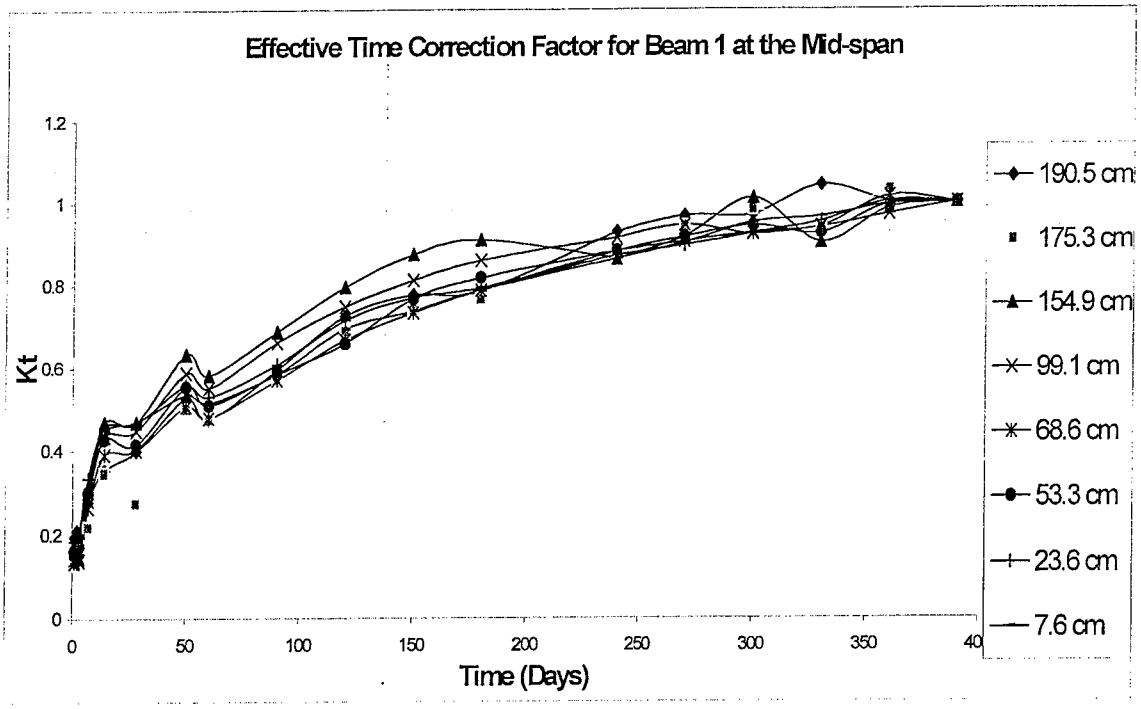

Figure 5-11 Effective Creep Time Correction Factor for Beam 1 at the Mid-span.

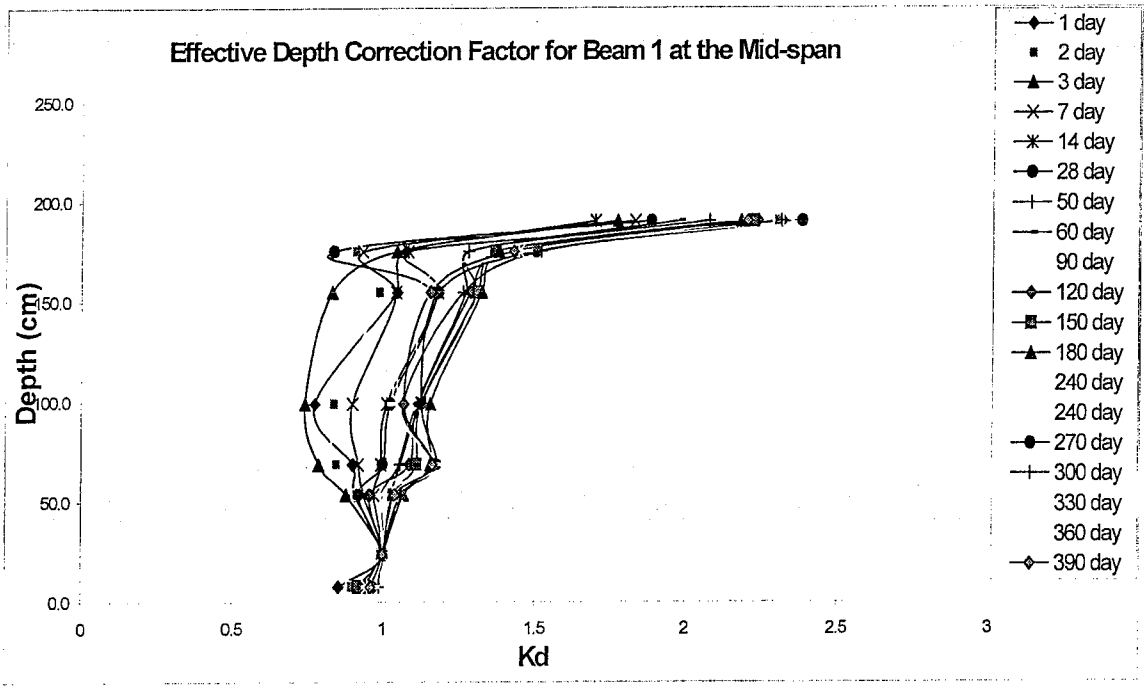

Figure 5-12 Effective Creep depth Correction Factor for Beam 1 at the Mid-span.

Figures 5-13 and 5-14 show the average time and depth correction factors respectively for Beam 1 at the mid-span. These averages are achieved from the previous charts of the time and depth effective correction factors. One must keep in mind, the multiplication of both time and depth correction factors yields the effective time and depth dependent effective creep coefficient. It is interesting to note that the effective correction factor K_t, compares well with the time functions used by PCI and ACI approaches.

Figures 5-15 and 5-16 show the average time and depth correction factors respectively for Beam 4 at the mid-span. These averages are achieved using the same method used to determine the time and depth correction factors of Beam 1 at the mid-span. Similar method is used to achieve the average time and depth correction factors of Beam 4 at 1.52 m away from the support. These averages are shown in Figures 5-17 an 5-18 respectively.

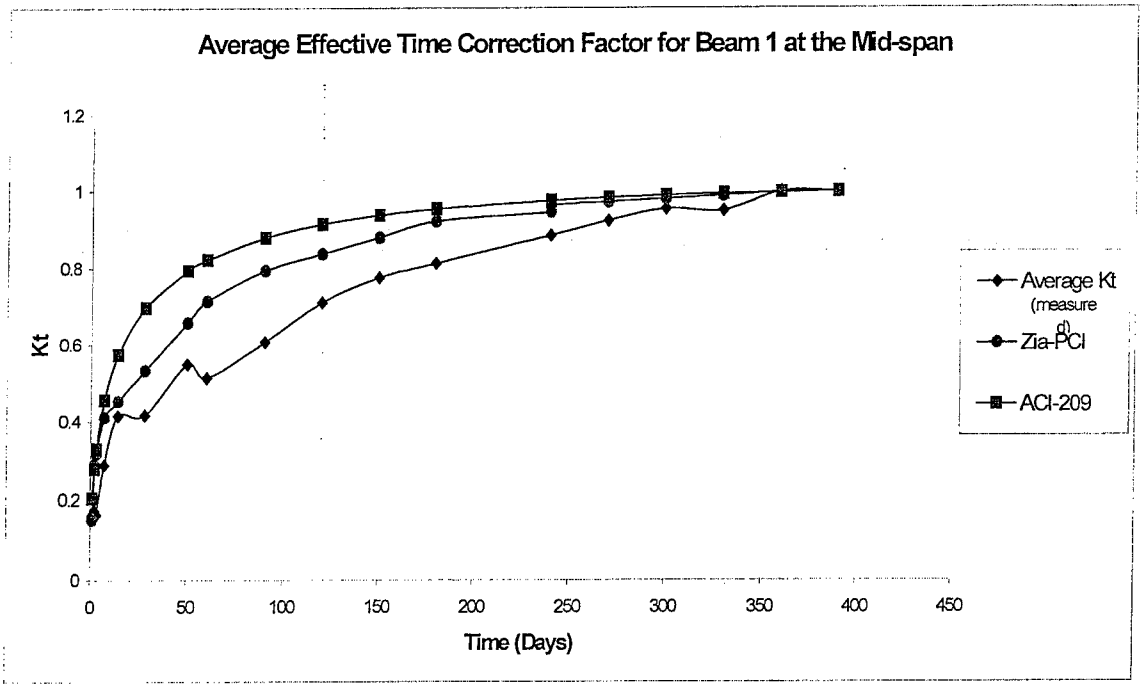

Figure 5-13 Average Effective Creep Time Correction Factor for Beam 1 at the Midspan

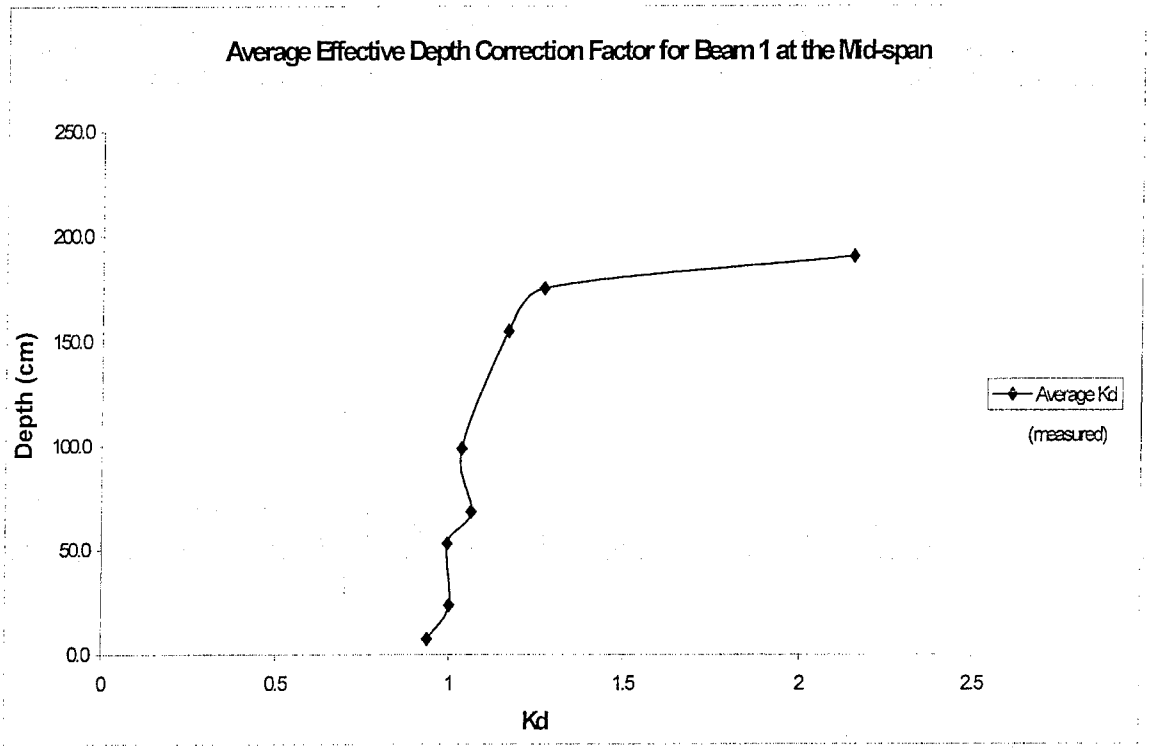

Figure 5-14 Average Effective Creep Depth Correction Factor for Beam 1 at the Midspan

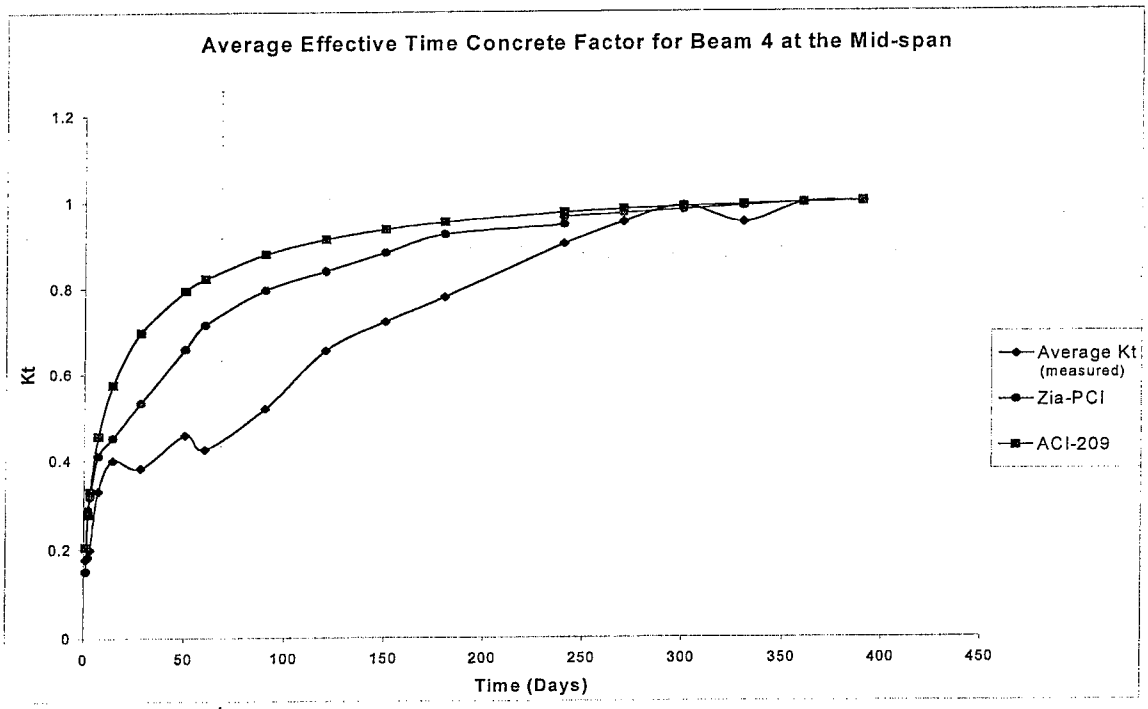

Figure 5-15 Average Effective Creep Time Correction Factor for Beam 4 at the Mid-span

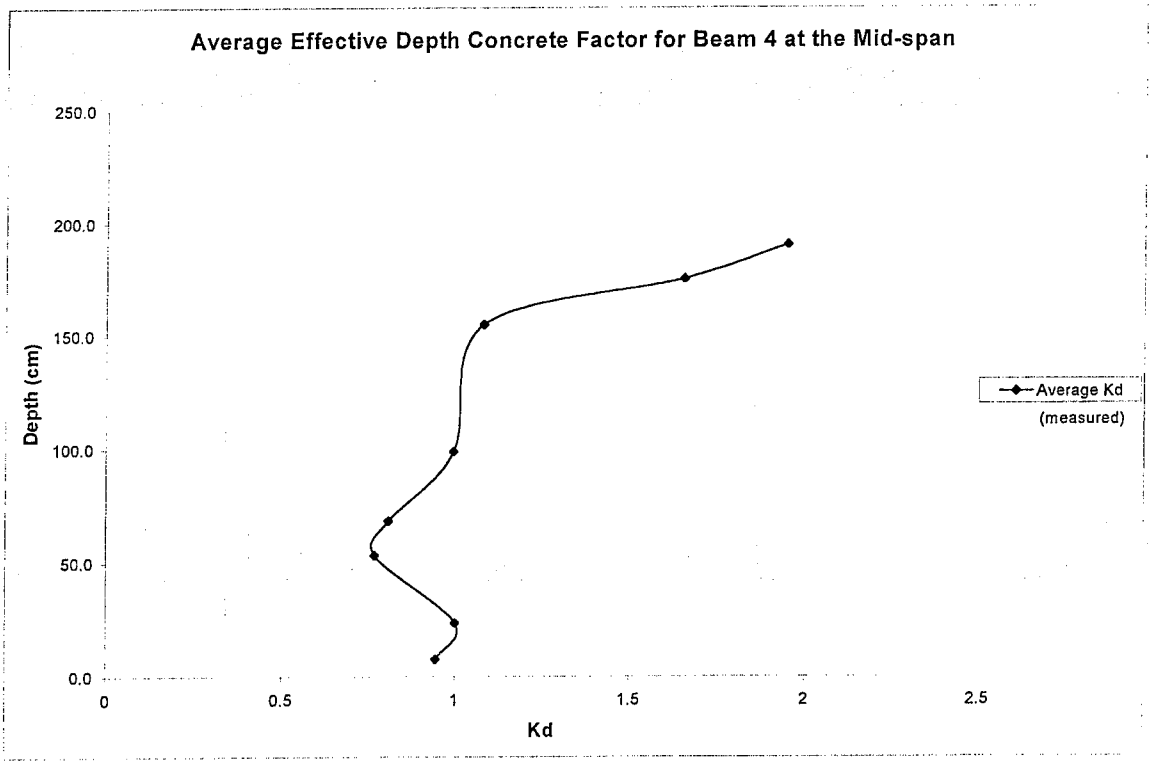

Figure 5-16 Average Effective Creep Depth Correction Factor for Beam 4 at the Midspan

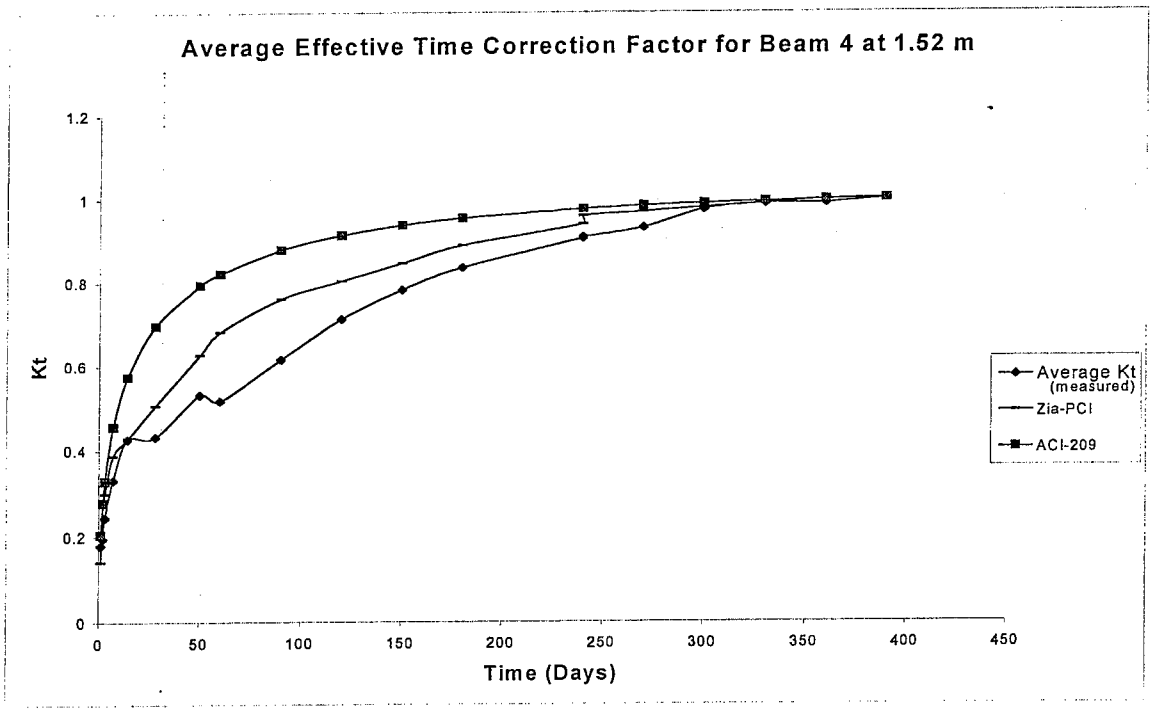

Figure 5-17 Average Effective Creep Depth Correction Factor for Beam 4 at 1.52m.

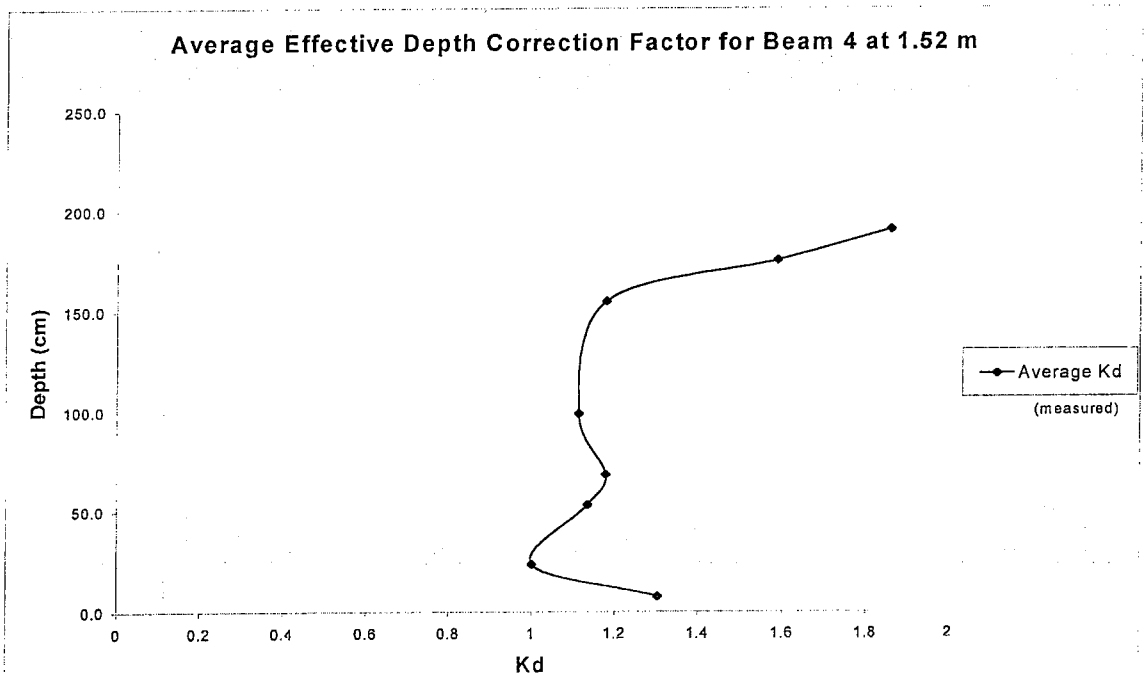

Figure 5-18 Average Effective Creep Depth Correction Factor for Beam 4 at 1.52m.

5.4.3 Using the PCI Code to Calculate Shrinkage, Creep, and Steel Relaxation

The measured strain readings constitute of both creep and shrinkage combined. Therefore, reliable measurement of the effect of the rate of the concrete's water loss ultimately leading to shrinkage is significant. In order to compute the magnitude of creep, the magnitude of strain by shrinkage must be primarily computed. The method for this computation is explained in chapter four and its implementation to the Gandy Bridge is extendedly shown in this section. The PCI time dependent approach for obtaining the various components is illustrated in this section. The values USH, SSF, AUS, PSH that appear in the equations utilized for this purpose are defined in chapter four. Each specific factor is computed for each specific time period. The SSF value is constant throughout the length of the project due to the assumption that the volume to surface area stays constant. The cumulative amount of shrinkage is then computed using all of these components. Once the cumulative shrinkage is computed, the amount of pre-stress loss due to shrinkage is known. The division of the shrinkage pre-stress loss value by the modulus of elasticity of the steel used yields the strain value of the pre-stress section due to shrinkage.

The PCI shrinkage values were incorporated into our study to capture the measured strain reading due to creep alone. The use of PCI shrinkage values was essential due to a field problem encountered in the early days of the project. Five different concrete cylinders were going to be used to account for shrinkage affect. All five cylinders were instrumented with strain gages. They were placed at the same

location as the concrete girders in order to experience the same weather conditions. However, the plastic shield for all the cylinders was not removed until 50 days later, thus affecting the rate of loss of excess water in the cylinders, and hence shrinkage strains. This error had forced us to implement the PCI time shrinkage values into our study. Plots of the cylinders shrinkage values are presented in Appendix A.

The Creep values are computed in a similar fashion to the shrinkage, the appropriate factors are mentioned in chapter four. From chapter four, the determination of all factors for each specific day was computed in order to determine the creep coefficient from the PCI code. Steel relaxation on the other hand involved an equation that uses time and the effective pre-stress. The result of these calculations are summed and compared to the result achieved experimentally as shown in the following section.

5.4.4 Using the ACI-209 to Calculate Shrinkage, Creep, and Steel Relaxation

The time-dependent pre-stress loss, using the ACI-209 method[6], is affected by many factors also. Among these factors are time, relative humidity, concrete and steel strength. The equations used to compute the various components were discussed in Chapter Four. A relative humidity of about 70 % was assumed. This relative humidity assumption is valid due to the geographical location of the Gandy Bridge. This method of computing time-dependent pre-stress loss is based on the steel centroid which compares will with the Zia-PCI study. It is important to use both studies for comparison with the measured time-dependent pre-stress loss from the Gandy Bridge measurements.

5.5 The Summation of the Code's Time Dependent Losses

The summation of all pre-stress loss components lead to the final values used for the time-dependent loss comparison. The various components of pre-stress losses are attained using the codes' findings. Similarity of the results from these theoretical values and the experimental findings from the Gandy Bridge are significant. The comparison between both pre-stress losses using strain data and the code's findings must be conducted at the level of the steel centroid. All theoretical values attained are based on the depth at the steel centroid level. The following figures represent pre-stress loss comparison between both code and experimental findings along with the pre-stress losses at various depths.

Figure 5-19 shows the experimental apparent pre-stress loss at various depths and the theoretical loss at the centroid of the mid-span of Beam 1. The PCI Committee pre-stress loss that is time dependent and is based on the steel centroid compares well with the experimental pre-stress loss at the steel level. The ACI code and AASHTO specifications do not vary with time or depth. They use a lump sum or single value throughout the lifetime of pre-stress loss.

Figure 5-20 show the experimental apparent pre-stress loss at various depths and the theoretical loss at the centroid at 1.52 m from the support of Beam 4. In comparison between both pre-stress measured loss and PCI Committee pre-stress loss, it is apparent that the PCI committee overestimates the pre-stress loss at 1.52m (5 ft) away from the support.

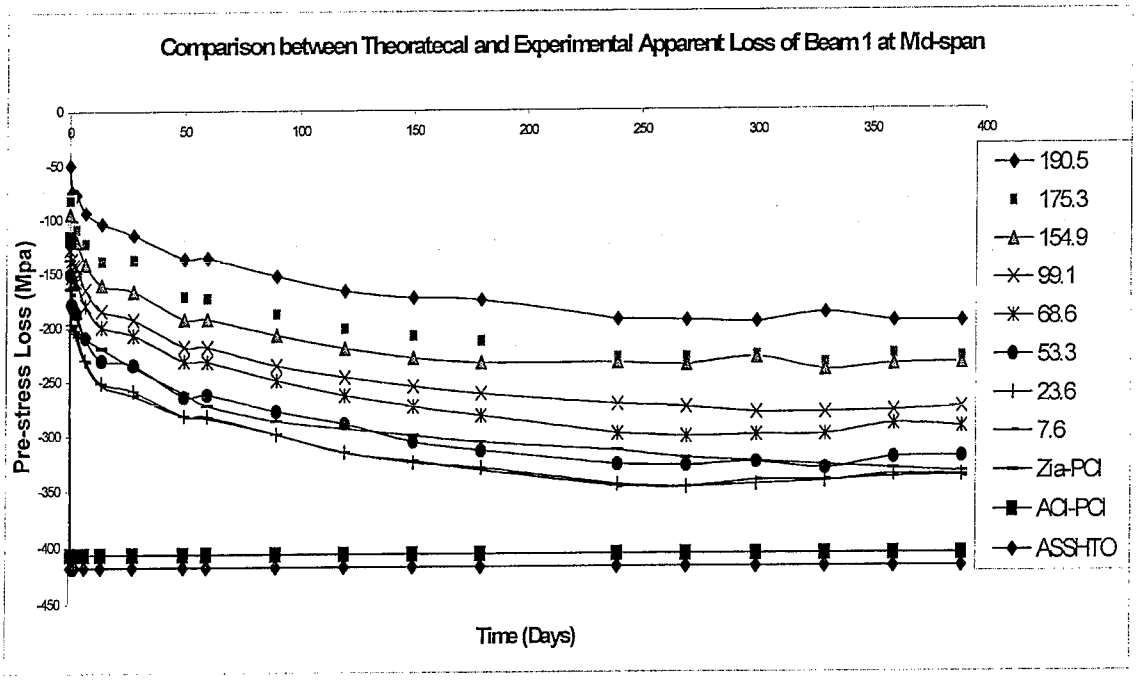

Figure 5-19: Experimental Pre-stress Losses vs. Theoretical Loss of Beam 1 at Mid-span.

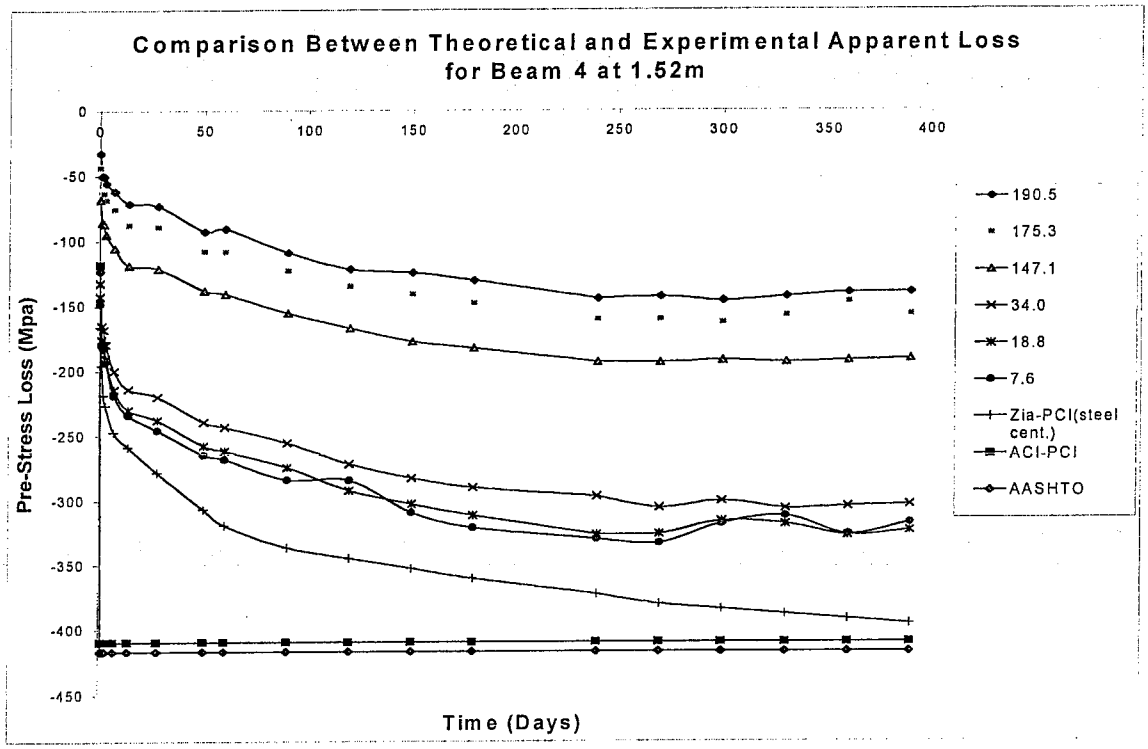

Figure 5-20: Experimental Pre-stress Losses vs. Theoretical Loss of Beam 4 at 1.52m.

Figures 5-21 and 5-22 show the experimental and theoretical pre-stress loss in terms of a ratio expressed with respect to the ultimate strength of the strands. These figures express apparent pre-stress loss in terms of effective pre-stress to ultimate strength ratio. In comparison between these figures and the previous ones, both show the amount of pre-stress loss.

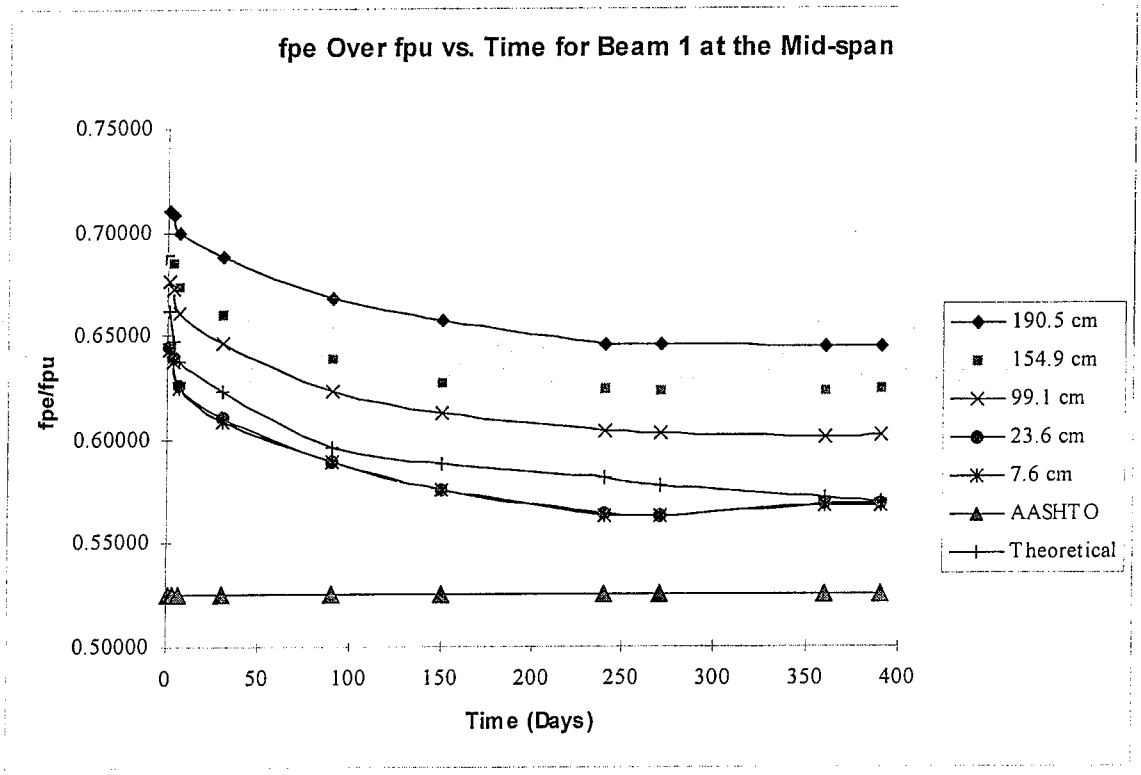

Figure 5-21: fpe over fpu vs. Time for Beam 1 at the Mid-span.

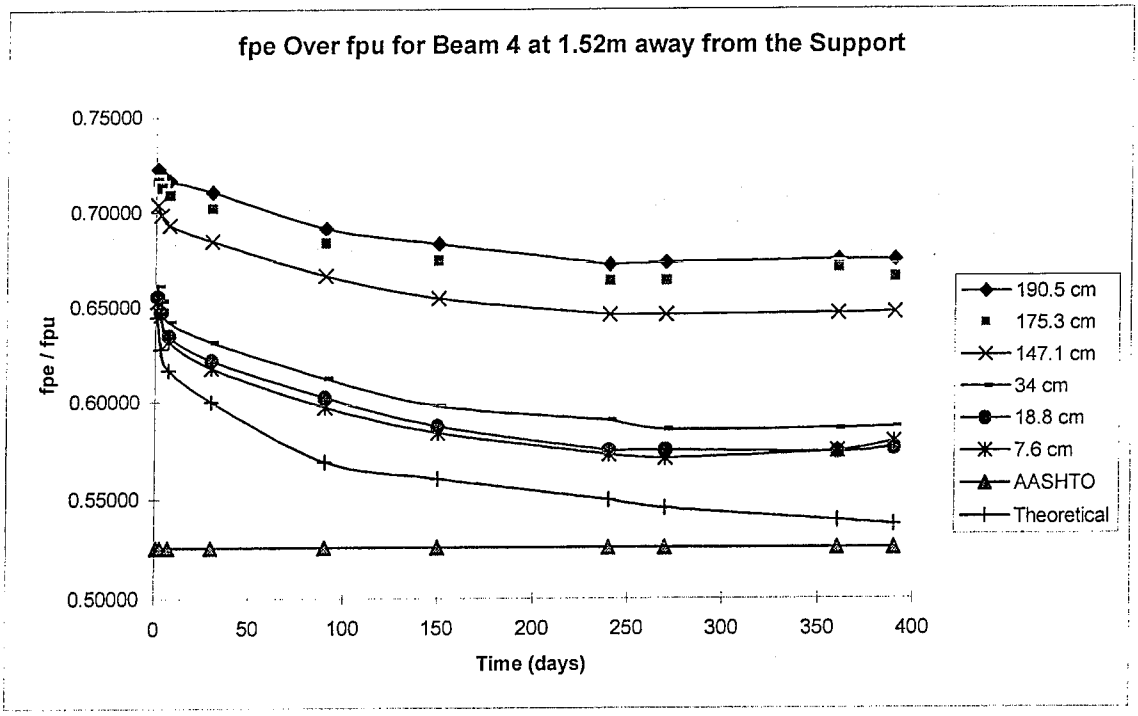

Figure 5-22: fpe over fpu vs. Time for Beam 4 at 1.52m away from the Support.

Another way to present the pre-stress loss is with respect to the jacking stress. It is important to note that this method of expressing pre-stress loss expresses both instantaneous and time-dependent pre-stress loss with respect to jacking stress. Figures 5-23 and 5-24 show the ratio of total loss to jacking stress for various depths. The measured total pre-stress loss compares well with Zia-PCI method of estimating pre-stress loss with respect to time at the steel centroid.

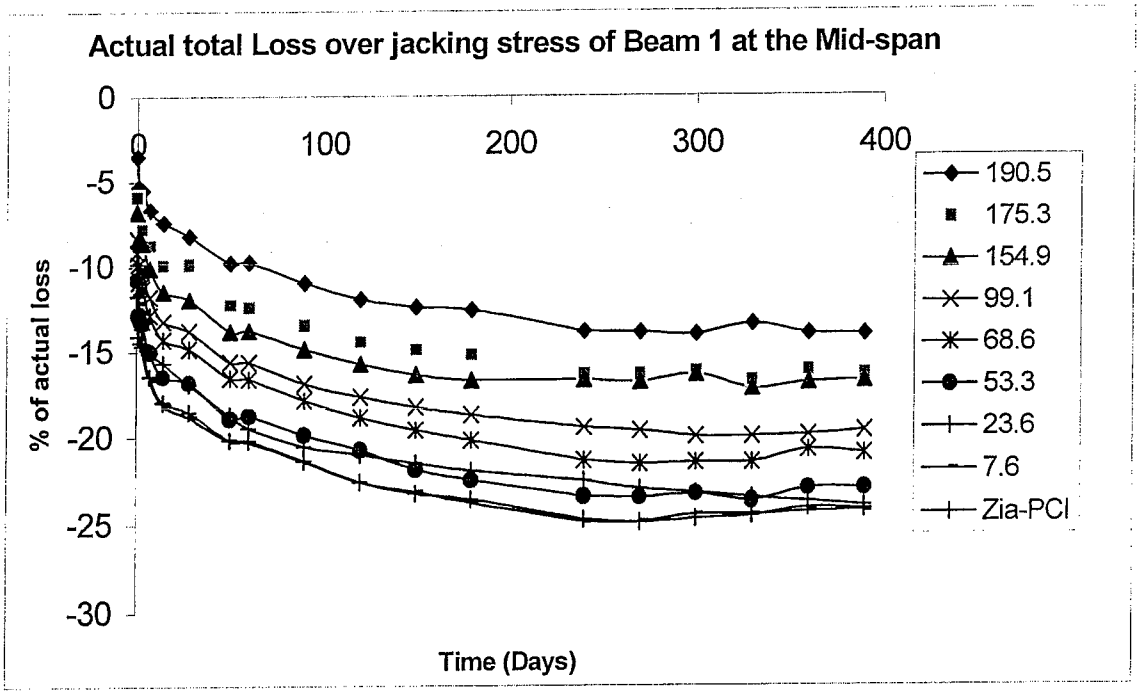

Figure 5-23: Actual Total Loss to Jacking Stress Ratio of Beam 1 at the Mid-span.

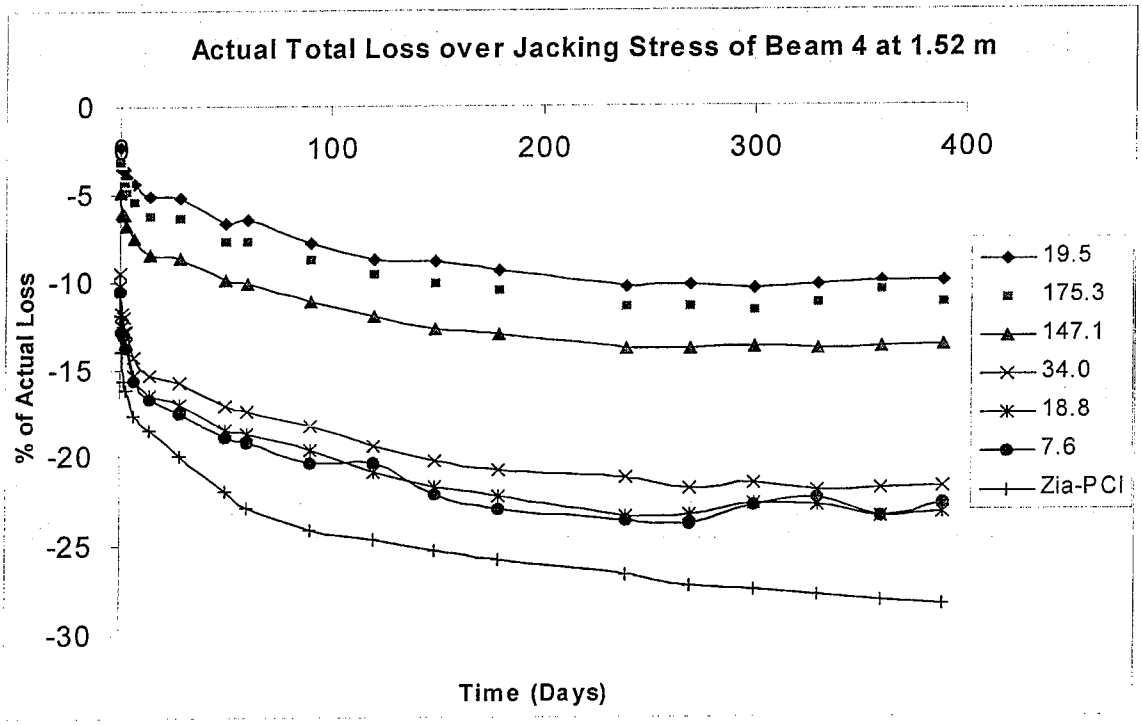

Figure 5-24: Actual Total Loss to Jacking Stress Ratio of Beam 4 at 1.52m.

Chapter 6

EFFECT OF TIME-DEPENDENT PRE-STRESS LOSS ON STRESSES, CAMBER & DEFLECTION

6.1 Introduction

Controlling stresses and deflection are some of the main objectives of pre-stressing a concrete member. Pre-stressing a member provides tensile stress and deflection control for the concrete section. Limiting both tensile stress and deflection to acceptable values are of vital importance for serviceability of concrete structures. Both stresses and deflection are related to one another. Sections that have tensile stress at the top portion and a compressive stress at the bottom portion are said to have negative deflection, camber. While sections that have the compressive stress at the top and the tensile stress at the bottom are said to be deflected. An ideal pre-stress concrete section has little or no tensile stress or deflection.

In the Gandy Bridge project, three simply supported spans of the bridge girders were studied. At the top of the three spans a continuous slab was cast. The effect of the continuity of the superimposed slab on the simply supported bridge girders was investigated in this study. The bending moment due to a strictly continuos slab is different from one that is caused by a simple supported one. Therefore, the comparison

between the use of a continuos superimposed and simple superimposed dead load was investigated, both in terms of stresses and camber. Findings from various results obtained at different sections along with comparison with various codes are discussed in this chapter.

6.2 Stress Distribution

The total concrete stress is composed of three parts. One is the stress of the section caused by pre-stressing alone. Another is the stress caused by the weight of the section. The last is the stress caused by any additional weight superimposed on the section. The equations used for the total stress and the various stress components were shown in chapter four and their results are presented here. The stresses at various depths of the section are presented for different days. Immediately after transfer, 150 days and 390 days are some of the days illustrated. The significance of these days is explained in the subsequent sections.

6.2.1 Immediately after transfer

Once the stress in the strands is transferred to the concrete section, the stress of the concrete section undergoes some changes. After transfer, the strands impose a compressive force on the concrete section. More compression at the lower half is

desirable than at the top half since this condition will be counteracted when additional loads are imposed on the structure later.

Figures 6-1 and 6-2 capture the stress distribution at mid-span Beams 1 and 4 respectively for various depths immediately after transfer. It is important to note that at this stage in the construction process, the beams act as simply supported members. Also the stress from the field measured data account for losses at different depths for any time considered. It can be seen from both figures that the stresses do not violate the code limitations based on AASHTO. Comparison between the actual and the design compressive limits vary. This variation is due to the fact that the design initial compressive strength of the section is about 72.3 % of the actual compressive strength when the strands were cut. These values are f_c'(design) is 34.475 Mpa (-5000 psi) while f_c'(actual) is 47.7 Mpa (-6919 psi). Since the actual compressive stress is larger than the design, exceeding the design compressive limits is perhaps not of major concern. However, the compressive stress should not exceed the limit based on the actual compressive strength of the concrete. Comparison between obtained stresses across the depth at the mid-span of Beams 1 and 4 with various findings are illustrated in both figures. AASHTO stress distribution is based on a time and depth invariant pre-stress lump sum loss value, where Zia-PCI is based on a time dependent pre-stress loss based on the steel centroid, that is depth invariant only. Comparison between all stress distribution at the mid-span immediately after transfer yields similar results across the depth.

Figures 6-3 and 6-4 depict the stress distribution of Beam 1 and 4 for various depths at 1.52 m away from the support. The compressive stress is increasing with depth. At the lower part of the section, the compressive stress exceeds the AASHTO design limit; however, it does not exceed the limit based on using the actual compressive strength. This is acceptable in practice since the actual section is stronger than expected in design. It is important to point out that the original designs of the girders were based on the CEB-FIP[7], European code. Based on that design, the initial stress was about 99 % of the allowed limit. In comparison between stress at 1.52 m (5 ft) from support and the mid-span, the compressive stress at 1.52 m (5 ft) from the support is lower at the upper part of the section and larger at the lower part of the section than at the mid-span. Comparison between using actual, AASHTO and Zia-PCI losses yields very little differences at this early stage. Stresses from all approaches are almost identical at this point in time.

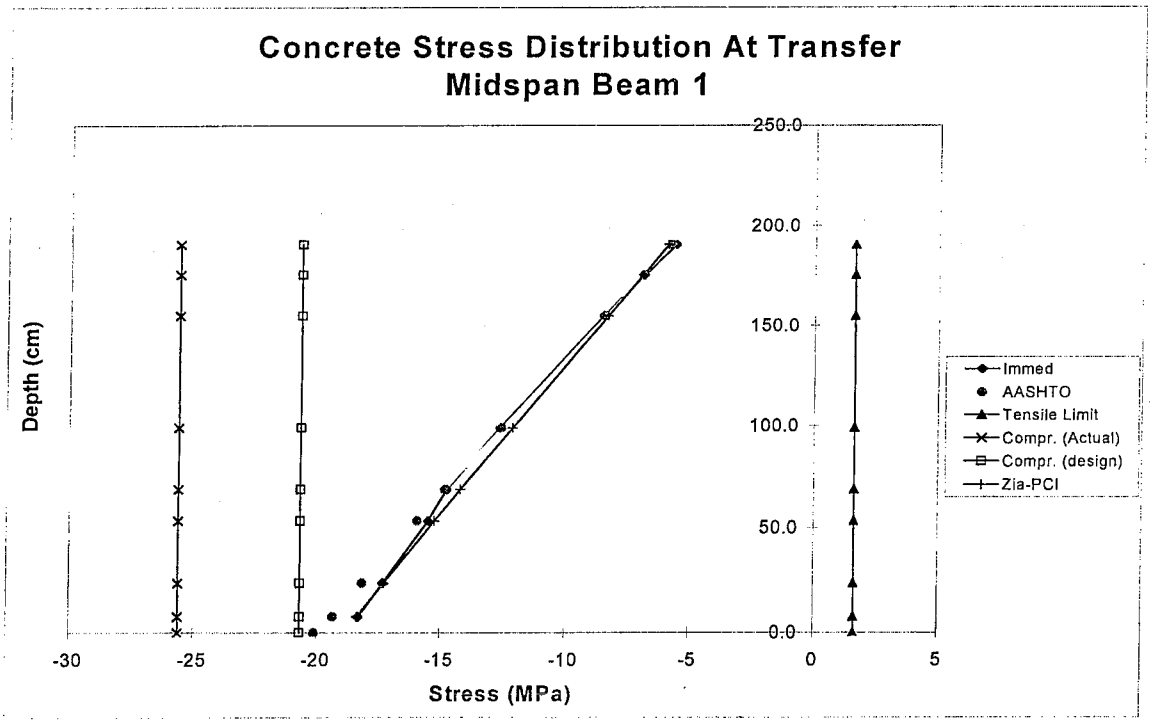

Figure 6-1: Concrete Stress vs. Depth for Beam 1 at Mid-span at Transfer.

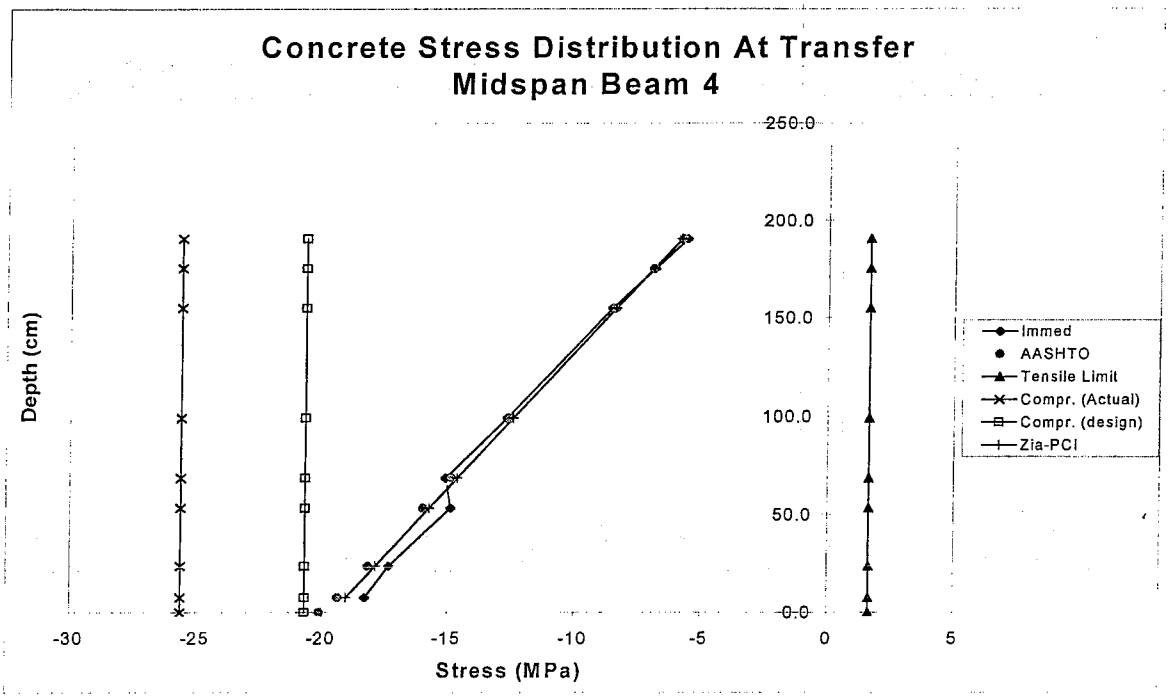

Figure 6-2: Concrete Stress vs. Depth for Beam 4 at Mid-span at Transfer.

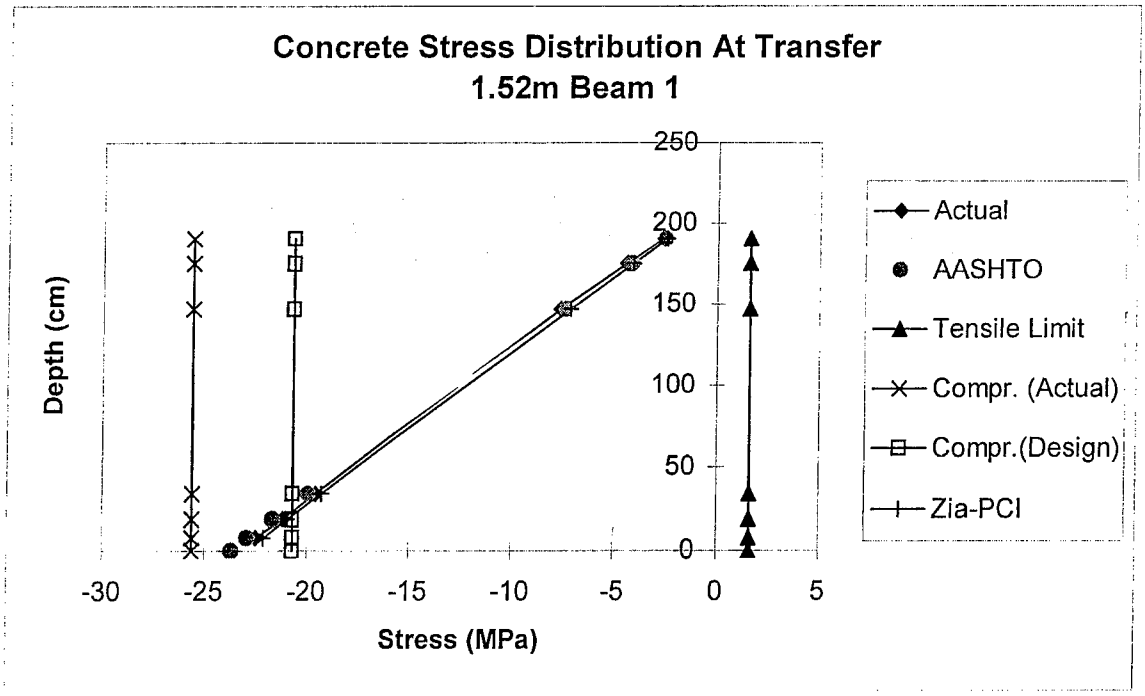

Figure 6-3: Concrete Stress vs. Depth for Beam 1 at 1.52m away from the Support.

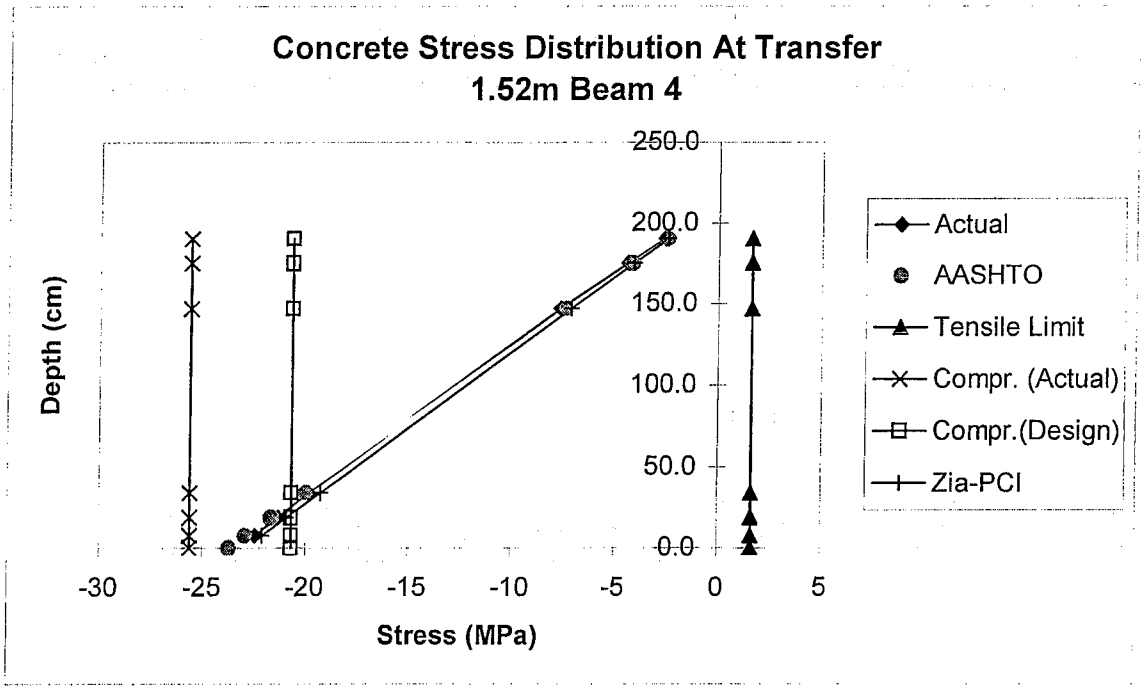

Figure 6-4 Concrete Stress vs. Depth for Beam 4 at 1.52 m away from the Support.

6.2.2 At 150 Days After Transfer

Time dependent losses are the ones that occur after the instantaneous loss has taken place. Shrinkage, creep, and steel relaxation play a major role in changing the initial pre-stressing force. Alteration to the pre-stressing force result in changes to the stress of the concrete section with time. At the 150-day mark of the construction, no superimposed dead load is placed on the girders yet. The pre-stressing force, the self-weight, and the time dependent parameters are the only factors affecting the girders alone. The difference between the effect of the immediate loss and time dependent loss on stresses can be easily observed in the re-distribution of the stresses in the concrete section between immediately after transfer and 150 days after transfer.

Figure 6-5 captures the stress distribution of Beam 1 at 150 days for various depths in the mid-span. The actual compressive stress at the lower part of the section is much greater than at the top of the section. The actual maximum and minimum concrete stresses are –14.75 Mpa (-2139 psi) at 7.6 cm (3 in) and –5.91 Mpa (-863 psi) at 190.5 cm (75 in) receptively. In comparison with time of transfer, the compressive stress on the lower part of the concrete section at 150 days has decreased from the compressive stress at transfer. This reduction in stress is expected and planed for in every pre-stress concrete design project. Comparison between the stress distributions form the various loss computation methods used yield different results than seen immediately after transfer. The obtained stresses based on measured pre-stress loss are greater at the bottom of the member than the stresses based on using AASHTO and Zia-PCI pre-stress

losses, and indicate a more non-linear distribution.

Figure 6-6 captures the stress distribution of Beam 4 at 150 days for various depths in the mid-span. The actual compressive stress at the lower part of the section is also much greater than at the top of the section. The actual maximum and minimum concrete stresses are –14.71 Mpa (-2133.43 psi) at 7.6 cm (3 in) and –5.92 Mpa (-858.6 psi) at 190.5 cm (75 in) receptively. Note that both AASHTO and Zia-PCI do not capture the nonlinear stress behavior across the depth of the member. Their stress distribution across the depth is based on the theoretical assumption of stress linearity used for simplicity. Both Figures 6-5 and 6-6 show that none of the concrete stress distribution exceed the allowable values in the mid-span. Thus, indicating that the time-dependency and depth-dependency of the losses do not dramatically affect the stresses in the mid-span. As a check, it is pointed out that at this stage in the construction, Beams 1 and 4 are similar and show same results as expected.

Figure 6-7 captures the stress distribution of Beam 4 for various depths at 1.52m at 150 days. The actual compressive stress at the lower part of the section is much greater than at the top of the section. The actual maximum and minimum concrete stresses are –19.37 Mpa (-2809 psi) at 7.6 cm (3 in) and –2.48 Mpa (-359.7 psi) at 190.5 cm (75 in). In comparison with time at transfer, the compressive stress on the lower part of the concrete section at 150 days has decreased from the compressive stress at transfer, however, it is still over the design limit. Analyzing the differences between the mid-span and 1.52m (5 ft) away from the support, the compressive stress at the lower part of the section at 1.52m (5 ft) is in more compression than at the mid-span. In this figure, both

stresses computed using measured and Zia-PCI pre-stress loss exceed the design compressive limit. The AASHTO stress does not violate the limit, and depicts a similar stress at the bottom of the member as the design compressive stress limit. Therefore, the effect of accounting for time-dependency and depth-dependency in the stress calculations seems to be more significant in the support region.

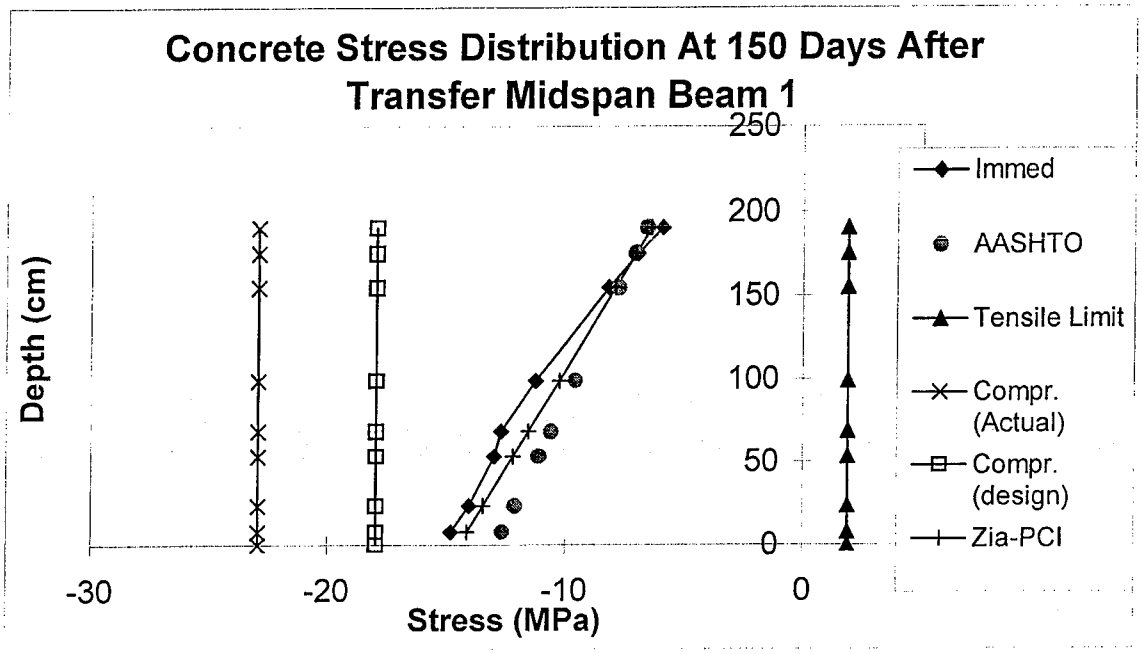

Figure 6-5: Concrete Stress Distribution vs. Depth at Mid-span of Beam 1 at 150 days.

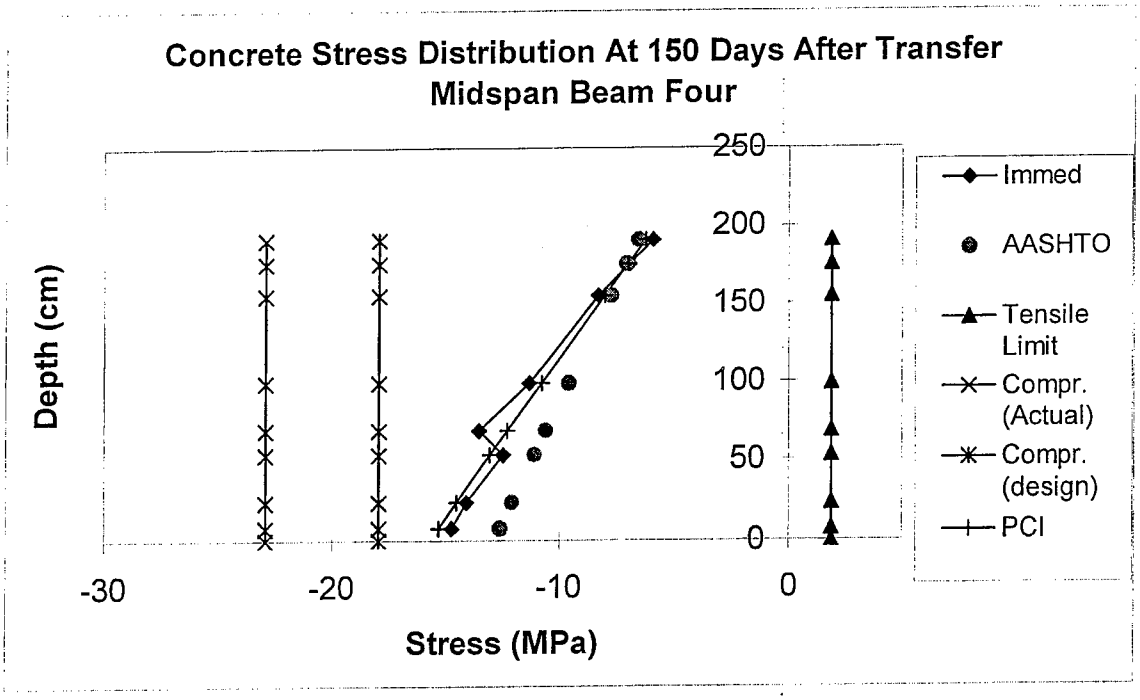

Figure 6-6: Concrete Stress Distribution vs. Depth of Beam 4 at Mid-span at 150 days.

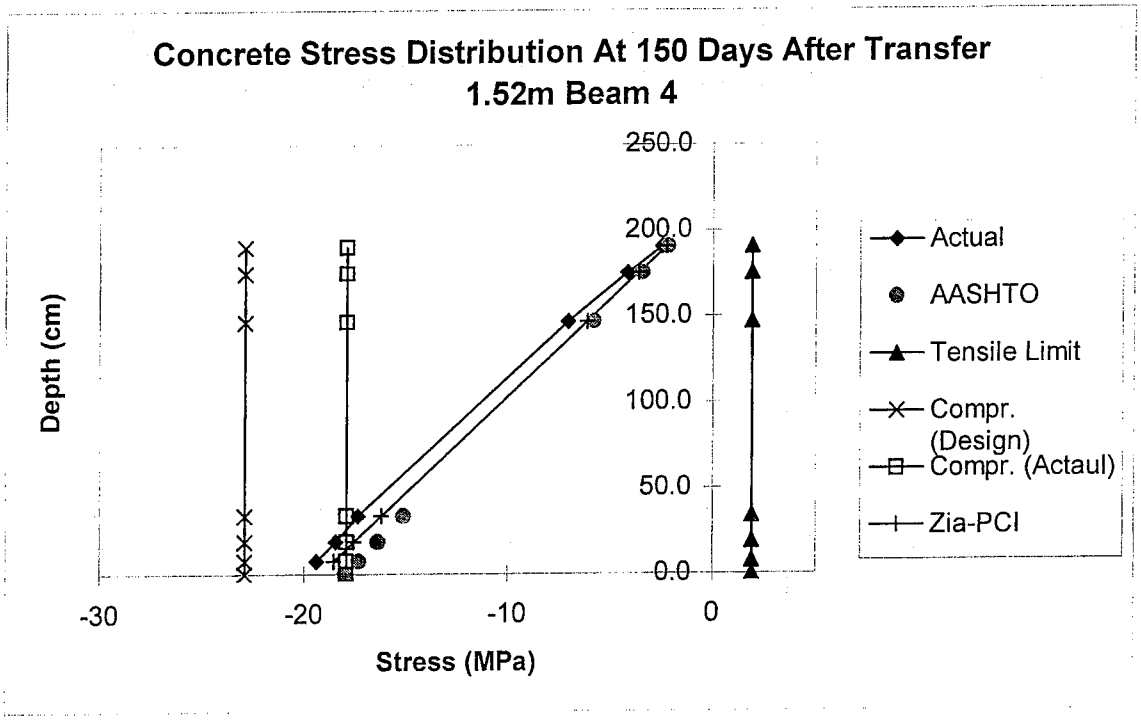

Figure 6-7: Concrete Stress Distribution vs. Depth at 1.52m of Beam 4 at 150 days.

6.2.3 At 390 days after Transfer

At 240 days after transfer the slab was cast. At which time the superimposed dead loads such as the slab, wearing surface, and railing were then considered part of the bridge loading in this study. The slab was cast over the three spans creating a dilemma in the design approach to be used for the bridge. Since the very deep girders (198 cm) were simply supported, questions such as whether to treat the slab (20 cm thick) as simply supported or continuous becomes an issue affecting the proper design method to be used. Procedures for both methods were studied and compared. Plots for stresses and deflections caused by considering the superimposed dead loads are simple or continuous are discussed in this chapter. Division of this section into simply supported girders carrying a simply supported superimposed load, and simply supported girders carrying continuous superimposed load are considered in the sections that follow.

6.2.4 Simply Supported Superimposed Dead Load on Girders

Figure 6-8 captures the stress distribution of Beam 1 for various depths at mid-span at 390 days. The actual compressive stress at the top part of the section is now much greater than at the lower part of the section. The actual maximum and minimum concrete stresses are - 9.37 Mpa (-1359 psi) at 190.5 cm (75 in) and –4.037 Mpa (-585.5 psi) at 7.6 cm (3 in). The top and bottom compressive stresses of this section at this point in time have changed from previously seen distributions for immediate and 150 days after

transfer. This change in stress distribution is due to the additional weight on the girders and the composite section considered. Comparison between the actual and the AASHTO code yields similar results to the ones seen earlier for 150 days. The actual compressive stress at the top is consistent with the AASHTO code and is greater at both the middle and lower fibers. The actual compressive stress at the bottom is consistent with Zia-PCI stress and is greater at both the middle and top fibers.

Figure 6-9 shows the stress distribution at the mid-span of Beam 4 for various depths at 390 days. The actual compressive stress at the top part of the section is much greater than at the lower part of the section. At 190.5 cm (75 in) from the bottom of the girder the compressive stress is –9.40 Mpa (-1363 psi) while the compressive stress at 7.6 cm (3 in) is only –3.59 Mpa (-520.7 psi). Comparison between the actual and the AASHTO code yields similar results to the ones seen earlier for 150 days. The actual compressive stress at the top is generally consistent with the AASHTO code and is greater at both the middle and lower fibers.

Figure 6-10 depicts the stress distribution of Beam 4 for various depths at 1.52 m (5 ft) at 390 days. The actual concrete stresses are –6.58 MPa (-954 psi) at 190.5 cm (75 in) and -6.02 MPa (-873 psi) at 7.6 cm (3 in). At this section, the compressive stress seems to be getting more uniform across the depth. The average compressive stress on the section is –6.30 Mpa (-913.7 psi). In comparison between the actual stresses, AASHTO code, and Zia-PCI, the pattern of stress distribution are similar. All the stress distributions based on the various methods are somewhat uniform across the depths. Thus, by assuming a simply supported superimposed dead load, the high compressive

stresses obtained in the bottom fibers close to the support seem to be compensated for as time proceeds. The stress distributions are well within the allowed limits in this case, suggesting a very conservative design.

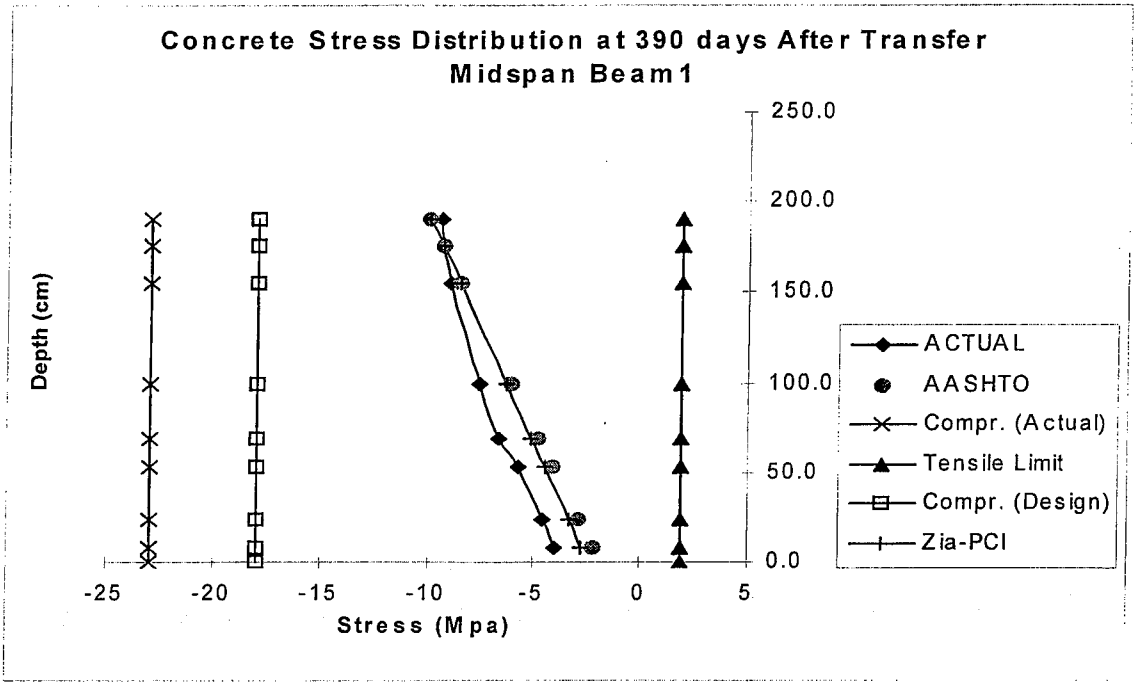

Figure 6-8: Concrete Stress vs. Depth for Beam 1 at Mid-span at 390 days.

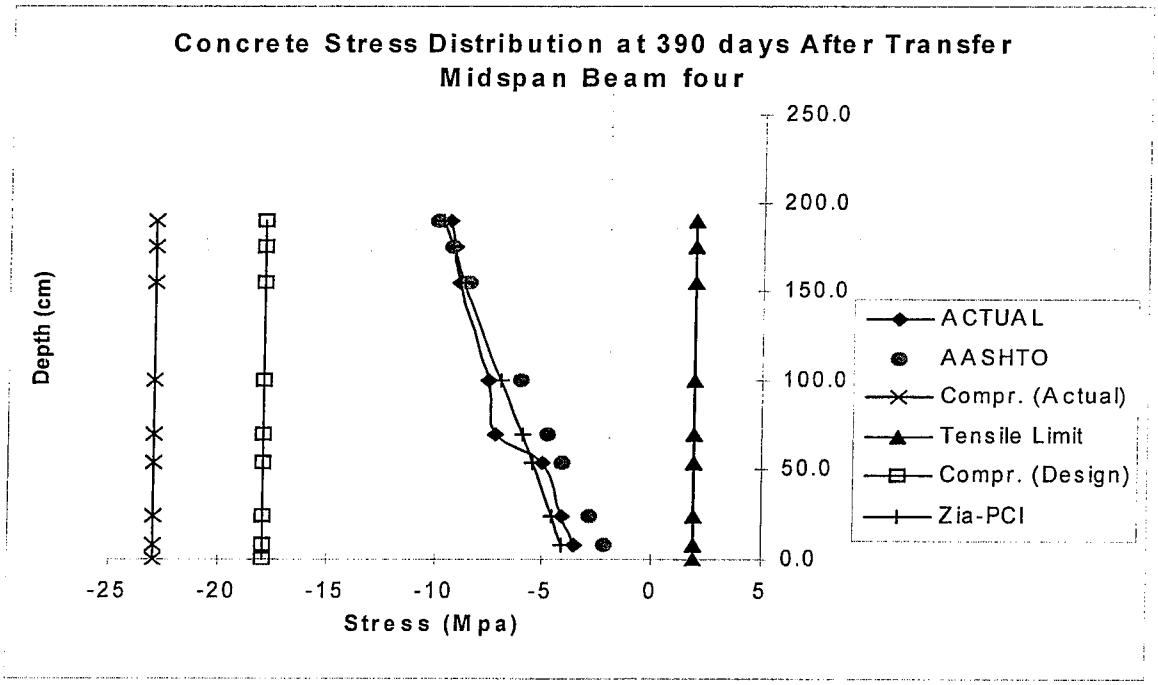

Figure 6-9: Concrete Stress vs. Depth for Beam 4 at Mid-span at 390 days.

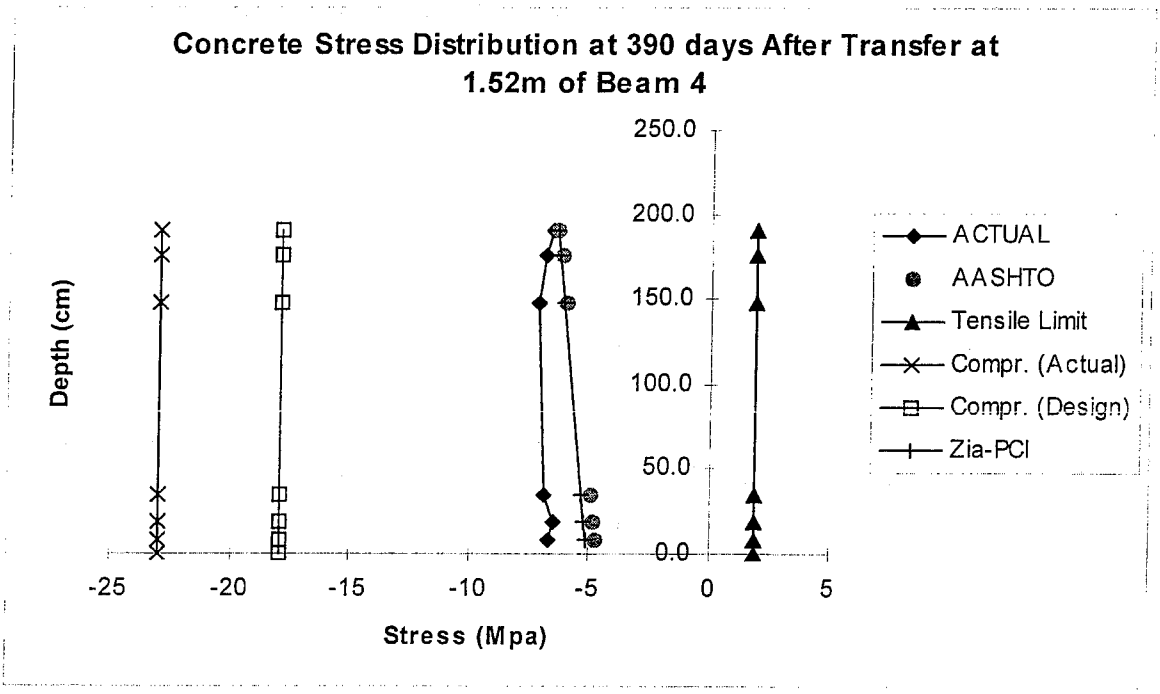

Figure 6-10: Concrete Stress vs. Depth for Beam 4 at 1.52m at 390 days.

6.2.5 Continuous Superimposed Dead Load on Girders

In Figure 6-11 the stress distribution from assuming continuous superimposed dead load for the mid-span of Beam 1 at various depths at 390 days is shown. This figure differs from the one assuming simply supported superimposed dead load. The compressive stress is more uniform across the depth. At the top most gage location, 190.5 cm (75 in), the concrete stress is – 8.27 Mpa (-1199 psi). Only –7.98 Mpa (-1157 psi) exist at 7.6 cm (3 in) at the bottom of the section. Comparison between the actual and the AASHTO code yields similar results to the ones seen earlier for simply supported case. The actual compressive stress at the top is consistent with the AASHTO code and is greater at both the middle and lower fibers. However, the actual measured stress distribution across the depth compares well with the Zia-PCI method.

Figure 6-12 captures the stress distribution at the mid-span of Beam 4 for various depths at 390 days. It is important to note that Beam 4 is in the interior span of the bridge segments. This figure significantly differs from the one obtained when assuming simply supported superimposed dead load. The actual maximum and minimum concrete stresses are –8.36 Mpa (-1212.5 psi) at 190.5 cm (75 in) and –7.83 Mpa (-1135.6 psi) at 7.6 cm (3 in). In comparison between both Beams 1 and 4 at the mid-span, the stresses at the top and bottom of the section are similar. In comparison between the actual, Zia-PCI, and AASHTO stress distribution across the depth, the Zia-PCI and the actual stresses compare well with one another. The AASHTO stress distribution across the depth is

consistent with the actual stress at the top of the section, while it is less at both the middle and the bottom of the section.

Figures 6-13 and 6-14 capture the stress distribution at 1.52 m of Beams 1 and 4 for various depths at 390 days. In Figure 6-13, The actual concrete stresses in Beam 1 are –2.83 Mpa (-410 psi) at 190.5 cm (75 in) and –18.53 Mpa (-2687.5 psi) at 7.6 cm (3 in). Where in Figure 6-14, The actual concrete stresses are –3.83 Mpa (-410 psi) at 190.5 cm (75 in) and –18.11 Mpa (-2626 psi) at 7.6 cm (3 in). The uniformity of the compressive stress seen in Figure 6-7 based on simple supported action seems to be altered when using a continuous superimposed dead load. In comparison between the actual and the AASHTO code, both yields similar results to the ones seen for mid-span. The actual compressive stress at the top is consistent with the AASHTO code and is greater at both the middle and lower section. Both AASHTO and Zia-PCI stress are consistent throughout the depth of the beam and seem to underestimate the actual compressive stress. The simply supported case, AASHTO and Zia-PCI compressive stresses at the bottom fiber in the support region meet the design requirements for all cases. However, the actual compressive stress seems to be right at the limit, hence, suggesting that using a simply supported assumption may be too conservative.

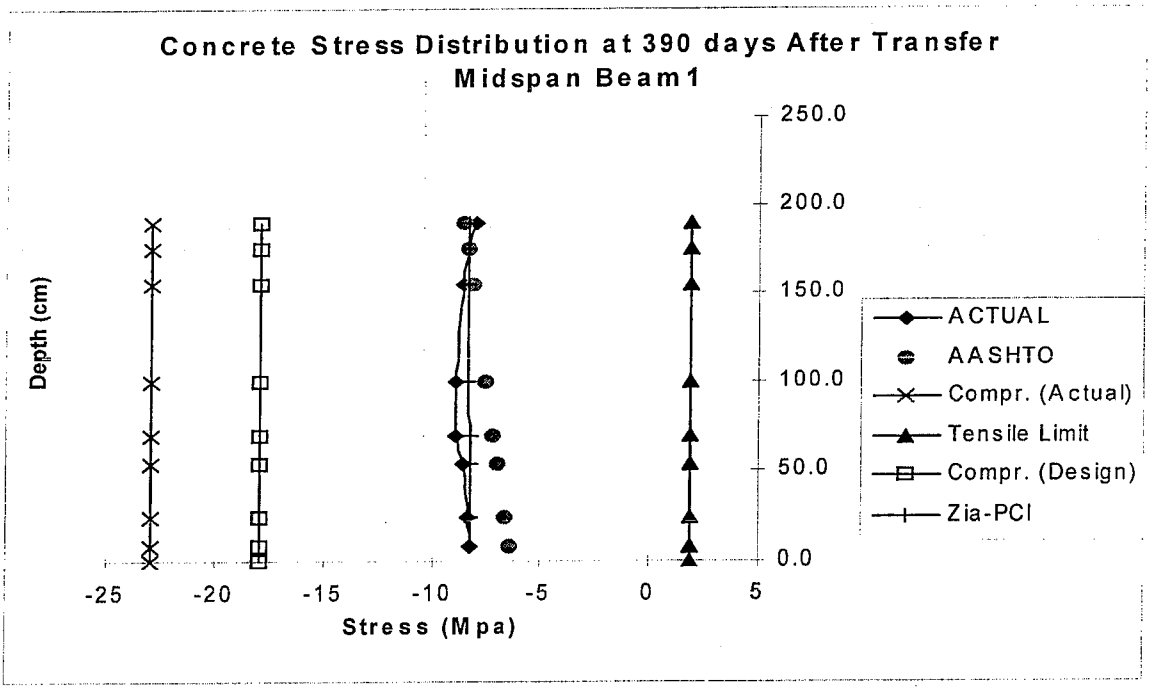

Figure 6-11: Concrete Stress vs. Depth for Beam 1 at Mid-span at 390 days.

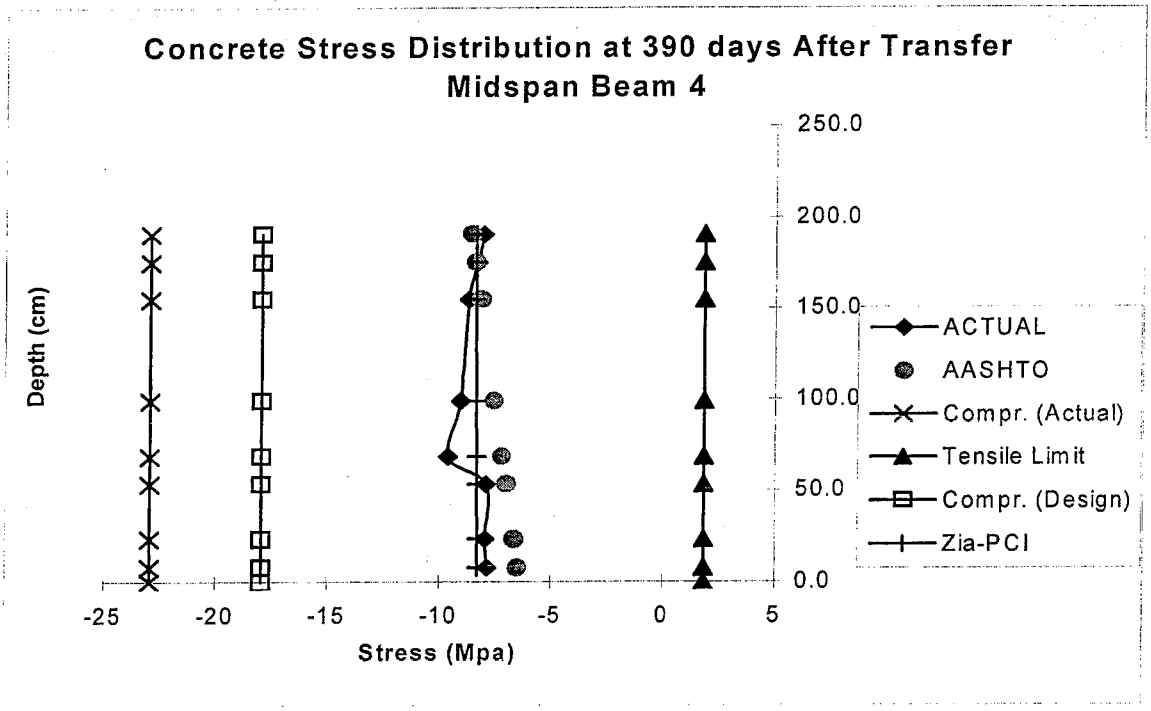

Figure 6-12: Concrete Stress vs. Depth for Beam 4 at Mid-span at 390 days.

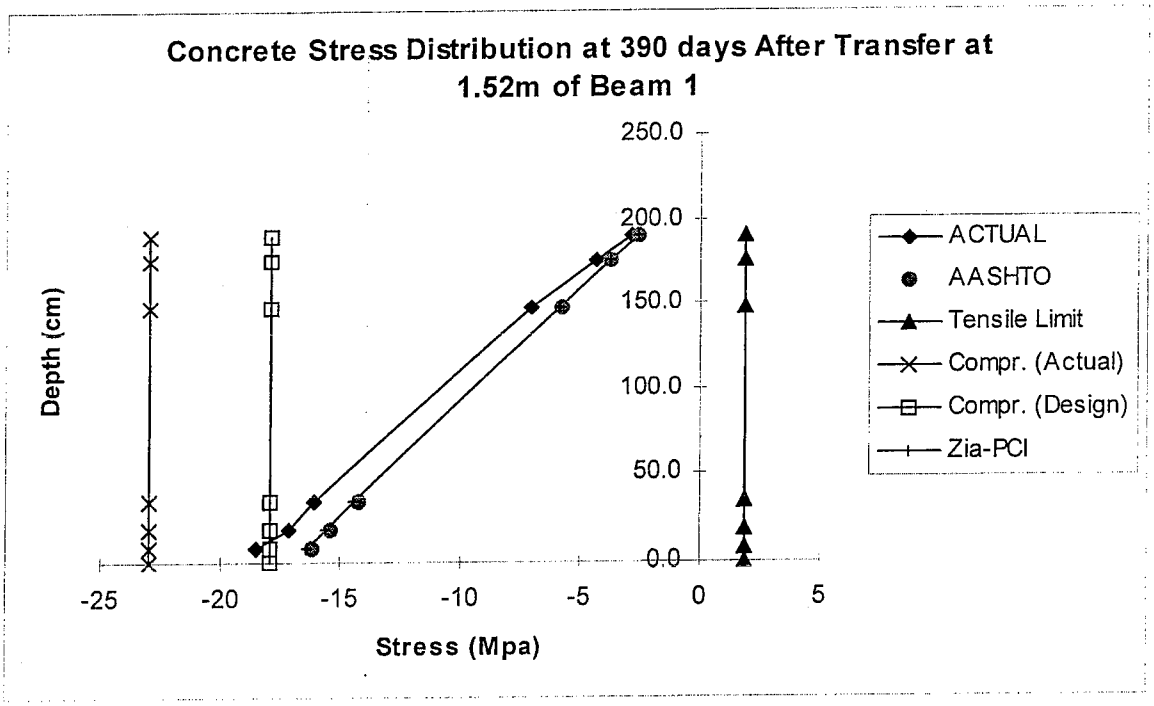

Figure 6-13 Concrete Stress vs. Depth for Beam 1 at 1.52 m at 390 days.

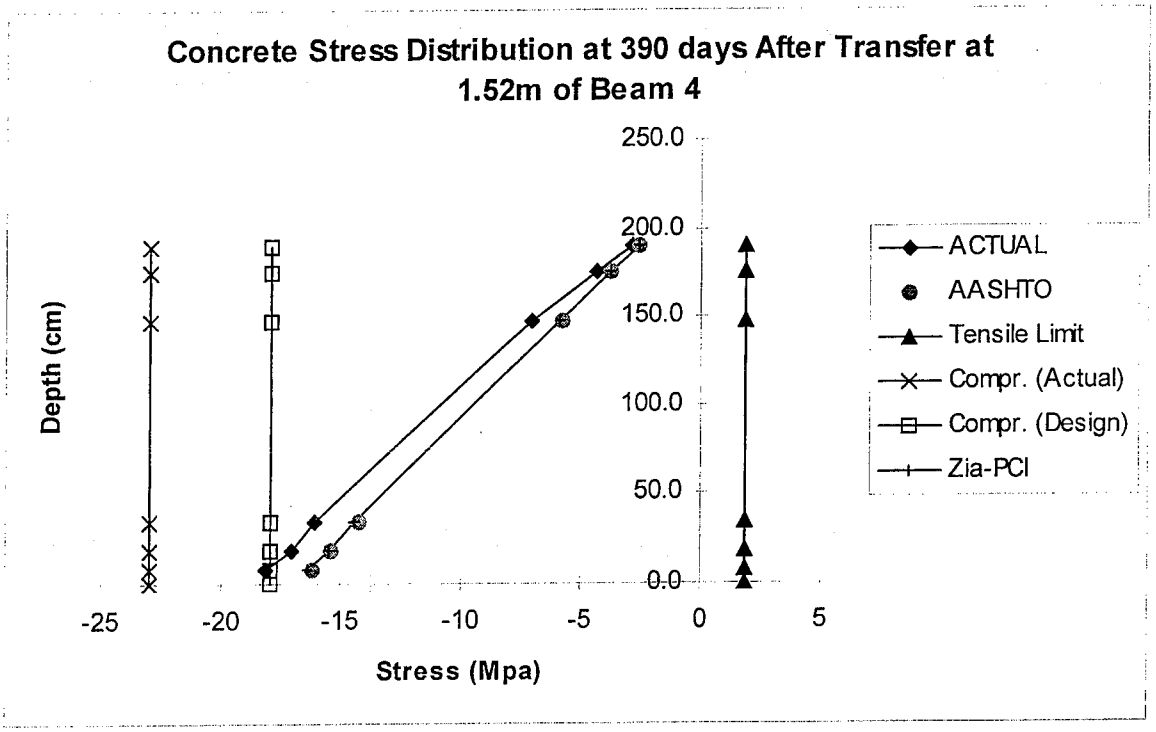

Figure 6-14 Concrete Stress vs. Depth for Beam 4 at 1.52 m at 390 days.

6. 3 Deflection and Camber of Modified AASHTO type VI Girders

The modified AASHTO type VI concrete girders of this bridge are subjected to a sustained eccentric compressive force. The level of this force affects the magnitude of time-dependent creep, and consequently camber of the girders. On the other hand, the sustained weight of the section and the superimposed dead load on the section cause it to creep and deflect as well. Controlling both camber and deflection to reasonable amounts is a significant task in design of pre-stress concrete members. The initial imposition of camber in a pre-stress member is done to counteract the deflection of the section at service. In this section the calculation of camber and deflection is divided into two.

6.3.1 Camber and Deflection

The details of methods used to compute the amount of camber and deflection were discussed in chapter four, and their implementation on the Gandy Bridge project is presented in this section of the report. For camber, the design of the modified ASSHTO type VI girder used in the Gandy Bridge consists of 14 doubly depressed strands and 50 straight strands extending throughout the length of the girders. Hence, 78 % of the strands are straight while only 22 % of them are depressed. Due to the combination of both straight and depressed strands, modification to equation (4.37) and (4.38) must be made in order to better predict the amount of camber due to the shape of the pre-stressing

strands. The following equation is used to determine the magnitude of camber that must be applied on the Gandy Bridge design.

$$\delta_i \uparrow = 0.78 * \phi_c \frac{L^2}{8} + 0.22 * \left[\phi_c \frac{L^2}{8} + (\phi_e - \phi_C) * \frac{a^2}{6} \right] \tag{6.1}$$

From chapter 4, the equation used to calculate the deflection of the girders due to the self-weight and the superimposed dead load was based on a simply supported member. Using the assumption that the whole bridge acts as a simple span lead to the use of equation (4.42).

$$\delta = \frac{5 * W * L^4}{384 * E_c * I_g} \tag{6.2}$$

On the other hand, since the slab is cast over all girders, equation (6.2) can not be used for a continuos superimposed dead load. The equation used to calculate the deflection due to the superimposed dead load based on continuos behavior is somewhat different from the one used in equation (6.2). The difference between both equations is the coefficient used in the deflection equation as shown below:

In the positive region of the exterior span:

$$\delta_{SD} = \frac{0.0069 * W * L^4}{E_c * I_c} \tag{6.3}$$

In the positive region of the interior span:

$$\delta_{SD} = \frac{0.000526 * W * L^4}{E_c * I_c} \tag{6.4}$$

6.3.2 Net Camber or Deflection

In order to sum all the contributions of camber and deflection, equation (6.5 or 6.6) must be used. This equation is based on the Approximate Time-Step Method[10]. It depicts the upward deflection or camber due to eccentric compressive stress of the strands as a negative value, and the downward deflection due to the various loads as a positive value. In equation (6.5), the deflection for a non-composite beam is shown.

$$\delta_T = -[1 - \frac{\Delta P}{Po} + \lambda(Kr * C_t)]\delta_{pi} \uparrow + [1 + C_t]\delta_D \downarrow + [1 + C_t]\delta_{SD} \downarrow + \delta_L \downarrow \quad (6.5)$$

For composite beams the total deflection is

$$\delta_T = -[1 - \frac{\Delta P}{Po} + \lambda(Kr * C_t)]\delta_{pi} \uparrow + [1 + C_t]\delta_D \downarrow + [1 - \frac{\Delta P - \Delta P_c}{Po} + Kr * C_t(\lambda - \lambda')]\delta_P * \frac{I_e}{I_{composite}} + [1 + C_t \frac{I_e}{I_{composite}}]\delta_{SD} \downarrow + [1 + C_t]\delta_D \frac{I_e}{I_{composite}} \downarrow + \delta_{df} \downarrow + \delta_L \downarrow \quad (6.6)$$

Where $\lambda = \frac{\Delta P}{2P_o}$

$\lambda' = \frac{\Delta P_c}{2P_o}$

$\Delta P = P_i - P_e$

δ_{pi} = camber due to initial pre-stress alone

δ_D = deflection due to weight of the girder alone

δ_{SD} = deflection due to superimposed dead load

δ_{df} = deflection due to deferential creep between slab and girder

δ_L = deflection due to live load

Equations (6.5) and (6.6) are modified and implemented to the Gandy Bridge project using the field measured time-dependent pre-stress losses and effective creep coefficient after some modification. In this modified equation, the loss of pre-stress is implemented into the camber due to pre-stressing alone. The creep coefficient is replaced by the time-dependent effective creep coefficient achieved in this study. The implementation of composite section is done at 240 days, when the slab is cast. When composite action takes place, the equations used to achieve the various displacements are modified to account for the change in the member's dimensions and properties. The Modified net Camber equation used is:

$$\delta_T = -[1+Ce)]\delta_P \uparrow + [1+Ce]\,\delta_D \downarrow + [1+Ce]\,\delta_{SD} \downarrow + \delta_L \downarrow \qquad (6.7)$$

Camber and deflection calculation is done for both simply supported and continuous superimposed loads. The division of this section into both methods of camber calculation is seen in the sequential sections.

6.3.3 Simply Supported Superimposed Dead Load

Figures 6-15 and 6-16 represent the camber-deflection at the mid-span of Beam 1 and 4 respectively when simple supported is assumed throughout. From the figures, it is obvious that the design camber is much higher than the camber achieved in this study. This is due to the fact that the design camber was based on concrete strength of 44.817

Mpa (6500 psi), where in reality the actual concrete strength is 57.318 Mpa (8313 psi). Additional weight such as slab, asphalt, parapets and other superimposed dead load were supposed to be applied on the girders at the 120th day of the project. The superimposed dead load was applied instead at the 240th day of the project. The effect of the superimposed dead load on the section is clearly illustrated in both graphs. In the design camber, the magnitude of camber drops significantly at the 120th day. In the achieved camber of this study, the affect of additional weight takes place at the 240th day of the project. The field measurement of camber is very consistent with those computed using the Time-Steps Method in this study. Although the camber measured in the field is not 100 % accurate, it gives an acceptable estimate to what the camber value should be. It can be clearly seen that these graphs along with others show the behavior of the concrete at various depths. This variation of camber with depth is seldom considered in pre-stress concrete behavior. The variation of the camber between various depths is due to the fact that different pre-stress loss and effective creep coefficient values are achieved at the various depths. Since pre-stress loss and creep coefficient are often computed as one value, sectional camber and deflection are often presented as one-value measurement as well.

Creep is one of the pre-stress loss components that affect camber a great deal. From equation (6.7), it is obvious that the effective creep coefficient plays a major factor in this equation. Using the maximum effective creep coefficient that occurs at 190.5 cm (75 in) from the bottom of the section, a more uniform distribution to camber can be seen. Figure 6-17 shows the camber-deflection at the mid-span of Beam 1. From the figures, it

is obvious that the design camber is much higher than the camber achieved in this study. This figure differs a great deal from Figure 6-15. In Figure 6-17 a more uniform camber with respect to depth is shown. This confirms that the use of a simple pre-stress loss value at the steel centroid and creep coefficient at this level will result in a uniform camber between top and bottom of the girder.

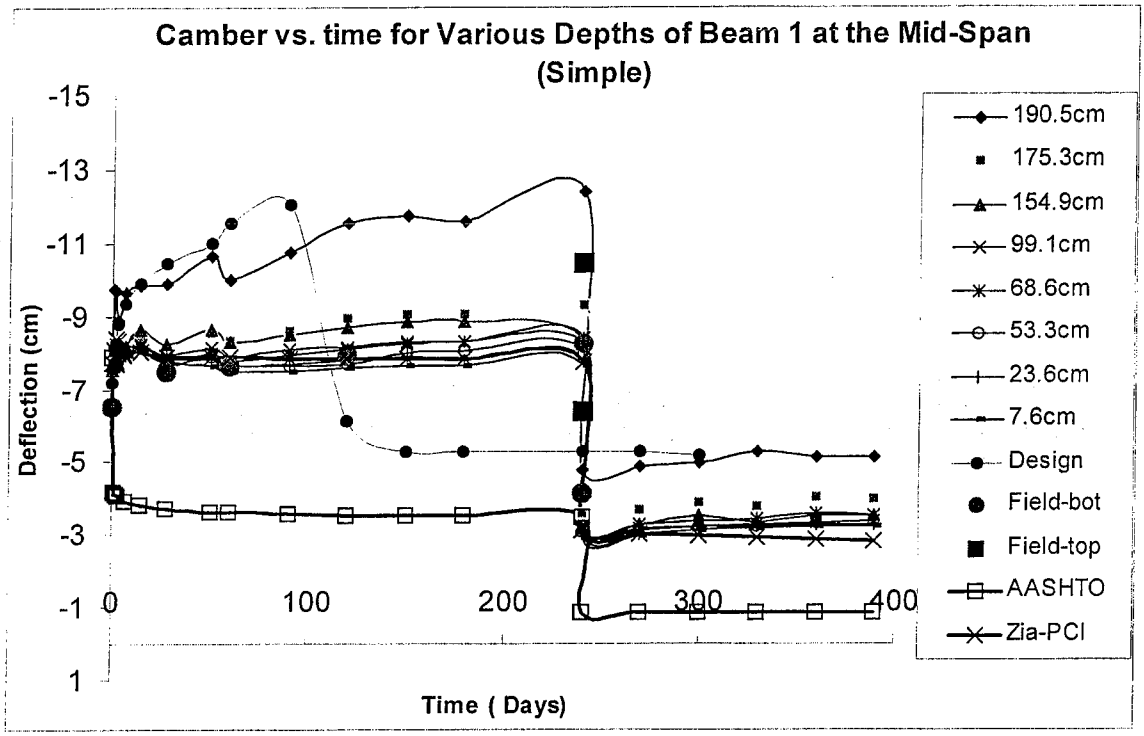

Figure 6-15 Camber vs. Time at Various Depths at the Mid-span of Beam 1.

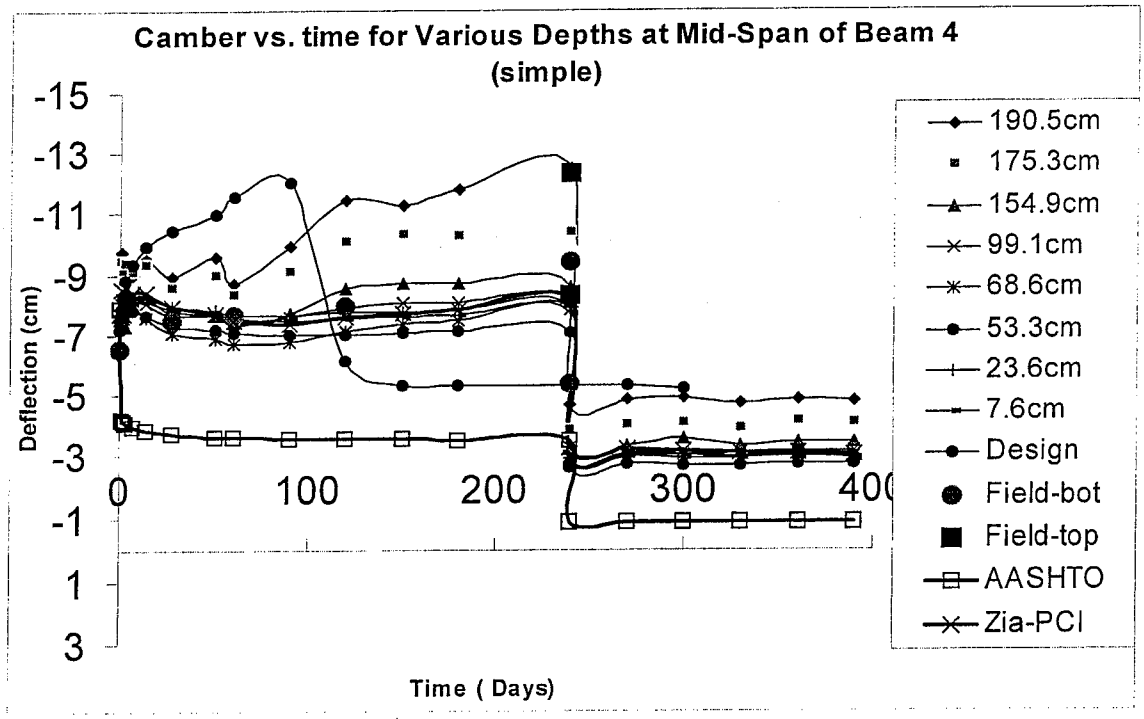

Figure 6-16 Camber vs. Time for Various Depths at the Mid-span of Beam 4.

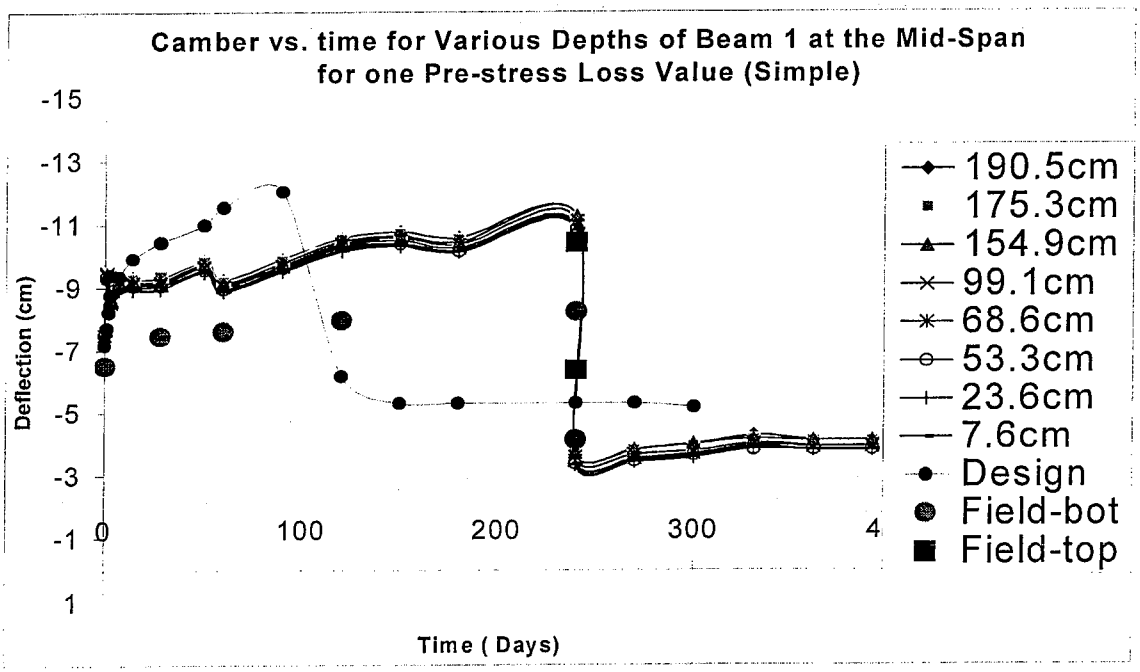

Figure 6-17 Camber vs. Time at the Mid-span of Beam 1 for One Pre-stress Loss Value.

6.3.4 Continuous Superimposed Dead Load

Figures 6-18 and 6-19 represent the camber-deflection at the mid-span of Beam 1 and Beam 4 respectively considering continuous superimposed load. From both figures, it is obvious that the design camber is much higher than the camber achieved in this study prior to imposing the additional weight on the section. The design of the Gandy Bridge had failed to account for continuity of the superimposed dead load. The field measurement of camber is more consistent with this research.

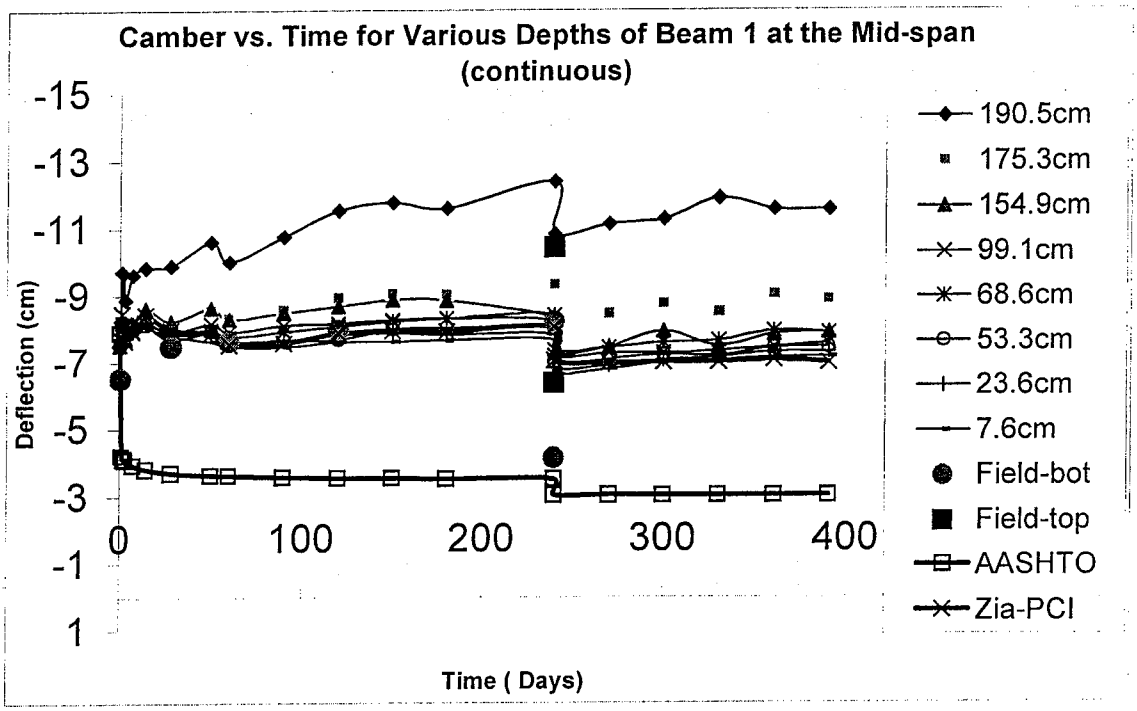

Figure 6-18 Camber vs. Time for Various Depths of Beam 1 at the Mid-span.

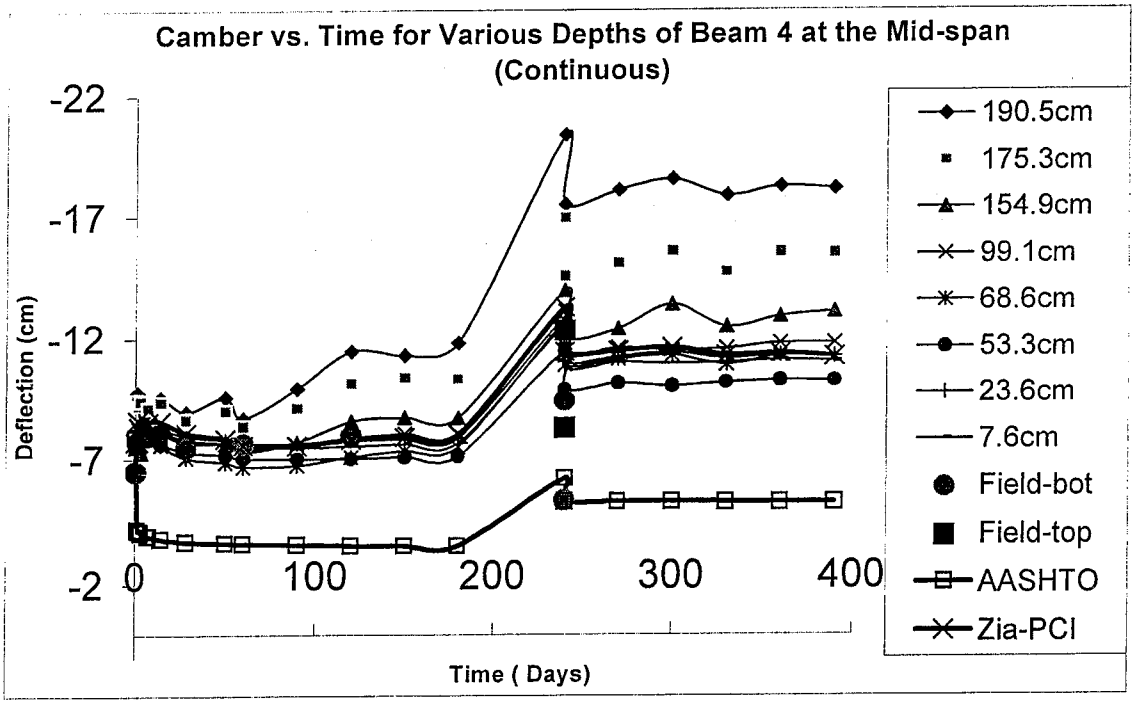

Figure 6-19 Camber vs. Time for Various Depths of Beam 4 at the Mid-span.

6.3.5 Comparison of Camber from Simple, Continuous and Field Data

Figures 6-20 and 6-21 show the comparison between simply supported and continuous superimposed dead load at the top and bottom sections of the girder respectively. Both figures are done at the mid-span of Beam 1. Both design and field camber values are implemented into these figures in order to better demonstrate the consequences of using simply vs. continuous superimposed slab. Although the Gandy Bridge consist of continuous slab sitting on simply supported girders, the camber values based on this study show that the actual camber is not equivalent to such a case. Due to the fact that the slab is sitting on a much stiffer girder, its ability to displace in the vertical direction is restricted especially when composite action is formed. Thus, the sections

seems to show more of a simple supported behavior, but is still not fully singly supported.

Figures 6-22 and 6-23 show the comparison between simply supported and continuous superimposed dead load at the top and bottom sections of the Beam 4 respectively. The use of slab continuity in the design approach of such structure is not proper, the method used in design assuming simply supported bridge was too conservative.

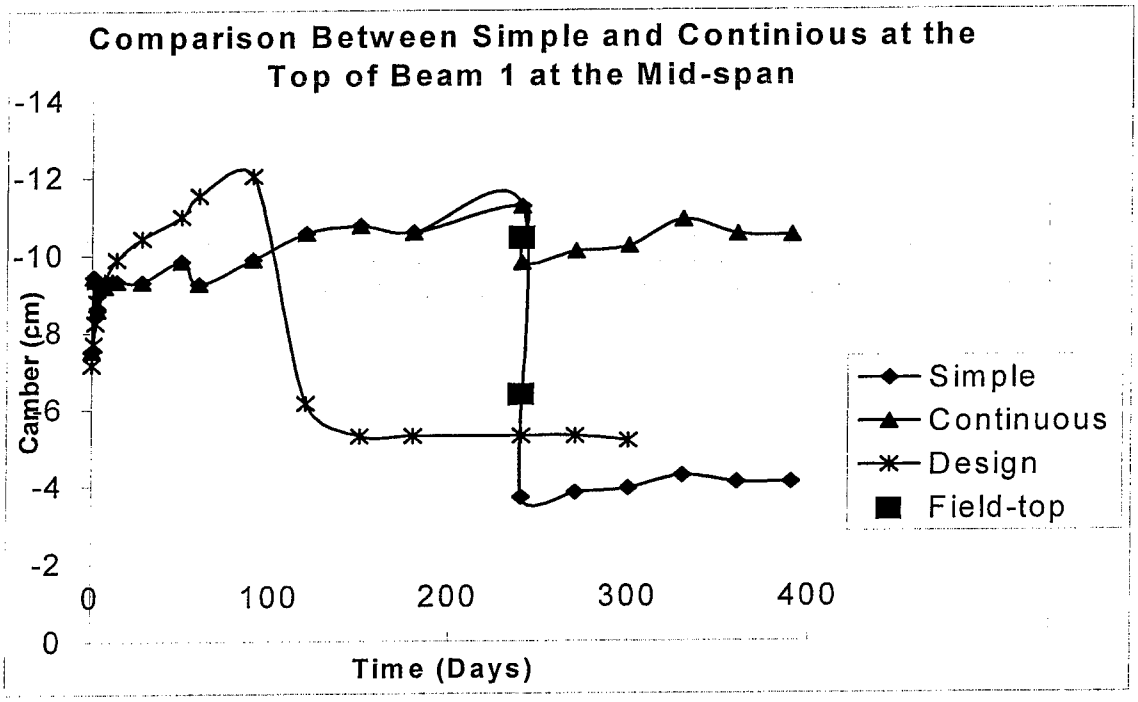

Figure 6-20 Comparison between Simple and Continuous slab at the Top of Beam 1.

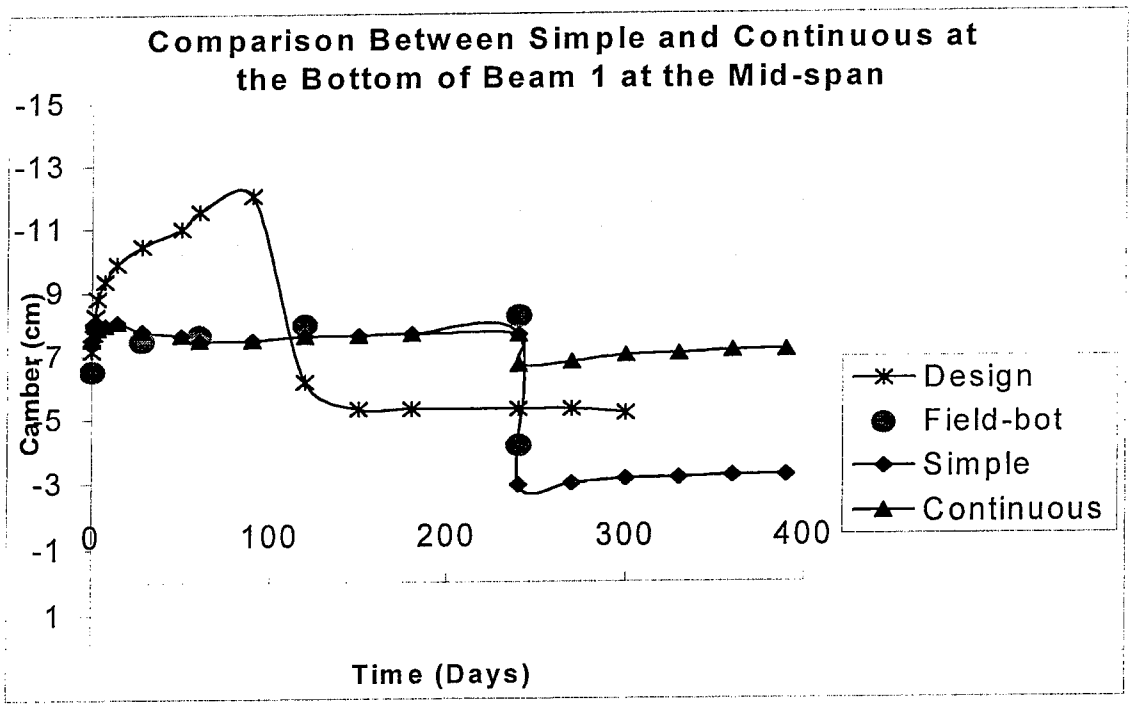

Figure 6-21 Comparison between Simple and Continuous slab at the Bottom of Beam 1.

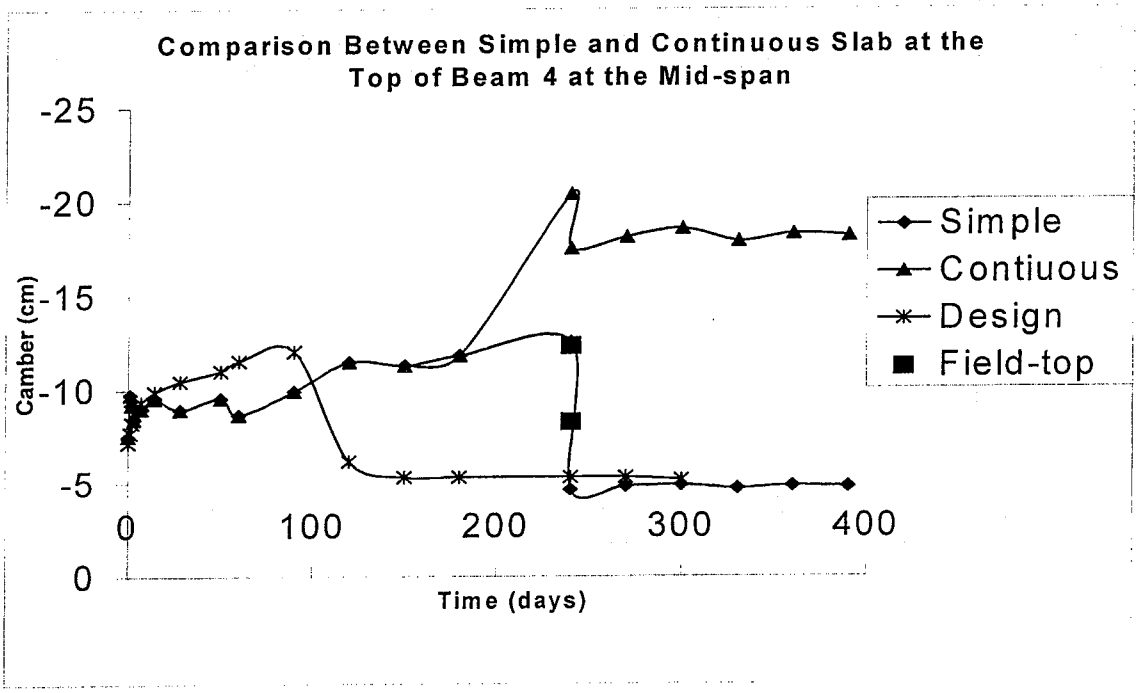

Figure 6-22 Comparison between Simple and Continuous slab at the Top of Beam 4.

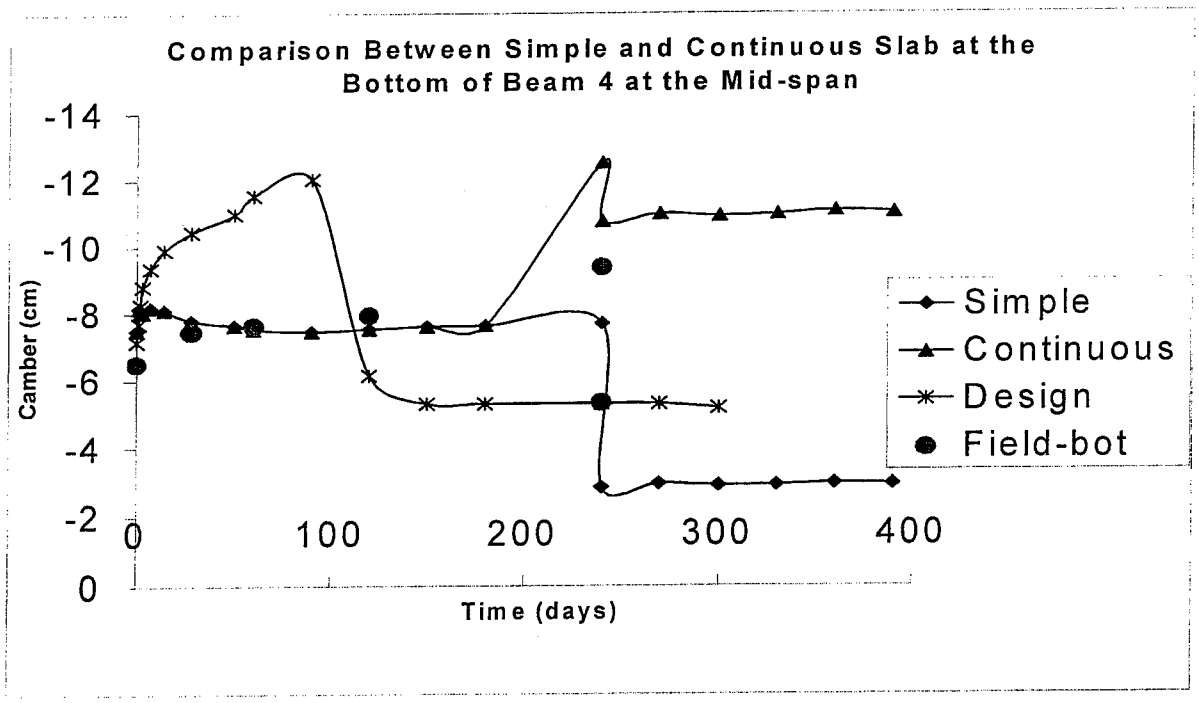

Figure 6-23 Comparison between Simple and Continuous slab at the Bottom of Beam 4.

Chapter 7

CONCLUSIONS AND RECOMMENDATIONS

7.1 Introduction

The main objective of the Westbound Gandy Bridge research project funded by the FDOT is to investigate the time-dependent behavior of the bridge girders. The unconventional design of the bridge is the main reason it was of interest to the FDOT. A typical portion of the bridge is a combination of simple supported beams and a continuous bridge deck.

Therefore, determination of the time-dependent pre-stress loss through actual measurement was of major interest in the study. Due to the relationship between pre-stress loss and stress, accurate determination of the time-dependent stress distribution or re-distribution within the girder depths was important. This stress distribution will enable engineers to better understand the effect of accounting for the deck continuity vs. the use of simply supported superimposed slab in the design of such bridges. Also of importance is the effect of time-dependent pre-stress loss on the magnitude of camber and deflection occurring in the girders. The conclusions from the various goals addressed in this study are discussed in the following sections.

7.2 Time-dependent Pre-stress Loss

It is essential in engineering design of structures built with pre-stress concrete members to estimate pre-stress loss with respect to time. Although the lump sum method of computing pre-stress loss is simple and convenient, it does not allow the designer to understand the structural behavior at various stages of construction and during service. The lump sum method is based on one value of pre-stress loss implemented at the level of the steel centroid and does not change with time. Its use often results in an over estimation of pre-stress loss especially in the early stages when most of the time-dependent pre-stress loss has not yet occurred. This overestimation of pre-stress loss in design may have negative effects on the behavior of pre-stress structures. Overestimating pre-stress loss in design suggests less camber, therefore ultimately underestimating the actual camber in the field. In bridges, the excessive camber resulting from this error causes an uncomfortable ride. Excessive camber is also undesirable from a construction point of view. In order to achieve a more even slab over a cambered beam, extra concrete must be placed at both ends of the section. On the other hand, underestimating pre-stress loss in design suggest more camber than anticipated for in the design. Therefore, it is equally as inconvenient from serviceability and construction point of view for structures to have excessive deflection as it is to have excessive camber.

- Based on the strain readings that are implemented at various depths of several Gandy Bridge girders the pre-stress loss was measured with respect to both time and depth. This measured time dependent pre-stress loss was then compared with those from

Zia-PCI[3], and ACI-209[6] methods of estimating time-dependent pre-stress loss at the steel centroid. Similar results were achieved for time-dependent pre-stress losses using Zia-PCI, ACI-209 and actual measured time-dependent pre-stress loss at the level of the strands. Both Zia-PCI, and ACI-209 lack the ability to depict the effect of pre-stress loss at different depth with the concrete member.

- Another approach was compared with the previous time-dependent pre-stress losses. This approach is based on the AASHTO method of estimating pre-stress loss. The AASHTO code uses a lump sum pre-stress loss value that does not vary with time or depth. This pre-stress loss value is an overestimation of the actual pre-stress loss of the member especially at the early stage. Although the consequences of using the different methods of estimating pre-stress losses may not be clearly seen in terms of loss values, their effect on the actual stress and camber values of the pre-stress element are of importance in practice.
- Also, K_d and K_t as described in this study are only a preliminary attempt to investigate ways for implementing the variability of the effective creep coefficient with respect to time and depth in design.

7.3 Stresses in the Modified AASHTO type VI Girders

The fact that the actual 28^{th} day concrete strength used for the girders of the Gandy Bridge was higher than specified in the design is a good conservative field practice from strand point of stresses. A stronger concrete section has a higher compressive stress limit than a weaker concrete section. Actual stresses at 1.52m away from the support immediately after transfer violated the design compressive limit provided by AASHTO but not the actual limit in the girders. The stress estimation of a pre-stress section may vary with the method of estimating pre-stress loss.

- In the Gandy Bridge Design Report[11], the stress at the bottom of the section did not violate the design compressive stress limit as was the case from actual measurement. The method used in estimating the stress distribution in the design manual was based on CEB-FIP[7].
- The variation of stress between those from the design report and from other codes used in this study suggests that the use of higher strength concrete in the field may be enough to accommodate for any inconsistency or variability in using different codes.
- It can be concluded that proper pre-stress loss estimation play a large role in depicting the amount of stress on the concrete section. Although the Zia-PCI stress distribution compared well with actual stress distribution especially at the mid-span, it showed similar stress distribution to the AASHTO code at 1.52 m away from the support.

The AASHTO stress distribution across the concrete showed less stress values especially at the bottom of the section.

- In comparison between both simply supported slab and continuos slab applied to simply supported girders, the stress distribution at the mid-span of the girders are very similar. However, the stress distribution at 1.52 m (5 ft) away from the support is very different.
- In the continuous slab case, there is very small reduction in the compressive stress at the lower part of the section near the support. It was determined also that the depth variation of losses did not significantly affect the stress-distribution, except making it non-linear. However, accounting for the time-dependency of the losses is necessary for a proper design.

7.4 Camber of the Modified AASHTO type VI Girders

Concrete sections are often assumed to be rigid structures. This assumption is not accurate. From the definition of rigid structures, they are said to have a constant shape and do not deform with time. However, concrete sections deform as time progresses. Deformation in the longitudinal direction causes strain of the concrete sections. Displacement in the vertical direction causes both camber and deflection. Camber is often thought of as one value across the depth of the concrete section. This assumption is as accurate as the assumption of stress linearity across the depth of the section. Stress linearity across a section's depth is assumed for simplicity of design. From the camber study conducted in this research, it was found that:

- the magnitude of camber differs between the top of the section and the bottom of the section.
- It also varies across the depth. This variation in the magnitude of camber is an important finding from this study that needs to be considered in both design and construction.
- This is attributed to the use of the depth varying effective creep coefficient value. In the field, camber is often measured at the bottom of the concrete section, and in the bed from the bottom of the bed to the camber point in the bottom of the member. In most cases, this is done by tying a rope at the bottom of both ends of the beam and measuring the spacing between the rope and the bottom of the beam at the mid-span.

Similar measurement should be done to compute the camber at the top most of the concrete member. Although field camber measurements done by this approach are not fully accurate, they give much better camber estimation than the camber values obtained in the original design. The design camber values are usually much higher than the actual camber. This is due to the fact that the actual strength of the concrete section at transfer is often higher than the design initial concrete strength as is the case in this study.

- The use of higher concrete strength in the field causes the member to camber less than anticipated in the design. Since the field concrete strength may be different from the design concrete strength, it is difficult to depict the actual magnitude of camber or deflection when all loads are applied.
- From this study, it can be concluded that the use of higher concrete strength in the field, while it is good for stresses, is not such a good thing for the camber and deflection. It is thus recommended that the use of higher strength concrete in the field is done with care.
- From the various methods used to achieve the magnitude of pre-stress loss, different camber estimations were obtained. In comparison between the camber values based on the field measured data of pre-stress loss, and Zia-PCI pre-stress loss, the camber based on Zia-PCI gives a good estimation of camber at the bottom part of the girder. However, Zia-PCI camber does not depict the camber values at different locations such as the top of the section.

7.5 Recommendations for Future Work

- The slab of the Gandy Bridge was instrumented with strain gages also. It will be of great benefit to investigate the effect of the slab continuity from analyzing the slab strain readings.
- Determining the amount of differential or inelastic creep if any resulting from the continuity of the slab is also of a great value.
- Continue efforts to implement the use of the effective concrete creep coefficient into a design methodology for pre-stress concrete girders. For proper use of this coefficient, factors affecting it such as strand profile, height of member, number of strands, and strength of concrete need to be investigated further.
- Similar study to the Gandy bridge research project should be done for post-tensioned members as well.
- It will be highly recommended to investigate the effect of different concrete strengths and steel profiles on the effective creep coefficient.

APPENDIX A

PLOTS OF STRAIN READINGS FROM SHRINKAGE CYLINDERS

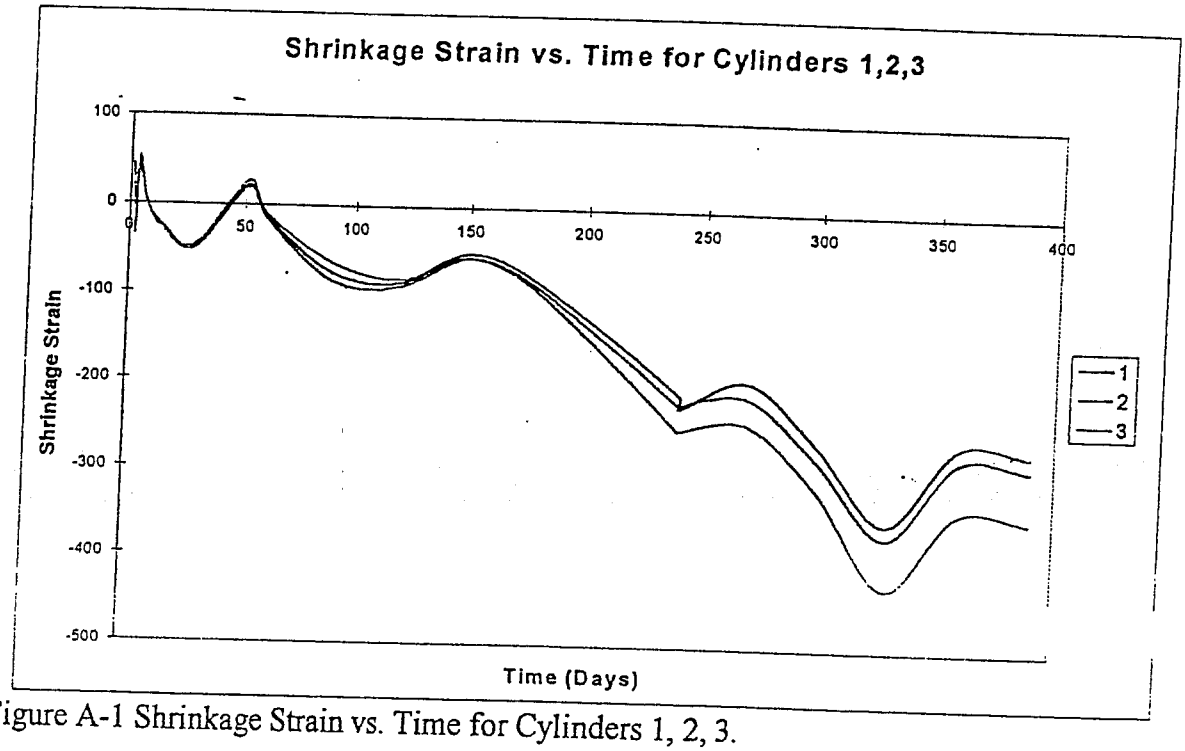

Figure A-1 Shrinkage Strain vs. Time for Cylinders 1, 2, 3.

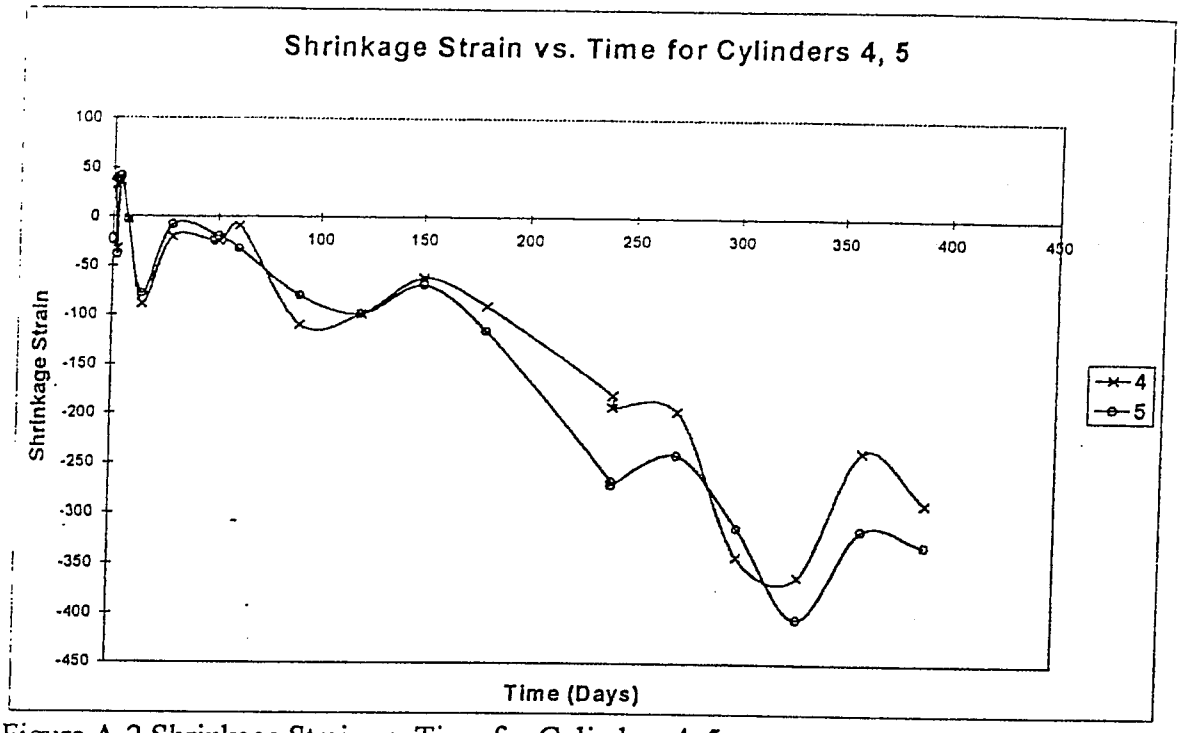

Figure A-2 Shrinkage Strain vs. Time for Cylinders 4, 5.

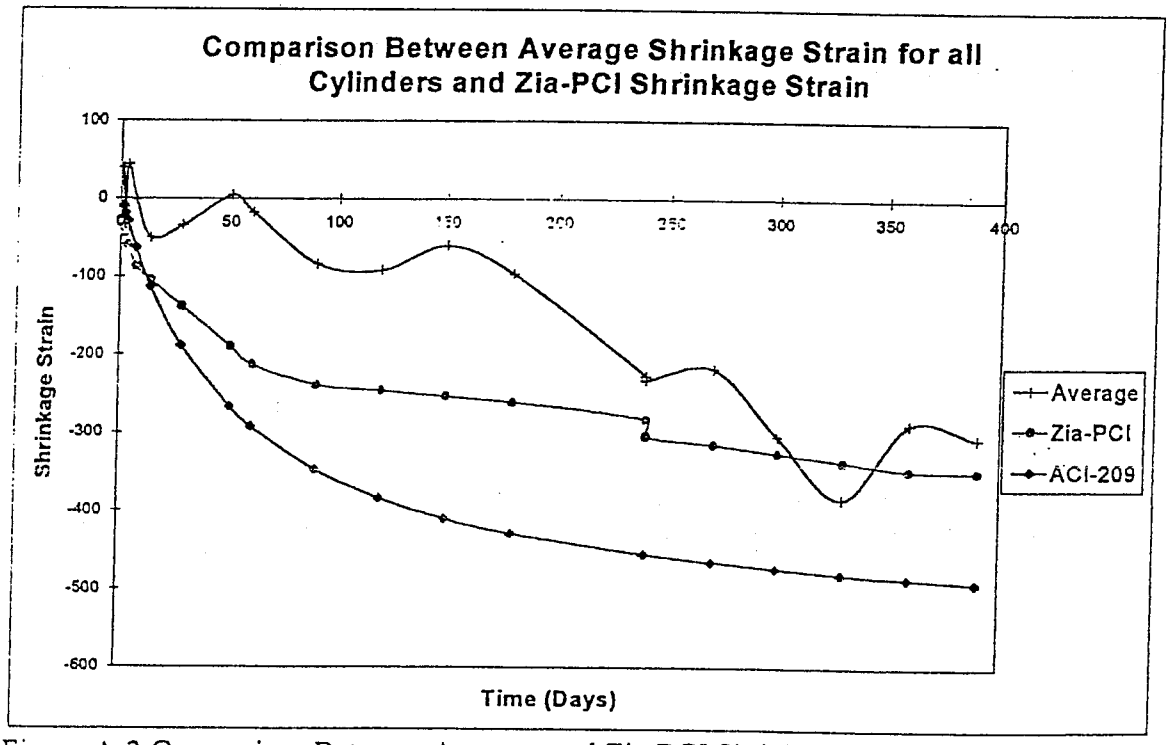

Figure A-3 Comparison Between Average and Zia-PCI Shrinkage.

APPENDIX B

FIELD SURVEY ELEVATION DATA OF GIRDERS COMPILED DURING CONSTRUCTION

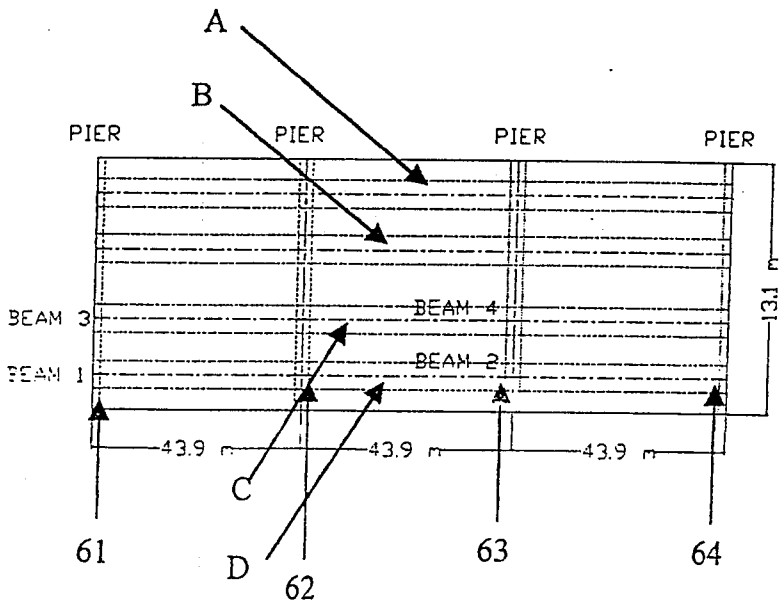

Figure B-1 Sectional Identification of the Westbound Gandy Bridge.

Table B-1 Field Measured Camber Data

	Beam A (ft.)	Beam B (ft.)	Beam C (ft.)	Beam D (ft.)	BP= Before Pour AP= After Pour D.E= Diff. in Elevation
W/FACE 61	17.401	17.636	17.850	18.040	BP
	17.405	17.639	17.856	18.045	AP
	+0.004	+0.003	+0.006	+0.005	DE
CL SPAN 60	17.399	17.656	17.829	18.006	BP
	17.284	17.550	17.724	17.891	AP
	-0.115	-0.106	-0.105	-0.115	DE
E/FACE 60	16.782	17.022	17.245	17.448	BP
	16.771	17.014	17.238	17.438	AP
	-0.011	-0.008	-0.007	-0.01	DE
W/FACE 60	16.827	17.048	17.266	17.482	BP
	16.818	17.040	17.260	17.472	AP
	-0.009	-0.008	-0.006	-0.010	DE
CL SPAN 59	17.082	17.255	17.494	17.669	BP
	16.962	17.134	17.375	17.545	AP
	-0.120	-0.121	-0.119	-0.124	DE
E/FACE 59	16.800	17.022	17.233	17.429	BP
	16.804	17.027	17.249	17.442	AP
	+0.004	+0.005	+0.016	+0.013	DE
W/FACE 59	16.768	16.984	17.203	17.400	BP
	17.774	16.989	17.207	17.404	AP
	0.006	+0.005	+0.004	+0.004	DE
CL SPAN 58	16.985	17.243	17.512	17.583	BP
	16.860	17.116	17.387	17.450	AP
	-0.125	-0.127	-0.125	-0.133	DE
E/FACE 58	16.781	17.004	17.232	17.420	BP
	16.772	16.994	17.224	17.411	AP
	-0.009	-0.01	-0.008	-0.009	DE

Table B-2 Continued Field Measured Camber Data

	Beam A (ft.)	Beam B (ft.)	Beam C (ft.)	Beam D (ft.)	BP= Before Pour AP= After Pour D.E= Diff. in Elevation
W/FACE 64	23.264	23.491	23.703	23.918	BP
	23.249	23.479	23.690	23.905	AP
	-0.015	-0.012	-0.013	-0.013	DE
CL SPAN 63	22.270	22.479	22.706	22.921	BP
	22.119	22.324	22.549	22.769	AP
	-0.151	-0.155	-0.157	-0.152	DE
E/FACE 63	20.728	20.960	21.181	21.385	BP
	20.728	20.960	21.180	21.383	AP
	0	0	-0.001	-0.002	DE
W/FACE 63	20.655	20.296	21.107	21.324	BP
	20.651	20.893	21.102	21.322	AP
	-0.004	-0.003	-0.005	-0.002	DE
CL SPAN 62	19.986	20.207	20.448	20.646	BP
	19.856	20.072	20.311	20.519	AP
	-0.130	-0.135	-0.137	-0.127	DE
E/FACE 62	18.712	18.962	19.174	19.410	BP
	18.723	18.957	19.170	19.398	AP
	+0.005	-0.005	-0.004	-0.016	DE
W/FACE 62	18.680	18.917	19.125	19.348	BP
	18.673	18.901	19.119	19.341	AP
	-0.007	-0.016	-0.006	-0.007	DE
CL SPAN 61	18.307	18.576	18.791	18.952	BP
	18.153	18.430	18.634	18.812	AP
	-0.154	-0.146	-0.157	-0.140	DE
E/FACE 61	17.377	17.601	17.827	18.018	BP
	17.372	17.594	17.831	18.012	AP
	-0.005	-0.007	+0.004	-0.006	DE

REFERENCES

[1] Onyemelukwe, O.U., "Field Measurement and Evaluation of Time-Dependent Losses in Prestressed Concrete Bridges, FDOT Report Grant No. 9908 99700-3318-119, Tallahassee, Florida, 1997.

[2] ACI. Building Code Requirements for Reinforced Concrete (ACI 318-89) (Revised 1992) and Commentary-ACI 318R-89 (Revised 992). Detroit, Michigan: American Concrete Institute, 1992.

[3] Zia, Preston, Scoot, and Workman, "Estimating Pre-stress Loss." Concrete International June 1979: 32-38.

[4] PCI Institute, PCI Design Handbook: Precast and Prestressed Concrete. 4th ed. Chicago: 1992.

[5] AASHTO, AASHTO LRFD Bridge Design Specifications 1st Edition 1994. Washington D.C.: American Association of State Highway and Transportation Officials 1994.

[6] ACI Committee 209, "Prediction of Creep, Shrinkage and Temperature Effects in Concrete structures." ACI 209R-92. Detroit: ACI, 1992.

[7] CEB-FIP 1990, Model Code for Concrete Structures (MC-90). London: Thomas Telford, 1993.

[8] Christopher Mills, Measurement of Time-Dependent Losses in Prestressed Concrete Bridge. M.S. Thesis, University of Central Florida. Summer, 1997.

[9] Antonio Montiel. Design and Analysis of Pre-stressed Concrete Bridge for Time Dependent Losses. M.S. Thesis, University of Central Florida. Fall, 1997.

[10] Nawy, Edward G. "Prestressed Concrete. Second Edition. New Jersey: Prentice-Hall, Inc. 1996.

[11] Finley McNary/Janssen Spaans. State Road No. 600 Westbound Gandy Bridge (Value Engineering Contract). Tallahassee, 1995.

[12] A. Ghali and R.Favre. Concrete Structures. 2nd edition. London: Chapman & Hall. 1994

[13] Antoine E. Naaman. Prestressed Concrete Analysis and Design. New York: McGraw Hill, Inc., 1982, pg. 65.